# An EEG modeling methodology based on the collective almost synchronization phenomenon

---

A thesis submitted in fulfillment
of the requirements for the degree of
Doctor of Philosophy

Department of Electronic and Information Engineering
Graduate School of Engineering
Tokyo University of Agriculture and Technology

*Author:*
Thi Mai Phuong Nguyen

*Supervisors:*
Prof. Toshiyuki Kondo

*Committees:*
Prof. Toshiyuki Kondo
Prof. Ikuko Shimizu
Prof. Seiji Hotta
Prof. Keiichi Kaneko
Prof. Hironori Nakajo

September 2022

# CONTENTS

# LIST OF FIGURES

# LIST OF TABLES

# ABSTRACT

Electroencephalography (EEG) is one of the essential non-invasive brain imaging methods for studying the human cognitive function and diagnosing brain diseases. A better understanding of how different types of brain activity are reflected in the cortical current dipole creates a better inverse model for sound source localization and the mechanism of human cortical activity. It may lead to a better understanding of brain diseases and the cure of diseases.

The EEG can measure the macroscopic collective activity of the brain with higher time resolution and is widely used to understand the electrophysiology of brain activity that correlates with cognitive function and motor regulation. Since EEG signals are complex and have stochastic, non-linear, and non-stationary characteristics, it is out of the question to apply classical time series analysis techniques. In this thesis, we have investigated that the EEG signal can be modeled as the sum of the action potentials of the oscillators that model the action potentials of living neurons. Hence, a neuron model-based approach is used to understand the dynamic nature of EEG signals better. EEG is a useful biological signal to distinguish different brain diseases and mental states. It is an technique for recording human brain signals, and is crucial for the Brain-Computer interface (BCI).

Firstly, we propose a model based on a complex network of weakly connected dynamical systems (Hindmarsh-Rose (HR) neurons or Kuramoto oscillators) configured to operate in the dynamic domain. This thesis shows that the best way to reconstruct an EEG signal from a complex oscillator network is to construct an output function (weighted average signal of action potentials of multiple neurons). Using this method, we show that the time-series orthogonal sets produced by the complex network of both HR and Kuramoto oscillators minimize the error function that fits the EEG data. The proposed model successfully reproduces EEG signal data in both healthy and epileptic patients and can also predict EEG characteristics such as the Hurst index and power spectrum.

Secondly, as a consequence of the modeling approach, a novel EEG feature extraction method which can improve the Motor Imagery (MI) classification introduced. Purpose of this study is to investigate the performance of the CAS model to identify features in the classification of MI states. To achieve this goal, a linear regression method is used and linear coefficients are extracted as feature vectors. Our approach boils down to identifying patterns in the MI-EEG by associating

them to the coefficients of a linear regression constructed to model the MI-EEG signal by signals generated by our dynamical network. MI-EEG dataset 2b from BCI Competition-IV was used to evaluate the performance of the proposed method.

The result of MI classification indicated that the proposed feature method is more robust in extracting distinguishable features from EEG signals as compared with Fast Fourier transform ($p < 0.05$). Moreover, the MI classification for across subjects was improved.

# ACKNOWLEDGMENTS

First I would like to express my sincere gratitude to my supervisors Prof Toshiyuki Kondo for his excellent guidance, continuous support, and motivation throughout my Ph.D. I would like to thank you for encouraging me, helping me to grow as a researcher, and challenging me at every step to do more. Thank you for your insightful comments and critical analysis of my work which helped me to broaden my research horizon.

I would like to thank Prof. Yoshikatsu Hayashi and Prof Murilo Baptista, thank you for giving me an opportunity to do joint research projects on dynamic systems for EEG modeling in my Ph.D. Thanks for your mentorship throughout all these years, the extended meetings, and the intriguing discussions. I truly appreciate and value everything I have learned from you.

I would like to thank all the academics in our department for their teaching, support, and encouragement throughout my master's and Ph.D. I would like to thank Prof Pham The Bao, my undergrad mentor for inspiring me to pursue Mathematics and Computer Science. I would like to thank the Yuasa Foundation, NEC CC Foundation, and Tokyo University of Agriculture and Technology for funding my research.

It was fantastic to have the opportunity to work with everyone in the Biologically-inspired Computing Laboratory. It was great sharing the lab and interacting with all of you. I enjoyed working on collaborative projects, and demos and doing science outreach to share the fascinating research we do in our lab.

I would like to thank my mother and my husband for the unceasing encouragement and support me to pursue a Ph.D. I am also very grateful to my family and friends for their constant support and encouragement.

# ABBREVIATIONS

| | |
|---|---|
| **AR** | Auto-regressive |
| **ARFIMA** | Auto-regressive Fractional Integrated Moving Average |
| **ARMA** | Auto-regressive Moving Average |
| **BCI** | Brain-computer Interfaces |
| **CAS** | Collective Almost Synchronization |
| **CNN** | Convolutional Neural Network |
| **dFC** | Dynamic Functional Connectivity |
| **DFT** | Discrete Fourier Transform |
| **DL** | Deep Learning |
| **EEG** | Electroencephalography |
| **EMD** | Empirical Mode Decomposition |
| **EPs** | Evoked Potentials |
| **ERD** | Event-related Desynchronization |
| **ERPs** | Event-related Potentials |
| **ERS** | Event-related Synchronization |
| **ESN** | Echo State Network |
| **EVC** | Eigenvector Centrality |
| **FC** | Functional Connectivity |
| **FFT** | Fast Fourier Transform |
| **HH** | Hodgkin-Huxley |
| **HR** | Hindmarsh-Rose |
| **HS-CNN** | Hybrid-scale Convolutional Neural Network |
| **ICA** | Independent Component Analysys |
| **LSM** | Liquid State Machine |
| **MA** | Moving Average |
| **MAE** | Mean Absolute Error |
| **MI** | Motor Imagery |
| **MLP** | Multi-layer Perceptron |

| | |
|---|---|
| **ODEs** | Ordinary Differential Equations |
| **PCA** | Principal Component Analysis |
| **PLV** | Phase Locking Value |
| **PSD** | Power Spectral Density |
| **RC** | Reservoir Computing |
| **RNN** | Recurrent Neural Networks |
| **SNN** | Spiking Neural Network |
| **STFT** | Short-time Fourier Transform |
| **SVD** | Singular Value Decomposition |
| **TFD** | Time-frequency Distribution |
| **WT** | Wavelet Transform |

# 1 INTRODUCTION

## 1.1 MOTIVATION

There are various approaches to understanding human thoughts and behaviors, but to really understand how the brain works, we need to look inside the brain. Recently, EEG has attracted the attention of researchers. This is because it provides faster, cheaper, and tighter time resolution insights into brain function. EEG is a recording signal of brain activity that mainly use for diagnosing and treating brain disorders [1]. EEG is an electrophysiological technique that records the electrical activity in the human brain. Due to its high temporal sensitivity, the primary use of EEG is to evaluate dynamic brain function. It is beneficial for assessing patients with suspected seizures, epilepsy, and extreme weather.

EEG has also been adopted for several other clinical indications. For example, EEG may be used to monitor the depth of anesthesia during surgical procedures [2]; given its great sensitive in showing sudden in neural functioning even as they first occur, it has proven quite helpful in this setting in monitoring for potential complications such as ischemia or infarction. EEG waveforms may also be averaged, giving rise to evoked potentials (EPs) and event-related potentials (ERPs), the potential that represented neural activity of interest that is temporally related to a specific stimulus. EPs and ERPs are used in clinical practice and research for analysis of visual, auditory, somatosensory, and higher cognitive functioning [3]. To discover more abilities of the EEG, current researches have focused on understanding how the brain works, the identification of biomarkers, and the construction of BCI [4–7].

Recently, much attention has been focused on interpreting the mechanism of memory formation from the viewpoint of brain connectivity and dynamics. The Collective Almost Synchronization (CAS) phenomenon, which represents the appearance of infinite patterns in a complex network with weak bond strength, produces an output that optimally models an experimental electroencephalogram (EEG) signal. Through computing models, this phenomenon is a promising ap-

proach to better understand the brain operation. However, this approach in EEG are not widely investigated.

This thesis considers that EEG signals can be modeled by oscillators by two approaches: linear and nonlinear. In the linear approach, weighted average signal of action potentials of multiple neurons were used to minimized the error function for fitting EEG signal. In the nonlinear approach, we used the non-linear transformations called Reservoir Computing (RC). RC is a recently introduced, biologically-inspired machine learning paradigm [8, 9]. This approach finds cutting-edge performance in the processing of empirical data. Even for complex calculations, such as chaos time series prediction and voice recognition, good results can be obtained by processing with high calculation efficiency [10, 11]. It aims to perform certain non-linear transformations of the input signal or to classify the input. In RC, the neural network ("reservoir") has fixed interconnections and input weights, only the linear output readout weights are trained by linear ridge regression. Importantly, the reservoir's fixed nature opens up using any dynamic system. Theoretical advantages of the proposed method are the model learn and adapt to the time-varying nature of EEG signal.

Using the proposed model, we also aim to understand how the field generated as the sum of the action potentials of neurons increases complex microscopic signals such as EEG signals. The first step in our modeling technique is to train the output measurements of the network to fit the initial training set of EEG data and then predict the following time points of EEG (not considered in the training set). Validating the model by finding the optimal configuration of the network to best predict the set of signals. The characteristic variables that make it possible to change the configuration of the network to predict the EEG signal better are: In (i) the strength of the interaction between the dynamic units that form the network, (ii) the type of dynamic unit, (iii) the topology of the network (random network and small-world network).

The BCI is a hardware and software communication system that allows a computer or external device to control brain activity. One of the essential components of the BCI system is the EEG signal feature extraction procedure because of its role in the proper performance of the classification stage that identifies mental states. As a consequence of the EEG model, this thesis proposed a new feature extraction method for MI classification by using the weight of linear model.

## 1.2 BACKGROUND

### 1.2.1 *Brain Computer Interface*

The BCI provides an interface for direct communication with computers and external devices without using the body's motor pathways [12]. BCI can do simple tasks by providing new means of communication for people paralyzed by severe movement disorders such as spinal cord injury and stroke and by leveraging their ability to create personalized thoughts. In recent years, BCI has also attracted attention in locomotor rehabilitation, and it has become possible to involve patients in more active rehabilitation [13]. Applications of BCI for healthy people include entertainment and brain training such as meditation, relaxation, and concentration by neurofeedback. BCI can also be used as a tool for studying various neuronal processes. BCI is controlled by neuronal activity recorded in an invasive or non-invasive manner.

The feature extraction plays a crucial part in BCI system. There are many methodologies for EEG signal analysis were presented. In this thesis, we focus on two common methods: Fast Fourier transform (FFT) and auto-regressive (AR) methods.

FFT is a Fourier transform developed in 1965 from the Discrete Fourier Transform (DFT) algorithm discovered by J. Fourie [14]. The FFT algorithm can calculate the transform faster because it can reduce loop processing compared to DFT. It can be calculated faster than DFT because it reduces loop processing. FFT is applied to systems that filter signals from the time domain to the frequency domain. This method is a good tool for stationary signal processing. It is suitable for narrowband signals such as sine waves [15]. In addition, its real-time applications are virtually faster than all other available methods [16]. However, this method has some drawbacks. FFT has a weakness in the analysis of unsteady signals such as EEG [15]. FFT does not work well for spectral estimation and cannot be used for the analysis of short EEG signals [17]. Also, the FFT cannot reveal the local spikes or complications characteristic of epileptic seizures. In addition, FFT has high noise sensitivity and is not suitable for short-time data recording [15].

A. Zabidi proposed AR as a feature extraction technique for classifying writing tasks from EEG signals [18]. By imagining a writing task, it is possible to obtain valuable information for improving writing disorders. They use an AR model that uses a multi-layer perceptron (MLP) to identify the alphabet. EEG signals change in amplitude and frequency while different mental tasks are being performed. Therefore, these features can be captured and extracted using modeling techniques such as AR models. The AR model is widely used for EEG analysis. This shows a linear combination of Independent Component Analysys (ICA) and past EEG and yields

the current EEG sample. The basic idea of the AR model is the assumption that the so-called AR process can approximate the actual brain waves. Based on this assumption, the order and parameters of the approximate AR model are selected to fit the measured EEG as closely as possible. For each particular AR model, alternative methods for the characteristics of the EEG spectrum are provided. The AR model can be applied to stationary signals. However, in the case of EEG, the concept of a local steady-state hardly holds, and the EEG signal leaves the steady-state at short time intervals. AR coefficients, model order, and power spectrum features help improve the accuracy of the classifier. As the AR order increases, the performance of the classifier increases linearly. Choosing the exact order plays the most crucial role in time series AR modeling [19]. The AR model has a problem in estimating the model's parameters when the length of the measured EEG signal is limited. In order to model brain waves using the AR model, it is necessary to set the predicted order and its coefficient values accurately. If the predicted order is high, the actual peak of the frequency spectrum cannot be divided, and if the predicted order is low, those close to the peak in the frequency domain are combined [15].

In summary, due to the characteristics of the EEG signal itself, it is difficult to achieve good extracted features. In this paper, we proposed a new method to extract a feature of EEG signal for the purpose of application to BCI.

### 1.2.2 *EEG*

The EEG is a recording of the electrical activity of the brain from the scalp (Fig. 1.1). The recorded waveforms reflect the cortical electrical activity. EEG activity is quite small, measured in microvolts.

The main frequencies of the human EEG waves are:

- **Delta**: The frequency is 3Hz or more minor. It has the largest amplitude and tends to have slow waves. Infants up to 1-year-old and sleep stages 3 and 4 are expected as the dominant rhythm. Localized subcortical lesions may occur globally in diffuse lesions, metabolic encephalopathy, hydrocephalus, and deep median lesions. The frontal region is most prominent in adults and the occipital region in children (e.g., Occipital Intermittent Rhythmic Delta).
- **Theta**: The frequency is 3.5-7.5Hz and is classified as "slow" activity. It is pretty standard in children up to 13 and during sleep but is abnormal during adult awakening. It may be seen as a symptom of localized subcortical lesions, but it is distributed systemically in diffuse disorders such as some cases of metabolic encephalopathy and hydrocephalus.

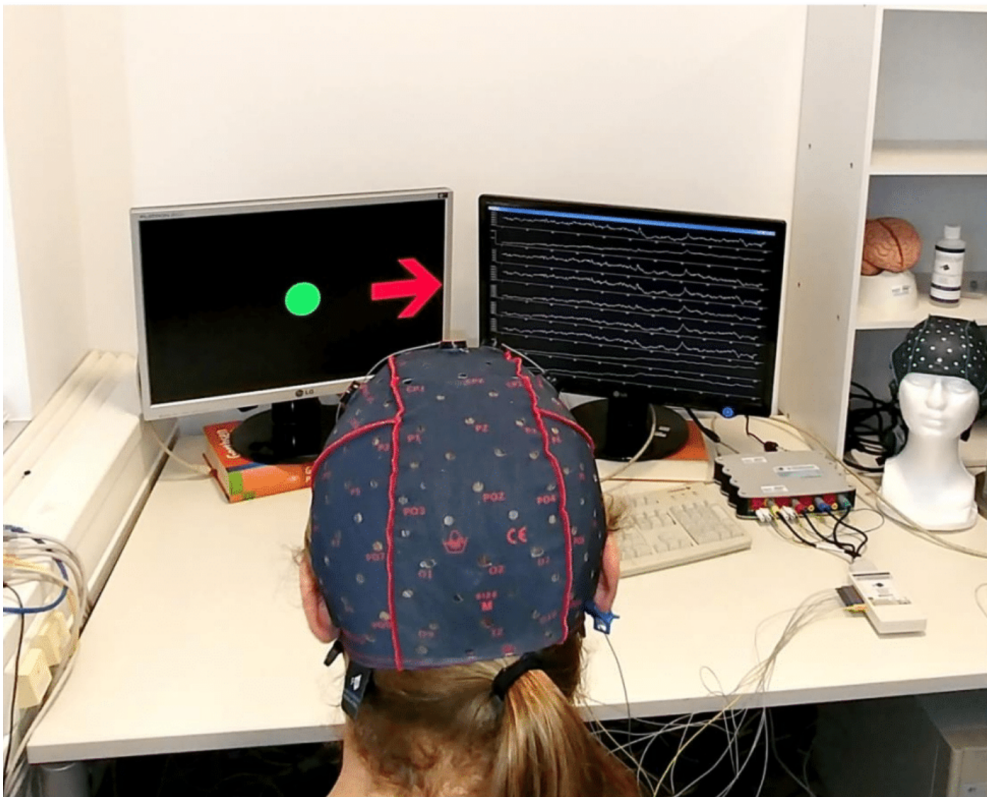

Figure 1.1: EEG record process [20]

- **Alpha**: The frequency is 7.5 to 13Hz. It usually appears on the left and right occipital regions, with greater amplitude on the dominant hand side. It appears when closing eyes and relaxes and disappears when eyes are opened or are alert by some mechanism (thinking, calculating). It is the main rhythm found in normal relaxed adults. It exists most of life, especially after the age of 13.

- **Beta**: Beta activities are "fast" activities. Its frequency is above 14Hz. It is usually symmetrically distributed and most prominent in the frontal region. It is enhanced with sedatives, especially benzodiazepines and barbituric acids. It may disappear or decrease at the damaged site of the cerebral cortex. Beta is generally a normal rhythm. This rhythm predominates in patients who are awake, anxious or have their eyes open.

- **Gamma**: Prior to the development of digital EEG, gamma waves were ignored because analog electroencephalographs are usually limited to recording and measuring rhythms below 25 Hz. One of the oldest reports was in 1964, recording the electrical activity of electrodes embedded in the visual cortex of awakened monkeys. Recent studies with a monkey and human microelectrodes have shown that gamma oscillations are present and are clearly correlated with the firing of single neurons (mainly inhibitory neurons) [21].

In humans, gamma oscillations were seen in all stages of the wake-sleep cycle and were maximally coherent during slow-wave sleep.

Richard Caton made the first neurophysiological records of animals in 1875 [22]. It took another half a century to record human electrical activity. In 1924, German psychiatrist Hans Berger established a method for recording human brain waves [22].

## 1.3 THESIS OUTLINE

The remainder of this thesis is organized as follows.

**Chapter 2** survey and discuss the methods for EEG modeling, but those are difficult to forecast even for short time intervals. Besides, the related works for dynamic functional connectivity and EEG classification are discussed.

**Chapter 3** shows the model that can reproduce and predict both healthy and epileptic EEG signals, as well as the characteristics of the EEG signals, Hurst exponent, and power spectrum of experimental EEG signals.

**Chapter 4** propose a novel approach for time-series forward prediction that was developed based on a CAS regime with an extension of an adaptive RC method. This chapter shows the proposed improved prediction for epileptic EEG signals compared with the linear regression model.

**Chapter 5** proposed a new method for EEG feature extraction. This chapter compares the performance of the proposed method with the FFT method and non-feature extracted studies. The feasibility of the proposed method is shown by measuring the accuracy and kappa value of MI-EEG classification.

**Chapter 6** draws the future works. We states and discusses the impact of novel findings of this thesis.

# 2

# RELATED WORKS

## 2.1 EEG MODELING

Computational models are at the junction of fundamental neuroscience and medical applications, allowing researchers to test hypotheses in silico and forecast the outcome of experiments and interactions that are extremely difficult in reality. However, the meaning of "computational model" is variously understood by researchers in various fields of neuroscience and psychology and hinders communication and collaborative research.

Over the last few decades, significant progress has been made in understanding brain function. Brain function is determined by how nerve cells are connected (the topology of nerve cell networks and the strength of synapses between nerve cells) and the intrinsic dynamics of the nerve cells that make up the brain. In general, information on the approximate course grain of the brain is obtained by inference from time-series measurements. EEG signals used to know the local state of the brain have been widely used in medical diagnosis and analysis because of their many advantages, such as non-invasiveness, low cost, high time resolution, and resistance to subject movement. Therefore, it is energetically studied to clarify the characteristics of this signal and to understand what kind of dynamic behavior of nerve cells produces the EEG signal. One of the biggest challenges of brain research, which also depends on EEG measurement, is understanding memory formation. The "bind hypothesis," in which perception occurs by synchronizing (binding) different brain cognitive and memory areas, is a specific research field of brain research that also depends on EEG measurement. Brain wave is the data obtained from several other methods. Thus, like data obtained from some other methods, brain wave data have network structures and neurons in the brain. Used to clarify the bonds that connect the strength of synapses. Modeling EEG signals is essential for understanding brain anatomy and tissue physiology and therefore supports the development of medical image analysis and neuroscience. However, consensus on the brain topology and synaptic mode is still an open question. On the other hand, the understanding of signals from the living brain is limited by

| Works | Sampling rate (Hz) | Period of prediction | Valuation |
|---|---|---|---|
| Autoregression model [26] | 500 | 100 ms | Phase locking value |
| Autoregression model [27] | 64 | 500 ms | Pearson correlation, mean square error |
| Artificial neural network and the combination of temporal and frequency of EEG [28] | 512 | 500 ms | Error measurement |
| Generalized linear model [29] | 50 | 5 ms | Number of spikes count prediction |

Table 2.1: Related work on the modeling and prediction of EEG signals.

non-invasive biological techniques. On the other hand, the method of estimating the connection structure of the brain from the measured values, such as EEG, can only roughly estimate the large-scale structure of the brain, and little knowledge about the connectivity of local clusters of neurons that generate EEG signals—not done.

Much research has been done on the simulation of neuron networks and the behavior of neuron networks as a function of bond strength and connection topology. Some studies have considered stochastic limit cycle oscillators to model EEG signals. Some studies also used a network of stochastic coupled nonlinear oscillators to describe dynamic units with Duffing oscillators or model with Jansen's one-column model [23, 24]. Probabilistic It was shown that the Duffing-van der Pol oscillator network model could capture important properties such as time-varying power spectra, Shannon entropy, and sample entropy of brain wave signals in healthy controls and patients with brain disorders. Recent studies have shown that EEG signals can be optimally modeled by a complex network of chaotic HR neurons that are weakly coupled and behave in a CAS state [5]. It suggests that weakly interacting chaotic neurons can generate brain activity. Therefore, we propose the idea that EEG signals can be successfully modeled and decomposed based on the chaotic signals generated by weakly connected neurons in a complex network. In a bibliographic study, [5] showed that a network of HR neurons could be configured to operate in the CAS region to produce data that best fits the EEG signal.

After a model for the EEG signal is proposed, one should attempt to validate it for future forecasts [25]. EEG signals are known to be high-dimensional, noisy, and difficult to forecast even for short time intervals. However, recent research approaches have shown promising results in the forecasting of these signals. as described in Table 2.1.

Our model follows the ideas outlined in Ref. [5]. Similarly, consider a network of weakly connected nonlinear oscillators to operate in the CAS region. However, a time series configured to be independent is used for the output function that models the brain waves. Details will be described later. Furthermore, we show that the signals generated by our model reproduce the main features of experimental EEG signals, such as the Fourier spectrum and Hurst index.

## 2.2 DYNAMIC FUNCTIONAL CONNECTIVITY OF EEG

The human brain is a complex network. These studies quantified the brain functional connectivity (FC) as the correlation between the time series of different regions across a whole scan without indicating the mediation of temporal covariation. They have a limitation in their ability to reveal this dynamic interplay. A growing number of studies have indicated that FC shows noticeable variation over a range of seconds to minutes, even in the resting state [30, 31]. This dynamic functional connectivity (dFC) exhibits highly structured spatiotemporal patterns in which a set of metastable FC patterns reliably reoccur across time and subjects. Recently, there are many studies considering dFC as a promising subfield [32–36]. Brain FC undergoes dynamics changes from the awake [37] to the unconscious.

DFC refers to the observed phenomenon that FC changes over short time. It is a recent expansion of traditional FC analysis which typically assumes that with several other mediums.

First, the FC refers the functionally integrated relationship between spatially separated brain regions. Unlike structure connectivity which looks for physical connections in the brain, FC is related to similar patterns of activation in difference brain regions regardless of the apparent physical connectedness of the regions. This type of connectivity was discovered in the mid-1990s and has been seen primarily using fMRI and Positron emission tomography. These methods assume the functional connections in the brain remain constant in a short time over a task of period of data collection.

However, in the mid-2000s, several studied examined the changes in FC often occur within the same individual and clearly relevant to the behavior. The dFC has now been investigated in a variety of different contexts with many analysis tools. Analysis of dFC has shown that far from being complete static, functional networks of the brain fluctuate on the scale of seconds to minutes.

The methodology to study dFC followed these steps.

- **Sliding window**

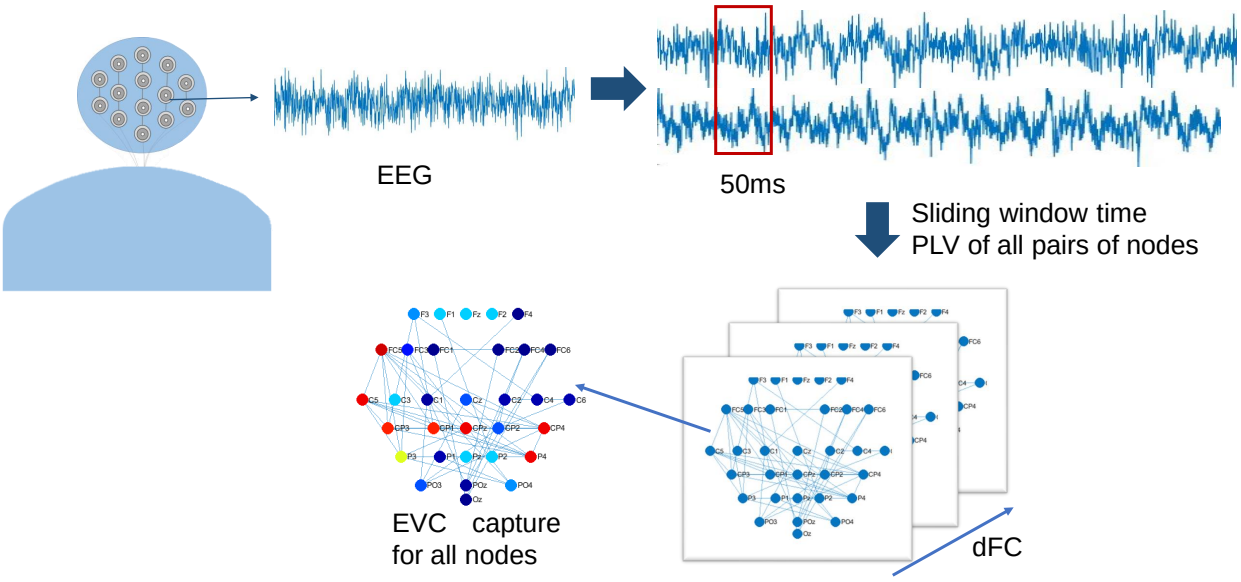


Figure 2.1: The dFC matrices are computed on windowed portions by PLV.

Sliding window analysis is performed by conducting analysis on a set of number of scans in a dataset. The number of scans is the length of sliding window. The movement of the window is usually referenced in terms of the degree of overlap between adjacent windows. One of principle benefits of sliding window analysis is that almost any steady state analysis can also be performed using sliding window if the window length is sufficiently large. It also has a benefit of being easy to understand and in some ways easier to interpret. In this study, the sliding window of 50 milliseconds is used (See Fig. 2.1).

- **Phase locking value**

The phase locking value (PLV) is a measure of the phase synchrony between two time-series, which has been previously applied to resting state connectivity analysis in MEG [38]. As pointed out by Lauchaux [39], phase locking analysis is particularly well-suited for connectivity analysis because it provides a measure of neuronal signal temporal relationships independent of their signal amplitude. In this thesis, we employs PLV as a measure of frequency-specific relationships between cortical regions. A FC metric known as PLV depends on the instantaneous phase of signals. The assumption is that if two brain regions are functional connected, the difference between the instantaneous phase of the signals from these regions should remain or less constant.

- **Eigenvector centrality**

The network analysis of brain connectivity was used to identify sets of regions that are critically important for enabling efficient neuronal signaling and communication. The eigenvector centrality (EVC) specify specifically weights nodes based on their degree of connection within the network. It does so by counting both the number and quality of links so that a node with few connections to some high-rank other nodes may outrank one with a larger number of mediocre contact [40]. Google's PageRank algorithm is a variant of EVC [41]. The EVC was introduced by Bonacich [42]. These produces establish undirected and weighted networks — the nodes defined as "hub" whose EVC are above or below the thresholds (Fig. 2.2). The mean EVC thresholds across subjects were calculated with the highest 10% [43].

Currently, there are many studies to examine how differences in dFC between different contexts relate to cognitive demands and behavioral performance [30, 44, 45]. Our analysis of dynamic functional connectivity follows these ideas. We employed a visuomotor coordination behavior approach to analyze the brain dFC. EEG data of three behavior tasks which had similar and different characteristics were used. The motion only had the same motion as tracking task and participant received the same sensory feedback as they were touching the haptic device. However, there were not any target on display; the participants did not have the visual feedback, versus from vision only task. Tracking task was the combination of mo-

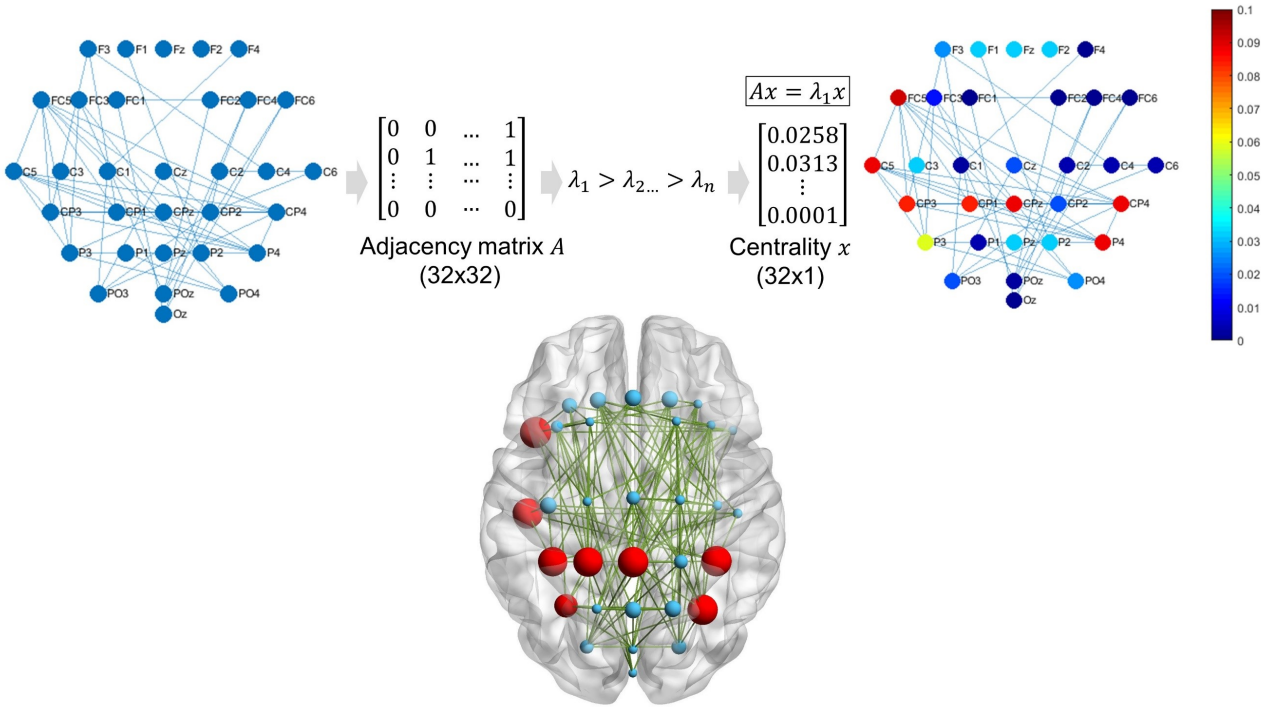


Figure 2.2: Mapping EVC values to electrodes. The red circle is the electrodes which has the high EVC level.

tion and vision. Hub represented for the channels which had high synchronization. Our result suggests that the hub of dFC patterns might remain the similarities and the differences of characteristics in visuomotor coordination behaviors. The most central brain regions are in the primary motor cortex. Synchronized activity in the primary cortex is modulated in the alpha, beta, and gamma frequency bands during various stages of movement planning and execution [46]. A significant difference is in superior parietal somatosensory association cortex. Motion only and tracking tasks have the hub in low-beta and gamma wave band at this region. While vision only and tracking only task have the hub in alpha wave band. A central role for pre-parietal flexible hubs in cognitive control of task demands [47]. That results show that the dFC patterns with hub feature represent the characteristic of brain at visuomotor coordination behavior [48].

## 2.3 EEG CLASSIFICATION

Categorization is predicting target variables or classes from a given input. To build a classification model, a learning algorithm is applied during the training phase to adjust the model's parameters. The same model is then used in the test phase to extract output. In the BCI system, features extracted by various feature extraction techniques are transformed into various motion picture tasks such as hand movement, leg movement, creating words, and be similar through classification algorithms. In a traditional neural network, weights have to be chosen very carefully. This is a significant obstacle to the efficient use of neural networks in many BCI applications. In recent studies, researchers have used the deep learning method because deep neural networks have high descriptive power and thus improve the accuracy of the system. Deep learning has been successful in computer vision and, in recent years, has also been applied in the classification of engine imaging tasks. Fig. 2.3 shows the category of the CNN method for EEG pattern classification.

Initially, Na Lu et al. propose an approach to use features that are manually extracted from FFT-based channels using deep belief network [50]. Among the various deep learning architectures, CNN is effectively used to classify motor imaging tasks due to its formalized structure and degree of immutability. CNN is a type of deep forwarding neural network that uses a variant of multilayer perceptrons. A simple CNN is a series of classes, and each CNN class converts one trigger amount to another through a distinguishable function. The CNN architecture consists of the input layer, convolutional layer, aggregate layer, fully connected layer, and the output layer. The convolutions class is the core building block of CNN and performs most of the computation. The pooled layer reduces the spatial size of the representation, and the neurons in the fully connected layer are fully connected to

the previous layer. Many studies proposed CNN architecture that uses dynamic energy based features for classifying multiclass MI EEG signals [51–53].

There is study proposed a parallel architecture using multi-layer MLP for static energy features and CNN for dynamic energy features with drop-out regularity [53]. The predictions from both networks are combined through averaging. The workframe significantly increases categorization accuracy compared to the supported vector machines. In Ref. [52] the author proposes an architecture that uses enhanced CSP to explore features. Energy features are arranged on a 2D matrix and CNN is then trained on this matrix to distinguish features.

Furthermore, the feature maps are selected using the post convolutional map selection algorithm. CNN was used to classify left and right motor images using a time frequency representation as an input. The author has proposed an architecture that uses CWT with wavelets and collisions to learn functionality [54]. Convolution 1D was performed in the convolution layer to analyze spectral features over time. The frame has achieved promising performance. More recently, CNN has been applied to classify multilayer engine image tasks using time representations. Another framework applied to multi-layer engine imaging tasks includes the temporal character extractor, the spatial feature extractor, and a generally learned classifier in an end- to-end. The framework uses convolutional classes that repeat and have shown acceptable performance.

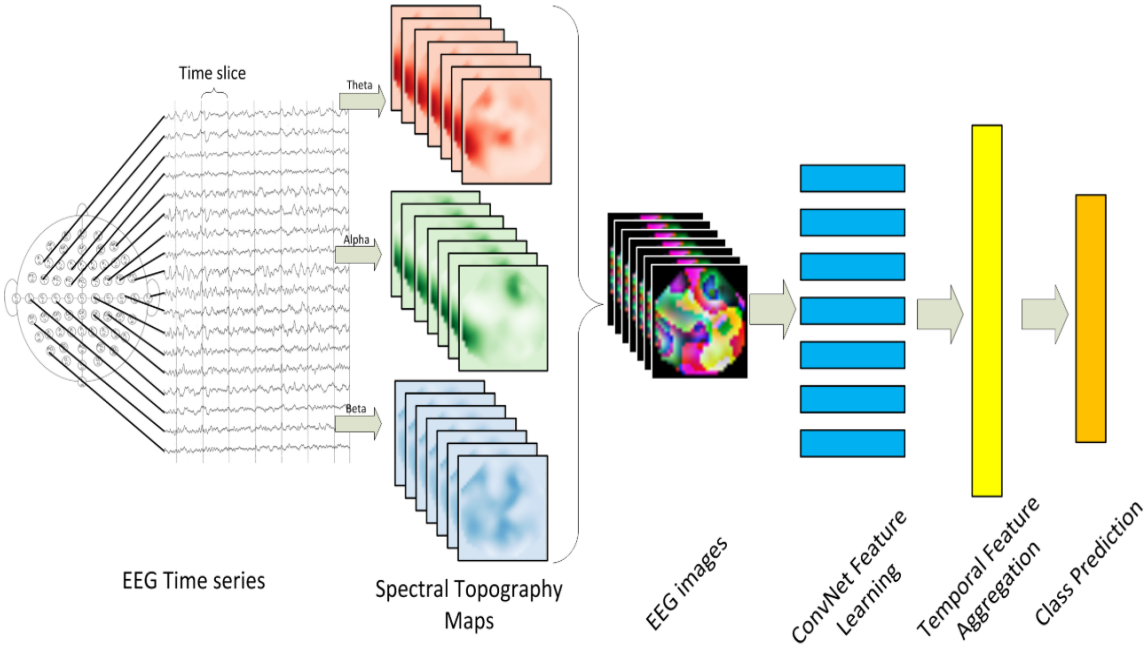


Figure 2.3: Overview of CNN approach [49].

# 3

# APPROACH FOR EEG MODELING

## 3.1 INTRODUCTION

One of the fundamental questions in neuroscience is how the activity of individual neurons represented by action potentials is combined to produce the collective dynamics observed at the population level that can be recorded by EEG. At the macro level, the neuronal network of the cerebral cortex can be modeled as a spatially continuous network that reproduces this same collective behavior, but its spatial resolution is limited to the specified one [55, 56]. However, an experimental constraint is that the activity of thousands, millions, or even billions of neurons cannot be measured to understand how cellular-level functions are transformed into macro-level functions [57]. To bridge this micro-macro gap, cell-level mathematical modeling plays an essential role in describing the activity of neurons [58–61].

EEG is a powerful non-invasive tool that can measure the macroscopic collective activity of the brain with higher time resolution and is widely used to understand the EEG of brain activity that correlates with cognitive function and motor regulation. Since EEG signals are complex, stochastic, non-linear, and non-stationary, applying classical time series analysis techniques is out of the question [62, 63].

Fourier analysis (finding the power spectrum or decomposing the signal into frequency components) is a classic method widely studied in the literature [64]. Other classic model-based techniques include AR, moving average (MA), auto-regressive moving average (ARMA), and auto-regressive fractional integrated moving average (ARFIMA) [26, 27, 65]. These methods focus on the analysis of signals in the time domain. Due to interest in machine learning methods, the modeling of EEG signals using a nerve cell model has attracted attention [66]. Fourier analysis was widely used to analyze EEG signals, and a phenomenon called event-related desynchronization/synchronization was discovered [67, 68]. Fourier analysis is the concept of Fourier series based on the assumption that functions that satisfy the general Dirichlet condition are represented as the sum of trigonometric functions. Therefore, a signal in the time domain can be decomposed into its frequency modes, and as the number of modes increases, the quality of the reconstructable

signal improves. Since nonlinear and unsteady signals also satisfy the Dirichlet conditions, it is plausible to study EEG signals by Fourier decomposition, at least from a mathematical point of view. However, the debate has continued whether it is appropriate to decompose non-stationary solid signals such as EEG [69]. Also, EEG should not be made from the sum of never-changing periodic signals that oscillate in such a static Fourier frequency mode distribution.

This chapter shows that the optimal method for reconstructing EEG signals from a complex oscillator network is to construct an output function (weighted average signal of action potentials of multiple neurons) that considers only orthogonal signals. Using this method, we show that the time-series orthogonal sets produced by the complex networks of both HR [70] and Kuramoto oscillators [71] minimize the error function for fitting EEG data under several conditions. Recently, the CAS phenomenon was introduced to model how spatial and temporal patterns emerge from complex networks in which neurons interact with small bond strengths. [72]. The CAS phenomenon appears when a number of individual neurons experience a near-constant local mean-field from other connected neurons. The HR network operating in the CAS region effectively models EEG signals. However, in this study, instead of constructing an EEG model from a time series collected from randomly selected neurons in a neuron network, a compressed set of independent vectors is generated by Principal Component Analysis (PCA) from the entire collection of data generated by the network. It is shown that the discrepancy between the measured value and the estimated value in the model can be significantly reduced by using. It is also shown that it is not necessary to rely on the network of the neuron model for modeling the EEG data, and it is possible to use the network formed by the coupling of the Kuramoto phase oscillators. Furthermore, the optimal model for predicting EEG signals is obtained when the oscillator is weakly coupled and shows that the existing condition of the CAS region is satisfied, supporting the results of Ref. [5]. Furthermore, we show that our model can reproduce and predict the EEG signals of healthy subjects and epilepsy patients and that the characteristics, Hurst index, and power spectrum of experimental EEG signals can be reproduced.

## 3.2 INTRODUCTION OF CAS PHENOMENON

### 3.2.1 *CAS phenomenon in network*

Consider a network of $N$ nodes, as described by

$$\dot{x}_i = \mathrm{F}_i\left(x_i\right) + \sigma \sum_{j=1}^{N} \mathbf{K}_{ij} \mathrm{E}\left[\mathrm{H}\left(x_j - x_i\right)\right], \tag{3.1}$$

where $x_i \in \mathbb{R}^d$ is a $d$-dimensional vector describing the state variables of node $i$, $F_i$ is the $d$-dimensional vector function representing the dynamical system of node $i$, $\mathbf{K}_{ij}$ is the adjacent connection matrix, and $E$ is the coupling function. Here, $H$ is an arbitrary differential transformation. Assume in the HR model that $H(x_j) = x_j - x_i$. For the Kuramoto model, $H(x_j) = \sin(x_j - x_i)$ is a nonlinear function, which is an extension of the analysis. If the $x_i$ is the variable of neuron $i$, the local mean field of node $i$ is defined as

$$\bar{x}_i\left(t\right) = \frac{1}{k_i} \sum_j \mathbf{K}_{ij} x_j. \tag{3.2}$$

Complete synchronization appears when $x_i = x_j = \bar{x}_i$ for all times when isolated from the network. For heterogeneity, one expects to find other weaker forms of synchronization behavior. CAS is a phenomenon that appears in a complex network that produces a weaker form of synchronization [72]. In this phenomenon, nodes are in weak interaction (weak coupling strength) and behave independently. The local cluster of neurons has roughly constant local mean fields. The CAS pattern is a solution of a simplified set of equations describing the network when $\bar{x}_i = C_i$. The expected value of the local mean field is defined as

$$C_i = \lim_{t \to \infty} \int \bar{x}_i\left(t\right) dt. \tag{3.3}$$

The following are the two criteria for node $i$ to present the CAS phenomenon (See Fig.3.1):

- **Criterion 1.** The central limit theorem can be applied. Therefore, the larger the degree of a node, the smaller the variation in the local mean field.
- **Criterion 2.** The CAS pattern describes a stable periodic orbit.

In this study, the HR neurons and Kuramoto oscillator were used to model the EEG signal.

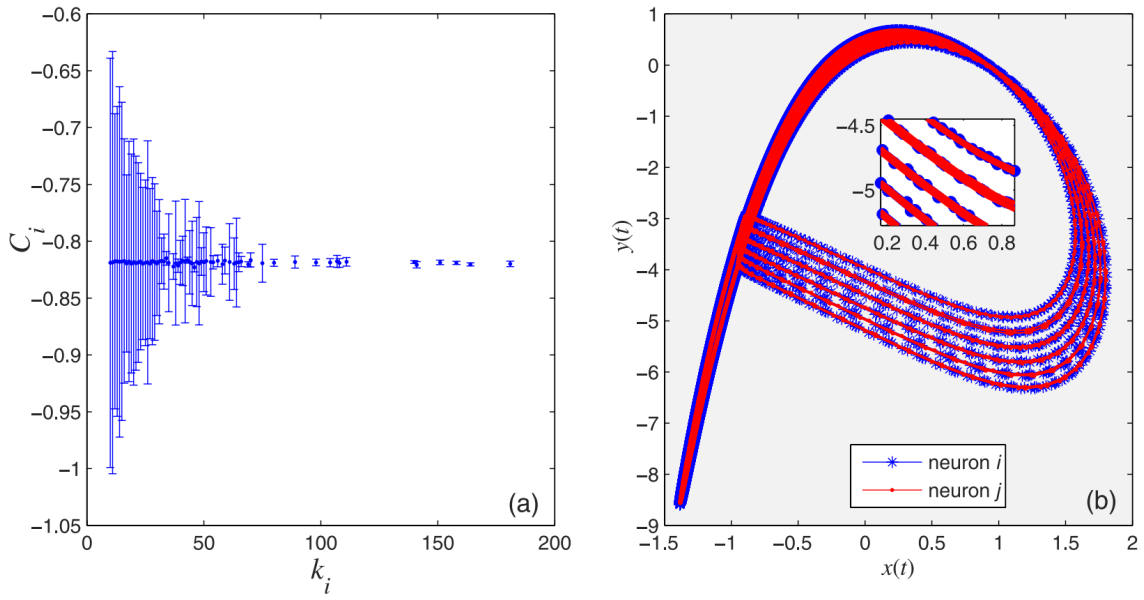


Figure 3.1: The two criteria for the existence of the CAS phenomenon.

### 3.2.2 *CAS phenomenon in HR network*

The HR neuron model is a well-known model for describing the patterned activity seen in neurons. The electrical synapses can be considered as follows:

$$\begin{cases} \dot{x}_i = y_i - ax_i^3 + bx_i^2 - z_i + \mathrm{I}_{ext} + \sigma \sum_{j=1}^{N} \mathbf{K}_{ij} \mathrm{H}\left(x_j\right) \\ \dot{y}_i = c - dx_i^2 - y_i \\ \dot{z}_i = -rz_i + sr\left(x_i + x_0\right), \end{cases} \tag{3.4}$$

where $(x_i, y_i, z_i) \in \mathbb{R}^3$ are the state variables of the neuron $i$, $i = 1 : N$. Here, $N$ is the number of neurons in the network. The parameters were selected as $a = 1$, $b = 3$, $c = 1$, $d = 5$, $s = 4$, $r = 0.005$, $x_0 = 1.618$, and $\mathrm{I}_{ext} = 3.25$, yield the HR neurons model to exhibit a multi-time-scale chaotic behavior characterized by spiking bursting. We use $\sigma$ to denote the electrical coupling strength. Simulations were performed using Matlab Simulink. The CAS patterns of node $i$ are described by

$$\begin{cases} \dot{\Xi}_{x_i} = \Xi_{y_i} - a\Xi_{x_i}^3 + b\Xi_{x_i}^2 - \Xi_{z_i} - R\Xi_{xi} + Q_i \\ \dot{\Xi}_{y_i} = c - d\Xi_{x_i}^2 - \Xi_{y_i} \\ \dot{\Xi}_{z_i} = -r\Xi_{z_i} + sr\left(\Xi_{x_i} + x_0\right), \end{cases} \tag{3.5}$$

where $R_i = p_i$, $Q_i = p_i C_i$, $p_i = \sigma k_i$ and $C_i \approx (1/k_i) \sum_{j=1}^{N} \mathbf{K}_{ij} x_j$. To illustrate the presence of the CAS phenomenon, we considered a random network formed by $N = 1000$ neurons.

### 3.2.3 *CAS phenomenon in Kuramoto oscillators*

The Kuramoto model was used to simulate brain interactions through synchrony on the basis of structural and functional implications of the organization of brain connectivity. The dynamics of node $i$ are described by

$$\dot{\theta}_i = \omega_i + p_i \tilde{r}_i \sin\left(\bar{\theta}_i - \theta_i\right), \tag{3.6}$$

where $p = 0.01$ is the probability that each two nodes are connected and $\omega_i$ is the natural frequency of node $i$ selected randomly from $[-\pi, \pi]$. Here, $\tilde{r}_i$ is the coupling strength of node $i$. The CAS patterns of node $i$ are described by

$$\dot{\Xi}_i = \omega_i + p_i \tilde{r}_i \sin\left(C_i - \Xi_i\right). \tag{3.7}$$

Eq. (3.7) describes a periodic orbit regardless of the values of parameters $\omega$, $p_i$ and $\tilde{r}$ because it is an autonomous two-dimensional system; chaos cannot exist [72]. Therefore, **criterion 2** is always satisfied in Kuramoto oscillators.

## 3.3 EXPERIMENT

Our model for the EEG was developed on a trained output from an autonomous dynamical complex network, set to operate in the CAS regime. We consider two topologies, random and small-world, and two systems for the node dynamical behavior: HR neurons and phase oscillators. We assume that this network has $N$ nodes. The HR networks are described by the system of ordinary differential equations (ODEs) in Eq. (5.5), and the Kuramoto-like phase oscillator networks are described by Eq. (3.6). Neurons in the HR network were coupled electrically with a strength given by $\sigma$, and each node in the Kuramoto-like network experiences a coupling strength of $\tilde{r}_i$, describing its dynamics coupled to the mean field.

Our networks have $N = 1000$ nodes, and we collect a time series from each node with $m = 3000$ data points. With these time series, we construct the matrix $X^* \in \mathbb{R}^{m \times N}$, where each column is a time series of length $m$ from a node. The dimensionality of this matrix is reduced using singular value decomposition (SVD) to produce a matrix $X \in \mathbb{R}^{m \times n}$ ($n < N$) with $n$ orthogonal columns and still contains 99% of the total variation of the original matrix, preserving 99% of all

the information of the original matrix. Here, $n$ is the number of retained principal components of $X^*$. This is accomplished using Eq. (3.19). This percentage of the total information was selected by optimizing the quality of our model.

Using $b_0$ to represent the experimental EEG time series, our network CAS-based EEG model of this experimental signal is denoted by $Y$, which is calculated using Eq. (3.11), where $Y \in \mathbb{R}^{(t_m - t_1)\times 1}$ constructed for the sample interval $[t_1, t_f]$ and $X \in \mathbb{R}^{(t_m - t_1)\times n}$ represents the reduced matrix obtained by Eq. (3.19). $a_0$ represents the vector of the coefficients trained by Eq. (3.10) and used to produce the output function of the network modeling the EEG signal. The sample interval $[t_1, t_m]$ is an EEG time-series interval $[1, 3000]$, and $[t_1, t_f]$ is the trained interval $[1, 2000]$.

The proposed model was applied to predict EEG signals in 5 datasets. The evaluation of the model was performed by comparing the experimental EEG signals in the "test data" time window (last 1000 data points) with the EEG predicted from the model. Regression models are used to predict brain waves, and this process is algebraic. Each HEG signal is only predicted using its information. The question is how to choose the time interval for the initial or "learning" data. In the data set used this time, by setting the time interval for calculating the coefficient to 2000 points, overfitting was avoided, and stable results could be obtained. Furthermore, to evaluate our model's performance, we considered four configurations of random HR, small world HR, random Kuramoto, and small world Kuramoto model, and the Hurst index (related to long-range correlation) of the experimental EEG data set. The power spectrum was compared with that obtained from our model.

The random network was generated by the Gilbert random graph method. Notated as G (1000; 0.01), all possible edges are generated independently with a probability of $p = 0.01$. The Watts–Strogatz network generation method was used for the small-world network, and the rewiring probability was equalized to $p = 0.01$. Both networks have an average degree of 10. Examples of network characteristics such as small world degree, average path length, and clustering coefficient were $(0.0304, 3.2632, 0.0098)$ for random networks and $(8.0536, 19.3226, 0.6622)$ for small-world networks.

The Fig. 3.2 shows the outline of the method adopted in this study. The figure on the left is a snapshot plot of the network configuration and its operation. The upper row is an example of the two network topologies examined, the random network and the small-world network. Each node has dynamics that can be described by an HR neuron or a Kuramoto phase oscillator. The network is simulated with a bond strength of $\sigma \in [0, 1.2]$. The figure below shows three network snapshots consisting of $N = 1000$ nodes and 3000 simulation trajectories with different bond strengths. The higher the bond strength, the more coherent patterns appear, and it is thought that such a configuration should be avoided for performance modeling.

The figure on the right shows how we built a model and used it to predict EEG data. In the figure above, the dashed box is the time window for the first 2000 points of EEG data ($b$) and the last 1000 points of test data (not used during the training phase of the model). The EEG signal and the $X$ generated by the dynamic network were split into training and test data. Before applying the prediction method, the measured signal of the dynamic network was reduced by SVD. The upper blue insertion frame is the calculation of the $a_0$ coefficient (Eq. (3.10)), and the lower blue insertion frame is the state where the predicted EEG signal is generated using this learned coefficient vector (Eq. (3.11)) is shown. The two figures below show EEG test data and predicted EEG signals (generated by Eq. (3.11).

### 3.3.1 *Simulation of the neuronal networks to predict a given series of EEG signals*

As an overall flow, HR neurons or Kuramoto oscillators were implemented in each node, and random or small-world networks were generated for neuronal networks. To test this hypothesis, we verified the types of neurons and network structures in the predicting regime (Fig. 3.2). The connectivity matrix $\mathbf{K}$ defines the weightings of the synaptic connections between neurons, defined by the electrical coupling strength $\sigma$. The neuron networks are obtained with $\sigma$ in the range from 0 to 1.2. The connections $\mathbf{K}$ are generated with random and small-world 1000-node networks. The median node degree is 10. A total of 3000 neurons were simulated using the Brain Dynamics Toolbox for HR neurons and Kuramoto oscillators [73]. Then, the local mean field $C$ of each node is calculated using Eq. (5.3), and $C$ are plugged into the differential equation to obtain the CAS pattern. For the HR model, we used $X = \{x_i\}_{i\in 1:1000}$ as a matrix composed of membrane potentials of the simulated neurons. For the Kuramoto model, we used the matrix $X = \{\theta_i\}_{i\in 1:1000}$ as a combination of neuron oscillations. Finally, using the matrix $\mathbf{X}(t)$ defined in Eq. (3.8), each $3000 \times 1000$ neuron network is reduced by using the PCA method. The dimensionally reduced matrix maintains 99% of the information of the original matrix. Training datasets of the EEG signals were used to determine the weight values of the individual neurons to fit the EEG signals as a function of time.

### 3.3.2 *CAS-network-based model for EEG signals*

To model the EEG signals, we used the property of linear algebra. Given an unknown vector $a \in \mathbb{R}^{n\times 1}$ of trained coefficients, a known matrix $\mathbf{X} \in \mathbb{R}^{m\times n}$ obtained using the methods to be further explained but are a function of measurements obtained from the dynamical network (where $m$ denotes the number of measure-

ments obtained or the discrete time interval), and a known vector $b \in \mathbb{R}^{m\times 1}$ (which is set to be equal to an EEG signal), the following equation

$$Xa = b, \tag{3.8}$$

has a unique solution by using least square method[74]

$$a = X^{+}b. \tag{3.9}$$

Here, $X^{+} \in \mathbb{R}^{n\times m}$ is the Moore–Penrose pseudoinverse of matrix $X$.

Given a training set of data from the EEG signals, denoted by $b_0$, we calculated the trained coefficients $a_0$ using

$$a_0 = X^{+}b_0. \tag{3.10}$$

Our CAS-network-based model for the EEG whose training set is $b_0$ is thus expressed as follows:

$$Y = Xa_0, \tag{3.11}$$

where $Y \in \mathbb{R}^{(t_m - t_1)\times 1}$ is our EEG model for a time interval of $t_m - t_1$, $X \in \mathbb{R}^{(t_m - t_1)\times n}$ is a matrix constructed from the dynamical network by taking $(t_m - t_1)$ observations, and $a_0$ the vector of coefficients trained by Eq. (3.10).

To validate our model, we calculated the Mean Absolute Error (MAE) function, which measures the averaged difference between the modeled EEG signal and the actual EEG signal denoted by $e \in \mathbb{R}^{(t_m - t_1)\times 1}$:

$$MAE = \frac{\sum_{t=t_f+1}^{t_m} |e_t - Y_t|}{(t_m - t_f)}. \tag{3.12}$$

### 3.3.3 *Dimension reduction of $X^* \in \mathbb{R}^{m\times N}$ by PCA*

Define $X^* \in \mathbb{R}^{m\times N}$ as the matrix that contains full information about the dynamical network operating in the CAS regime. Every row is a time series of values obtained from a node of the network, and the entire network is set with a total of $N$ nodes.

The matrix $X^*$ can be factorized using SVD

$$X^* = U\Sigma V^T, \tag{3.13}$$

where $K \leq \{m, N\}$ is the rank of matrix $X^*$ and $\sigma_1 \geq \sigma_2 \geq \cdots \geq \sigma_K$, with $\sigma_i = \Sigma_{ii}$ are the singular values of $X^*$. Here, $\Sigma \in \mathbb{R}^{m \times N}$. $U \in \mathbb{R}^{m \times m}$ is the left singular vector, and $V \in \mathbb{R}^{N \times N}$ is the right singular vector of $X^*$.

The eigenvector with the highest eigenvalue is the principal component of $X^*$. In fact, the eigenvector with the largest eigenvalue represents the most significant relationship between the dimensions. An approximate compact matrix can be constructed with a specific rank $k$ such that $k < K$, whose singular values only contain the $k$ largest singular values of $X^*$. Using this approach, the matrix $X^*$ can be approximated by

$$X^* \approx X_k = U_k \Sigma_k \left(V_k\right)^T. \tag{3.14}$$

Matrix $U_k \in \mathbb{R}^{m \times k}$, $\Sigma_k \in \mathbb{R}^{k \times k}$, and $V_k^T \in \mathbb{R}^{k \times N}$. Making the definition

$$U = (u_1\ u_2\ u_3 \ldots u_k) \text{ and } V = (v_1\ v_2\ v_3\ \ldots\ v_k), \tag{3.15}$$

we can write that

$$X_k = \sum_i^k \sigma_i u_i v_i^T. \tag{3.16}$$

The standard measure of the quality of $X_k$ is the proportion of total variance, which is defined by the Frobenius norm of the difference between two matrices:

$$\frac{\|X_k\|_F^2}{\|X^*\|_F^2} = \frac{\sum_{i=1}^k \sigma_i^2}{\sum_{i=1}^K \sigma_i^2}. \tag{3.17}$$

Thus, the proportion of the total variance is higher if $k$ is larger. This is an important theorem that helps determine the matrix approximation based on the amount of information required. Therefore, we want to maintain at least 99% of the information of $X^*$ and selected the smallest $k$ such that

$$\frac{\sum_{i=1}^k \sigma_i^2}{\sum_{i=1}^K \sigma_i^2} = 99\%. \tag{3.18}$$

Suppose that $n$ is the value of $k$ such that the proportion of total variance is equal to 99%. The truncated $m \times n$ of matrix $X$ can be obtained by considering only the first $n$ largest singular values and their singular vectors [75, 76]:

$$X_{m \times n} = U_{m \times n} * \Sigma_{n \times n} = X^* * V_{N \times n}, \tag{3.19}$$

where $V_{N\times n}$ is the $n$ first columns of $V$. These $n$ vectors in $X_{m\times n}$ are called the principal components that are linearly uncorrelated and have 99% variance with $X^*$.

### 3.3.4 *Hurst exponent*

Let a single EEG signal to be represented by $e \in \mathbb{R}^{(t_m - t_f)\times 1}$, with $e = \{e_1, e_2, \ldots, e_n\}$, with $n = t_m - t_f = 1000$, which is the time interval considered in our study. The average value of $e$ is denoted by $\mathbb{E}(e)$.

Defining the adjusted range as

$$R(n) = max(0, w_1, w_2, \ldots, w_n) - min(0, w_1, w_2, \ldots, w_n), \tag{3.20}$$

where for each $k \in [1 : n]$, $w_k = \sum_{j=1}^{k} \left(e_j - k\mathbb{E}(e)\right)$, then the Hurst exponent is defined by finding the scaling that fits to

$$\frac{R(n)}{S(n)} \sim cn^H \tag{3.21}$$

with $S(n)$ representing the standard deviation of $e$. An estimation of the Hurst exponent adopted in this work can be calculated by using a rescaled range formula [77]: $\frac{R(n)}{S(n)} \sim \left(2^{(2H-1)} - 1\right) n^H$.

## 3.4 RESULTS

Our model was constructed considering both EEG signals in healthy and epileptic patients. Previous studies have shown that output functions constructed from the average of time series weights (" trained") collected from randomly selected neurons can reproduce EEG signals well in networks operating in the CAS region. Specific neurons in the network operating in the CAS region behave as if they have a weak correlation. Therefore, a time series in which neurons in such a network were randomly selected and collected is likely to form a set of almost independent time series ("orthogonal"). This study proposes a new strategy to select neurons that make up the weighted output function, based in part on this principle. In this study, PCA was used to determine the collection of orthogonal neurons as a function of time (see Methodology for details). PCA is a well-known tool that can reduce the dimensions of a dataset of correlated variables while preserving most information.

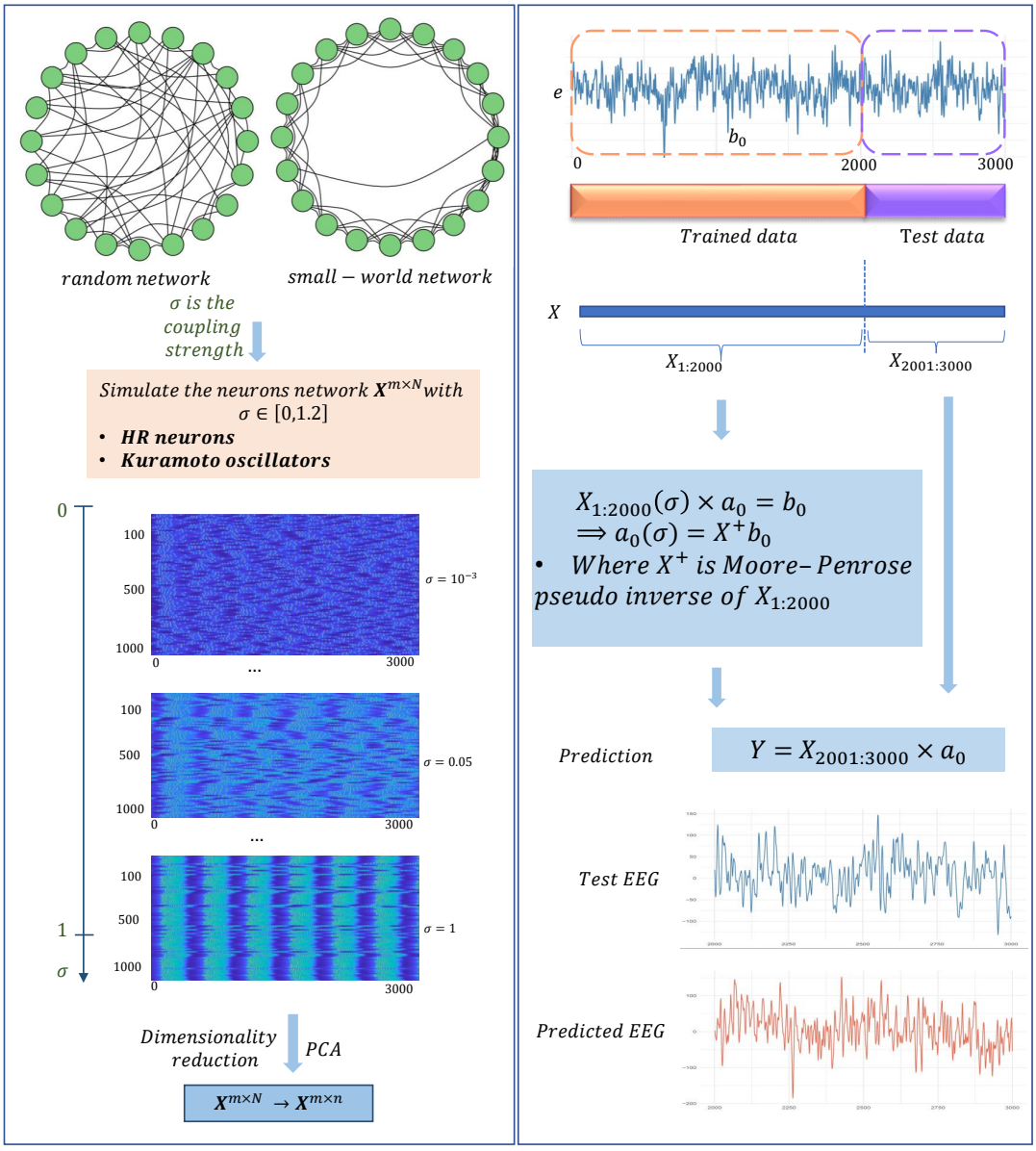


Figure 3.2: Overview of proposed method with dynamical networks and two types of topology.

### 3.4.1 *Comparison of methods to generate X*

The local mean field of the neuron depends on the coupling strength $\sigma$. Therefore, the value of $\sigma$ was tuned from 0 to 1.2 to find the CAS regime. In this regime, we found that $\sigma \leq \sigma^{CAS}$, where $\sigma^{CAS} \cong 0.001$ for all HR and Kuramoto models. The CAS phenomenon exists when a node has an approximately constant local mean field. If the equation for the CAS pattern presents the coexistence of attractors, nodes are still in a CAS state if the CAS condition is satisfied. Fig. 3.3a shows the

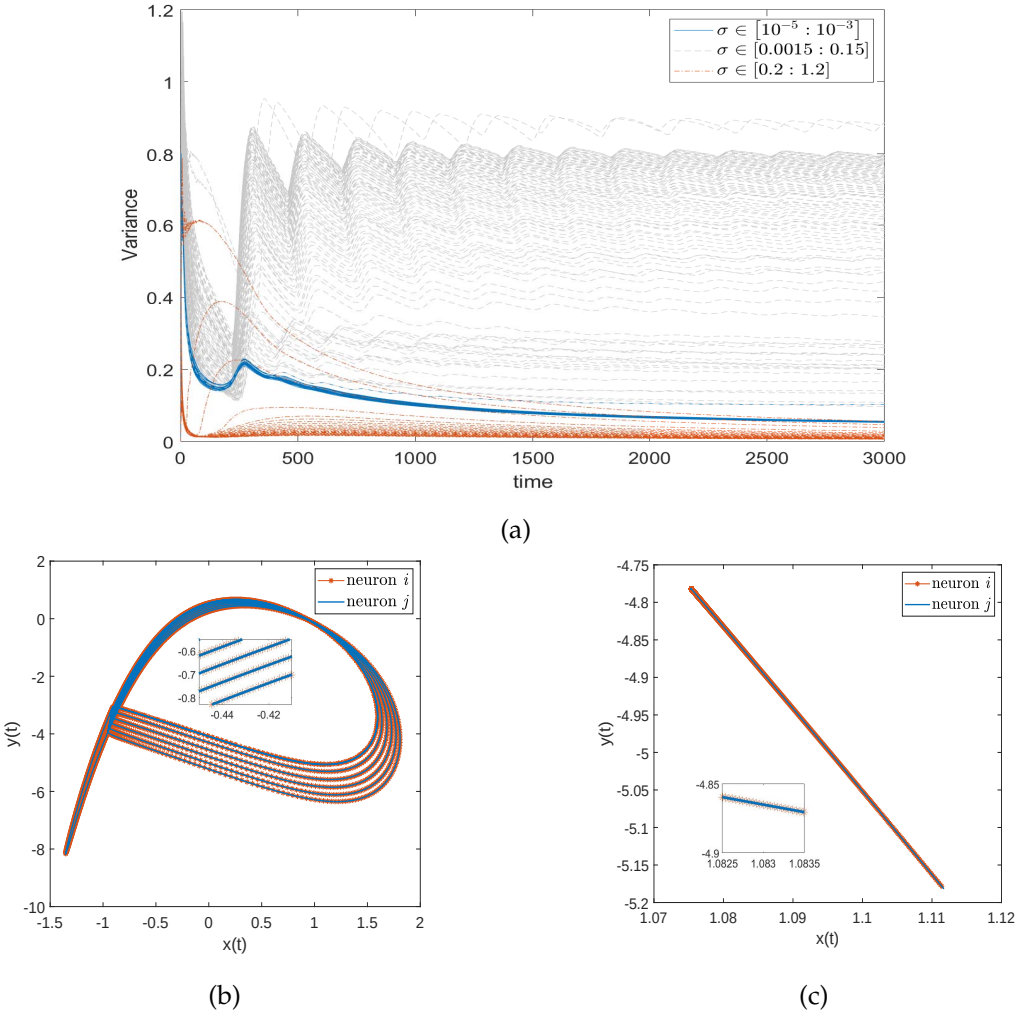


Figure 3.3: Results validating the two criteria for the HR neurons to exhibit the CAS pattern.

variances of the local mean field at every time point. In particular, the variance of the local mean field of neuron $i$ at time point $t$ is calculated as follows:

$$Variance_i\,(t) = Var\,(\{\bar{x}_i\}_t) \tag{3.22}$$

where $\{\bar{x}_i\}_t$ is the vector of the local mean field from the starting time point to time point $t$. As time increases, the blue lines show that the variance values of the nodes of the weakly coupled network converge to 0 (**criterion 1**). The variances of the nodes of the strongly coupled network are still high (gray lines). For the coupling strength in $[0.2 : 1.2]$, the variances also converge to 0 (the red lines). However, Fig. 3.3c shows these neurons are not a stable periodic orbit. In Fig. 3.3b, the CAS pattern of coupling strength $\sigma = 0.001$ described a stable periodic orbit (**criterion 2**).

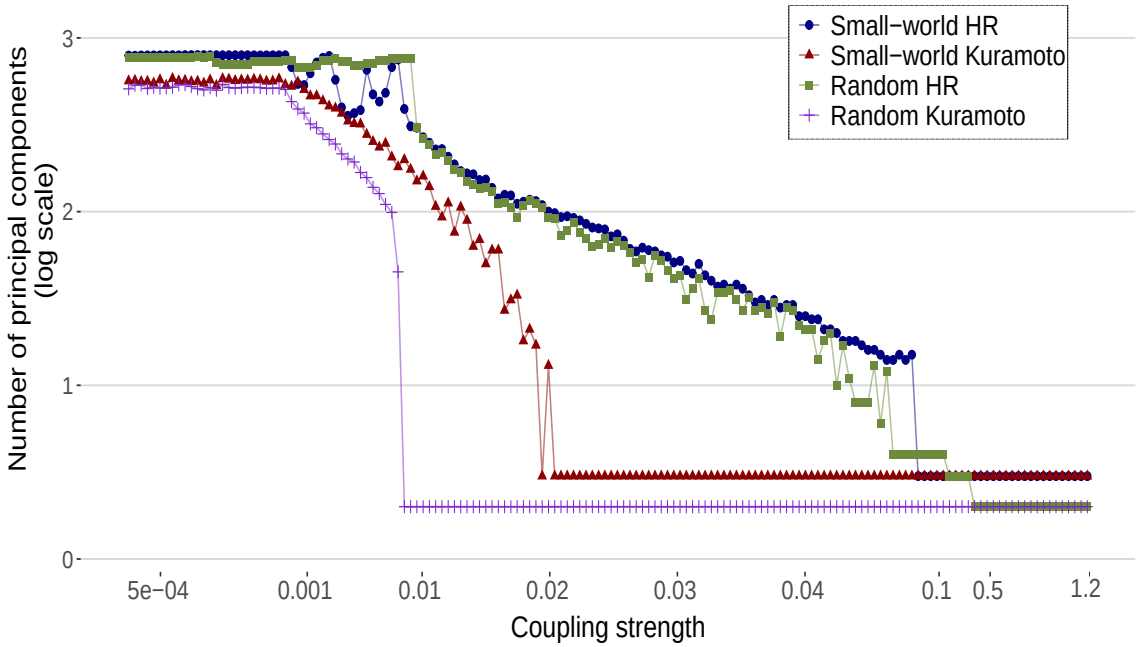


Figure 3.4: Number of principal components $n$ that were retained as a function of the coupling strength $\sigma$ to maintain 99% of the total variance, as in Eq. (4.2).

Our proposed method to generate the matrix $X$ is based on reduction using PCA. We considered the matrix $X \in \mathbb{R}^{m\times N}$ for the entire network simulated considering all $m = 1000$ nodes. Then, we reduced it to $X \in \mathbb{R}^{m\times n}$ using PCA. The new matrices contained the $n$ principal components, which were constructed as mixtures of the initial networks. These principal components are uncorrelated.

Understanding how the coupling strength changes behavior in the network and how this affects the ability of PCA is important to reduce the dimension. Figure 3.4 shows the relation between the coupling strength value and the number of retained principal components for all network models to maintain 99% of the total variance.

The coupling strengths of networks that produced the smallest fitting error were selected to generate the matrix $X$ from which we calculated the predicted EEG signal. These values of $\sigma$ are smaller than 0.001 for both the HR model and the random Kuramoto model.

To justify the novelty of the proposed approach, we compare it with the method proposed in Ref. [5], in which the nodes of the HR network considered to construct the reduced matrix $X \in \mathbb{R}^{m\times n}$ are selected randomly.

The value of $\sigma$ was chosen by minimizing the value of the MAE in Eq. (3.12); thus, it is the coupling that creates behavior such that our model fits the best EEG signals. The values of $\sigma$ obtained for all our network models were within the interval determined in which the CAS phenomenon existed, so $\sigma \leq \sigma^{CAS}$.

For comparison, the MAEs of the two methods were compared using 100 channels of dataset A (healthy individuals with closed eyes). The results are shown in Fig. 3.5. Both methods fit the EEG signals well. However, as demonstrated by the distribution of the error in Fig. 3.5c, our proposed method can fit EEG signals with more than twice the accuracy (Wilcoxon test, two-tailed $p$-value $< 0.01$).

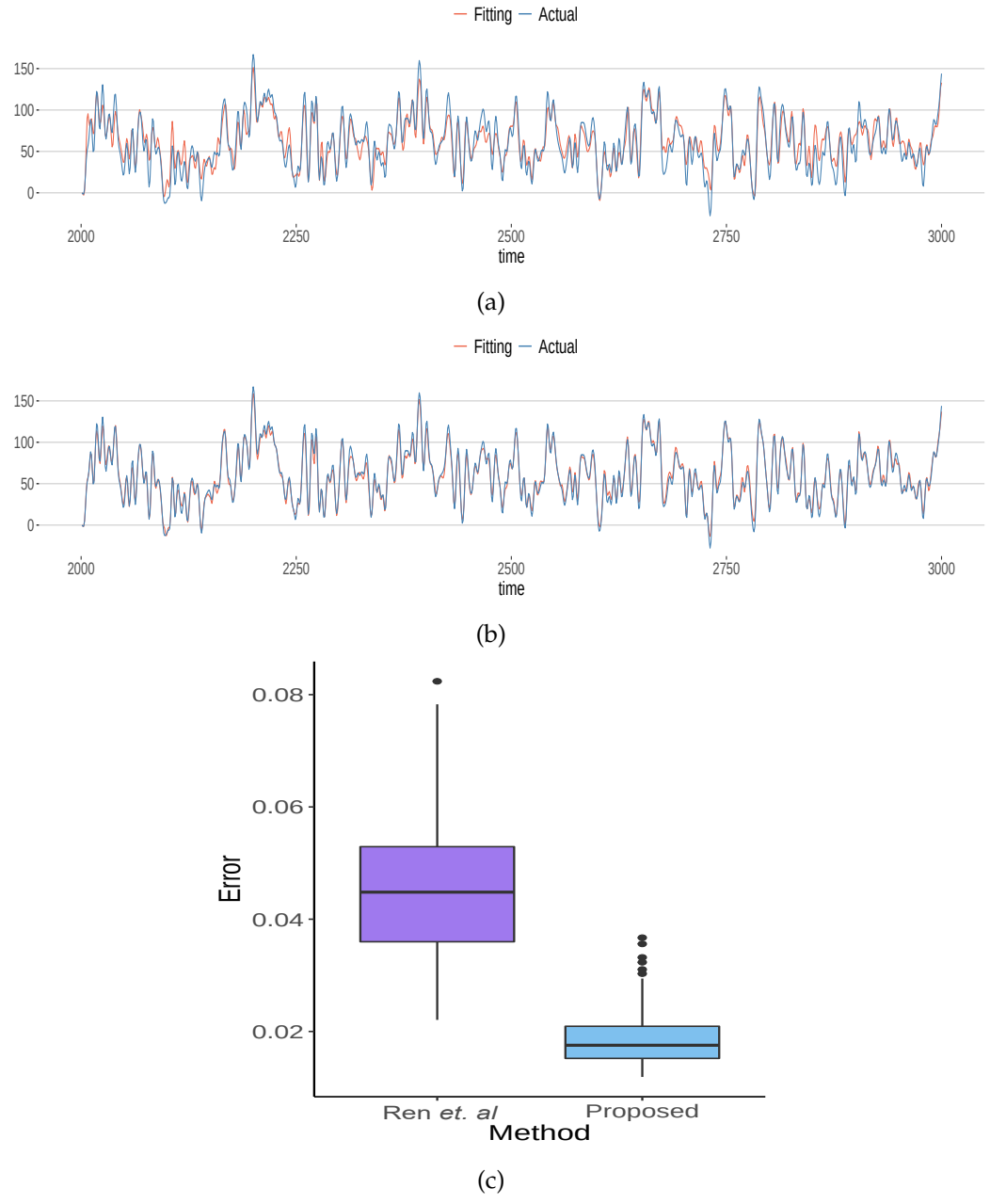


Figure 3.5: Comparison of the efficiency to model the EEG signals between the method being proposed in this work and that in Ref. [5] to model EEG signals.

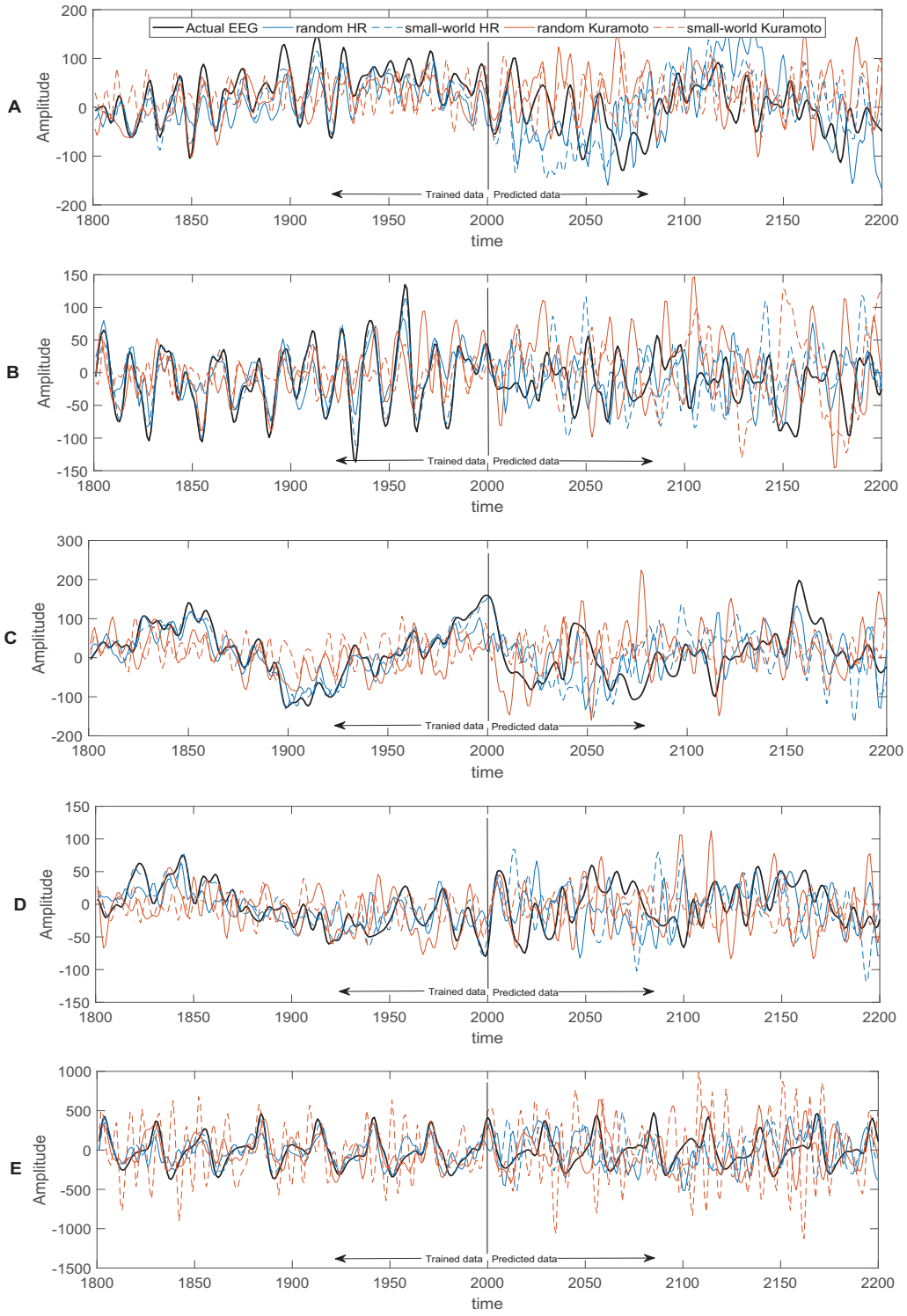


Figure 3.6: EEG data obtained experimentally, training and prediction of five datasets: A, B, C, D, and E

### 3.4.2 *Validation of the two different neuronal models*

This study used an open-source database from Bonn University: A (closed eyes, healthy records), B (opened eyes, healthy records), C and D (seizure-free interval,

epileptic records), and E (during seizure activity, epileptic records) [78]. From the five participants for each set, the EEG recordings were obtained using the 10–20 international electrode positioning system. Each set consisted of 100 single-channel EEGs under a sampling rate of 173.61 Hz. The datasets were band-pass filtered (0.5–30 Hz, EEGLAB embedded Fourier infrared (FIR) filter). In this study, 3000 sampling points collected over approximately 17.28 s were used. The first 2000 points were training data and the last 1000 points were predicted data.

A sequence of network configurations was considered, with coupling strength varying within the range of $\sigma \in [0, 1.2]$. For a given 2000 sampling points over approximately 11.52 s for a single channel, the weighted parameters of the proposed model were calculated using Eq. (3.9). Then, MAE values between the EEG signals and the reconstructed EEG signals based on our proposed model approach were calculated using Eq. (3.12). The predicted signal shown is generated be considering a network whose coupling strength $\sigma$ minimizes the MAE function.

Figure 3.6 shows several representative single-trial predictions that are used as a typical example from datasets of four models, considering different network configurations, particularly different topologies, with various dynamical units and for a range of values for $\sigma$. These trials demonstrate that random and small-world HR networks (Fig. 3.6 (A, B, C)) and the random Kuramoto network (Fig. 3.6 (D, E)) allow for a predictive signal that can accurately capture the general underlying trend of the data. In particular, the reconstructed EEG signal for the random Kuramoto network can capture prominent peaks in the power spectra (Fig. 3.6 (E)). The EEG reconstructions that use the small-world Kuramoto networks had the worst modeling performance; that is, they could not capture the general trend and the frequency spectral component of the EEG signal (Fig. 3.6 (E)).

In addition to conducting an error analysis of our predicted EEG signal, we evaluated our modeling approach by checking whether the generated EEG signals in the predicting regime could reproduce the characteristic features of the power spectrum (comparing similarities with the EEG signals in the frequency domain) and the Hurst exponent (comparing similarities with the EEG signals in the long-term correlations).

### 3.4.3 *Error analysis of the predicted EEG signal*

The average error scores computed using the MAE quantity in Eq. (3.12) for the different prediction models are presented in Table 3.1. Owing to the differences in range between the five datasets, the MAE was divided by the range of EEG signal to obtain the ratio. We found that the MAE ratio values obtained from the

different datasets do not differ much for the EEG signals predicted by our four network models.

To further evaluate the efficacy of our predicted EEG signal in modeling real EEG signals, we considered standard deviations of the MAE ratio values. The results are listed in the MAE part of Table 3.1. Set A was best modeled by the small-world Kuramoto network ($10.97 \pm 40.05\%$), set B by the random HR ($7.82 \pm 15.90\%$) and small-world Kuramoto ($7.95 \pm 15.98\%$) networks, set C by the random HR network ($7.95 \pm 6.69\%$), set D by the small-world HR network ($8.17 \pm 7.48\%$), and set E by the random Kuramoto network ($11.21 \pm 23.89\%$). We note that the epileptic EEG signals (sets C and D, 7.95% and 8.17%, respectively) have smaller prediction errors than the healthy EEG signals (set A, 10.97%) with closed eyes and comparable performance with healthy subjects with closed eyes. Data from subjects during epileptic seizure were only well modeled by the Kuramoto networks; this suggests that the epileptic brain becomes highly coherent, something captured by the Kuramoto phase oscillator network.

| Data | Random HR | Small-world HR | Random Kuramoto | Small-world Kuramoto |
|---|---|---|---|---|
| **MAE of prediction (%)** | | | | |
| Set A | $11.28 \pm 40.79$ | $13.43 \pm 58.88$ | $12.35 \pm 47.34$ | $\mathbf{10.97 \pm 40.05}$ |
| Set B | $\mathbf{7.82 \pm 15.90}$ | $11.58 \pm 50.44$ | $9.35 \pm 20.26$ | $\mathbf{7.95 \pm 15.98}$ |
| Set C | $\mathbf{7.95 \pm 6.69}$ | $8.27 \pm 9.11$ | $9.09 \pm 98.54$ | $7.39 \pm 10.49$ |
| Set D | $9.40 \pm 10.50$ | $\mathbf{8.17 \pm 7.48}$ | $9.91 \pm 9.32$ | $9.41 \pm 12.31$ |
| Set E | $45.84 \pm 352.61$ | $73.73 \pm 649.34$ | $\mathbf{11.21 \pm 23.89}$ | $34.56 \pm 268.48$ |
| **Hurst exponent prediction mean error** | | | | |
| Set A | $0.09 \pm 0.06$ | $0.19 \pm 0.11$ | $\mathbf{0.08 \pm 0.05}$ | $0.17 \pm 0.11$ |
| Set B | $0.08 \pm 0.07$ | $\mathbf{0.07 \pm 0.06}$ | $0.08 \pm 0.05$ | $0.20 \pm 0.13$ |
| Set C | $0.11 \pm 0.07$ | $0.13 \pm 0.07$ | $\mathbf{0.08 \pm 0.05}$ | $0.16 \pm 0.09$ |
| Set D | $\mathbf{0.06 \pm 0.06}$ | $0.09 \pm 0.07$ | $0.07 \pm 0.06$ | $0.14 \pm 0.10$ |
| Set E | $0.18 \pm 0.10$ | $0.15 \pm 0.11$ | $\mathbf{0.10 \pm 0.07}$ | $0.17 \pm 0.11$ |
| **Power spectrum prediction mean error** | | | | |
| Set A | $2.53 \pm 1.60$ | $2.64 \pm 1.76$ | $2.20 \pm 1.37$ | $\mathbf{2.13 \pm 1.65}$ |
| Set B | $3.88 \pm 4.57$ | $4.30 \pm 6.19$ | $3.38 \pm 4.89$ | $\mathbf{3.34 \pm 4.87}$ |
| Set C | $4.68 \pm 3.91$ | $4.83 \pm 4.19$ | $4.30 \pm 3.42$ | $\mathbf{3.30 \pm 2.44}$ |
| Set D | $6.03 \pm 12.84$ | $6.14 \pm 12.56$ | $5.86 \pm 11.01$ | $\mathbf{5.09 \pm 15.31}$ |
| Set E | $4.64 \pm 5.48$ | $5.76 \pm 13.29$ | $5.02 \pm 17.35$ | $\mathbf{4.58 \pm 9.67}$ |

Table 3.1: Key values for this table are the datasets and the network topologies considered. Bold values represents the best result in each row.

In addition, to ensure that our best fit models are obtained when the networks are set in the weak coupling regime responsible for the presence of the CAS phe-

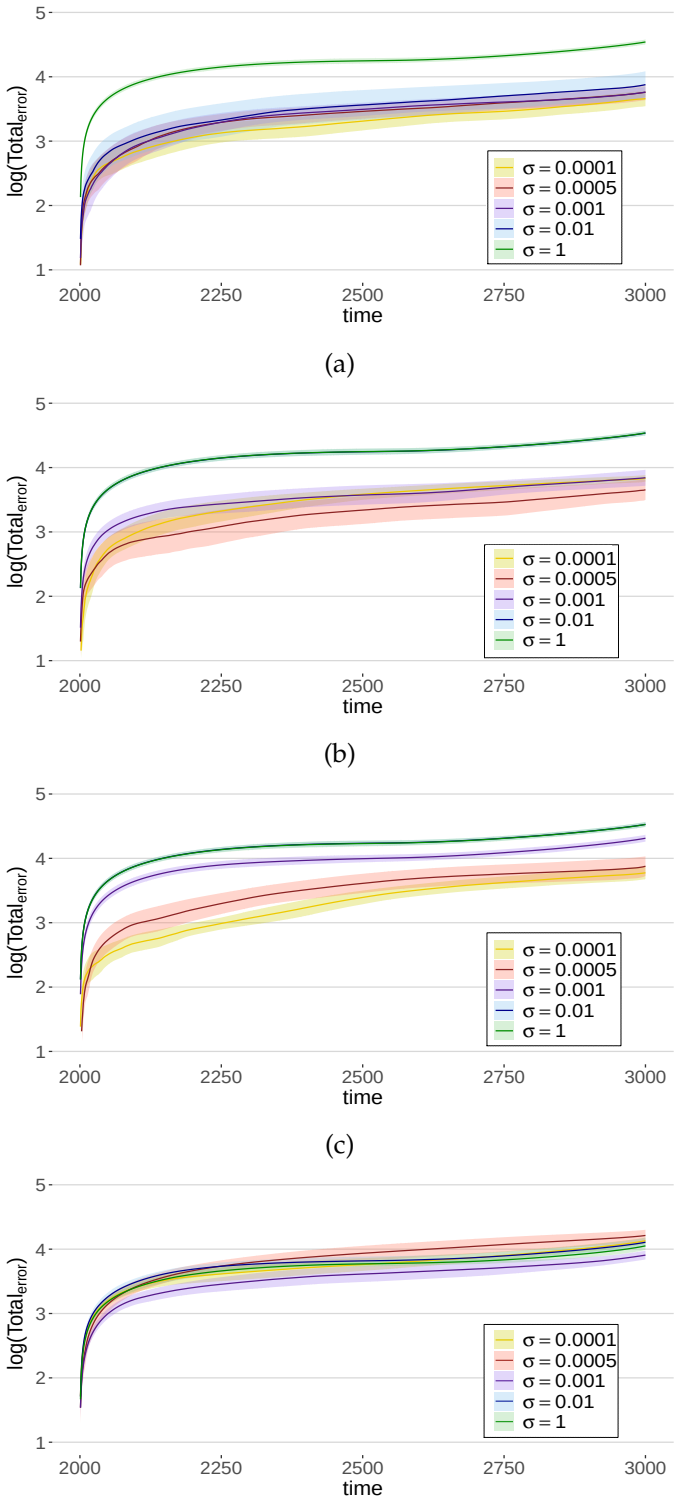


Figure 3.7: Total error of prediction from channel 4 of five subjects in dataset A.

nomenon, we calculated the cumulative total error of our model as a function of

time for each network model and different coupling strengths using the following formula:

$$Total_{error}(t) = \sum_{i=t_f+1}^{t} |Y_i - e_i|, \tag{3.23}$$

which is simply the MAE multiplied by the time interval, where $Y$ defines the predicted EEG signal and $e$ is the actual EEG signal.

From Fig. A.4, we can conclude that, independent of the types of oscillatory node dynamics and the types of network topology (excluding results from the small-world Kuramoto network), small $\sigma$ values that produce the CAS phenomenon can lead to the smaller errors between the EEG signals and the regenerated EEG signals, i.e., better prediction of the EEG signals after the weights were trained using the EEG dataset (training session). The results of datasets B, C, D, and E are shown in Supplementary Fig. A.

### 3.4.4 *Hurst exponent*

The Hurst exponent is a measure of the long-range correlation of a signal, and it is broadly used to analyze EEG signals from healthy control subjects and epileptic patients [77, 79, 80]. In clinical applications, the Hurst exponent was used to identify seizure-free EEG signals from seizure interval subjects and distinguish between healthy individuals and patients suffering from epilepsy [81, 82].

The datasets contained healthy (A, B), seizure-free (C, D), and seizure (E) EEG signals. The Hurst exponent was calculated for all 100 single-channel EEG signals from each dataset for several sigma values. This exponent is calculated by rescaled range (R/S) analysis [83] in a time window of 1000 time points corresponding 5.76s.

We calculated the mean error and standard deviation of the difference between the Hurst exponent calculated from the predicted signal and the Hurst exponent of the experimentally obtained EEG signal. The results are listed in Table 3.1. In general, the random Kuramoto network model produced the smallest errors for the Hurst exponents.

### 3.4.5 *Power spectrum*

Spectral analysis is a standard method for the quantification of EEG signals. The power spectrum reflects the frequency content of the signal or the distribution of the signal power over frequency [84–86]. An important application is the measurement of event-related desynchronization (ERD)/event-related synchronization

(ERS), which is widely used in brain–computer interface applications. ERD/ERS is related to the power spectrum changes at specific frequency bands during physical motor execution and mental motor imagery [67, 87].

The "actual" spectrum calculated directly from the EEG signal and the "predicted" spectrum calculated from the modeled signal in the predicting regime for the representative channel Fp1 from dataset A are presented in Fig. 3.8 with red and blue colors, respectively. The rows of this figure represent the power spectra ("actual" and "predicted") for several values of $\sigma$ increasing from top to bottom. The "actual" spectra in a row are the same.

For the HR network models and the random Kuramoto network model, the difference between the predicted and original power spectra increases as $\sigma > 10^{-2}$. It is worth recalling that the CAS phenomenon exists in the networks when $\sigma \leqslant 0.001$, which exactly matches the range for which the power spectrum can be well reproduced. The results of datasets B, C, D, and E are shown in Supplementary Fig. B.

## 3.5 DISCUSSION

It has long been shown that the HR neural network operating in the CAS region reproduces EEG signals [5], but in this study, PCA is not from the time series collected from randomly selected neurons but from the actual data generated by the network. Using the compression set of independent vectors generated by the above for the model, the fitting error of the model was reduced (from the Fig. 3.5). We also show that it is possible to use a mechanical network formed by the Kuramoto phase oscillator instead of the connected neuron model to reproduce the EEG data.

The challenge in neuroscience is to discover the vibrations regions in which the brain functions [58]. In this study, we further demonstrate (as provided in Ref. [5]) That the brain can operate at least locally in the CAS region. Because for all kinds of nonlinear networks studied, the best model of EEG signal can be obtained from the data generated from the network operating in the CAS region, as the result of Fig. A.4 shows. Networks in the CAS region are characterized by small clusters of weakly connected neurons behaving as if they were nearly synchronized neurons.

There is increasing empirical support for the idea that network topology plays an essential role in understanding brain function. This study tests two different topology models, random and small world, for networks, and two types of neurons, HR neurons and Kuramoto phase oscillators. The error analysis of the distance of the EEG signal modeled with the experiment, and the average difference of the feature amount, Hurst index, and power spectrum were shown in Table 3.1. As a result, set A was best modeled by considering the small-world Kuramoto network,

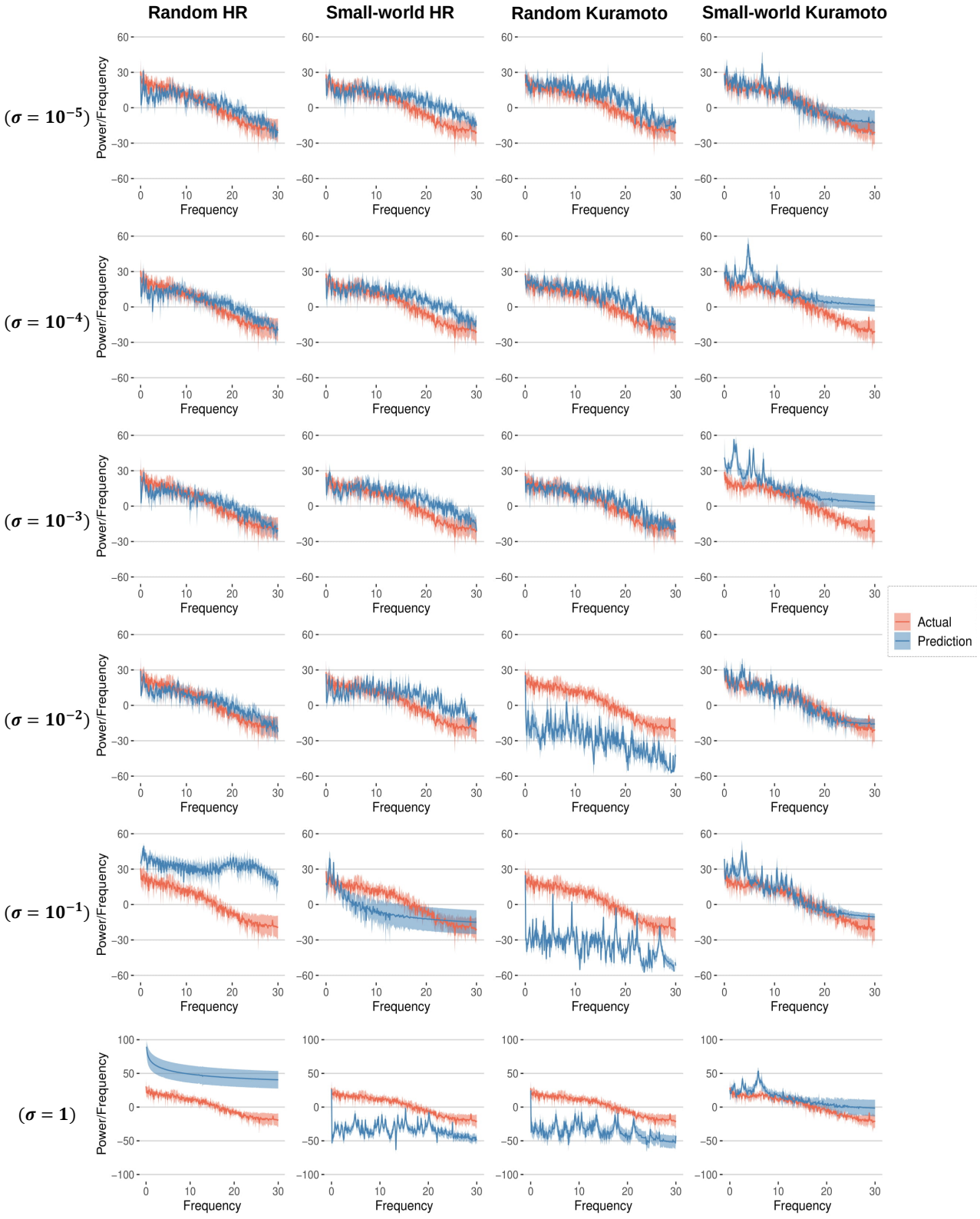


Figure 3.8: Experimental and predicted power spectrum for dataset A.

set B by random HR and small-world Kuramoto, set C by random HR, set D by small-world HR, and set E by random Kuramoto. In addition, the epileptic EEG

signals (sets C and D) have more minor prediction errors than the EEG signals of healthy subjects with eyes closed (set A) and have the same performance as healthy subjects with eyes closed. Data from subjects during seizures were successfully modeled only by the Kuramoto network. These results suggest that the epileptic brain was captured by the Kuramoto phase oscillator network and was highly coherent.

Some studies have reported that the network of Kuramoto phase oscillators is essential for understanding seizure activity, as in the papers by Yan and Li [88]. These authors estimated the human brain network from diffuse magnetic resonance images of healthy individuals. Thus, a computational model using a delayed version of the Kuramoto model connected to the estimated network provided the basis for the authors' hypothesis that the frontal hub could drive seizure activity. Another study has shown that in the Kuramoto phase oscillator network, the appearance of hyper synchronization similar to seizures was manifested as a result of the network topology [89].

Using dynamic descriptions of other neurons, such as the Hodgkin-Huxley (HH) model and the integrate-and-fire model, could also be considered a dynamic unit of the network used in the proposed unsupervised learning method. The only requirement is that the network is set up in the CAS area. The network of HH model and phase oscillator was considered in this study because the parameter group in which CAS exists in the network of HH and phase oscillator was clarified by the previous study [72].

This study used a network with $N = 1000$ nodes and collected a time series of $m = 3000$ data points from each node. EEG signals for 17.28 seconds were analyzed, corresponding to data frequencies 173.61 to Hz. This time is sufficient to perform several analyzes in a short period for the detection of epileptic seizures and the classification of motor images. In the future, we will increase the time points of data and the number of neurons to explore the possibility of clinical analysis. The model's performance for other types of data, such as ECG, should also be studied, depending on the type of dynamics that form the network. Given that the modified Van der Pol oscillator is a reasonable basis for modeling ECG, it was thought of as the mechanical unit of the proposed network.

## 3.6 CONCLUSION

This study shows that it is possible to supply data to a machine learning model that can be learned by an unsupervised approach using a nonlinear network set to operate in a weakly coupled region called CAS. Notably, the output from the CAS model can reproduce the EEG signals of healthy and epileptic patients in the

predicted region and can reproduce the EEG signals features of the Hurst index and power spectrum.

We used model data from healthy individuals and epilepsy patients to validate the performance of CAS models based on various neuron and network types. Interestingly, the prediction error between the EEG data set and the signal generated by the CAS is that it is essential to allow artificial neurons to interact weakly to generate the CAS in order to predict the EEG signal better. Thus, it was suggested that the CAS model, which is a weakly connected chaotic system, has generality that can express the dynamics of the brain without depending on the dynamics of nerve cells or the type of network.

However, there are some limitations we need to address to improve this model in the future. Our model is based on linear regression, which approximates the experimental EEG signal, but with a unique set of constant weighting factors, a network with an invariant topology, and a constant coupling strength between nodes. However, the EEG signal is originally unsteady. Therefore, in order to make long-term predictions, it is necessary to incorporate into the model some time-varying configurations tuned to adapt to the variation of the modeled experimental signal.

The standard approach to modeling EEG relies on autoregressive or artificial neural networks [26–28]. Although these methods have succeeded in reproducing the characteristics of EEG signals, they can be predicted well only at time intervals shorter than 1 second. The reason why the EEG signal is difficult to predict is that the EEG signal is unsteady. The proposed method is based on a nonlinear network in which the nodes are configured to operate in the CAS region (in effect, the orbit wanders along a large periodic orbit) and predicts a time interval of 5.76 seconds.

# 4

# CONSTRUCTIVE UNDERSTANDING OF EEG ACTIVITY USING RESERVOIR COMPUTING

## 4.1 RESERVOIR COMPUTING

### 4.1.1 *General introduction*

RC has been developed by three types of methods: "liquid state machine", "echo state network", and "backpropagation-correlation learning rule". These methods aim to facilitate a new approach to modeling complex dynamical systems in the fields of mathematics and engineering with artificial Recurrent Neural Networks (RNN) [90]. Each method consists of a fixed-weight recurrent network, which, given a dataset, outputs a series of activation states. These intermediate values are used to train the output connected to the second part of the system that outputs the description of the dynamics of the original model obtained from the data. The first part of the Reservoir system is an a RNN with fixed weights that acts as a "black box" model for complex systems. The second part, called Readout, is some classifier layer (usually a simple linear) that connects to the Reservoir with a series of weights. A primary characteristic common to these techniques is a kind of intrinsic memory effect due to the iterative connection of the Reservoir, the size of which is expressed in the time steps required to use up the effect of the input on the calculated output of the Reservoir. One of the main behaviors to consider in the construction of the Reservoir is the activation function used to characterize the node's behavior. In the literature, it is mainly used from simple linear models to more elaborate nonlinear models such as "echo states" and sigmoids often used in backpropagation-correlation approaches or "liquid state" techniques to be seen later.

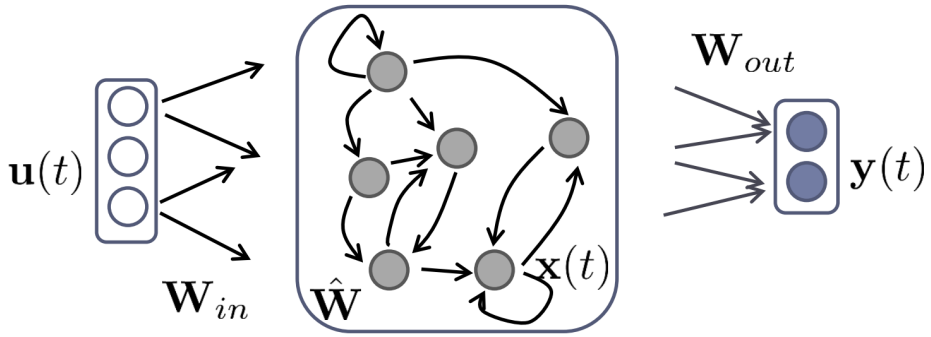


Figure 4.1: General structure of an ESN.

### 4.1.2 *Echo state network*

The Echo State Network (ESN) approach was introduced in 2001 [91]. The main idea is (1) to drive a random, large, fixed recurrent neural network with the input signal, thereby inducing in each neuron within this "reservoir" network a nonlinear response signal, and (2) combine a desired output signal by a trainable linear combination of all of these response signals (See Fig. 4.1). In detail, a generic ESN model is composed of a discrete-time neural network $\mathbf{u}$, reservoir network $\mathbf{x}$ and output $\mathbf{y}$. Activation's of network at time step $t$ are described by $\mathbf{u}(t) = [u_1(t), u_2(t), ..., u_N(t)], \mathbf{x}(t) = [x_1(t), x_2(t), ..., x_K(t)]$, and $\mathbf{y}(t) = [y_1(t), y_2(t), ..., y_L(t)]$ where $N, K, L$ are the number of units of input, reservoir, and output respectively.

In the ESN approach, this task is solved by the following steps.

**Step 1. Harvest reservoir states.** Drive the reservoir with the training data $u(t)$. This results in a sequence $x(t)$ of K-dimensional reservoir states. An $K$ weight matrix $W$ collects reservoir node weights and recurrent. The input and reservoir was connected by an $NxK$ weight matrix $W_{in}$. Sigmoid-unit echo state network is governed by the state update equation:

$$x(t+1) = f\left(W_{in}u\left(t+1\right) + Wx(t) + W_{back}y(t)\right) \tag{4.1}$$

Where $W_{back}$ is the connections that project back from output to reservoir units.

**Step 2. Compute output weight.** Connection's weight from system to output, an L x (N + K + L) matrix is prepared $W_{out}$. Compute the output weights as the linear regression weights of the outputs $y(t)$ on the reservoir states $x(t)$.

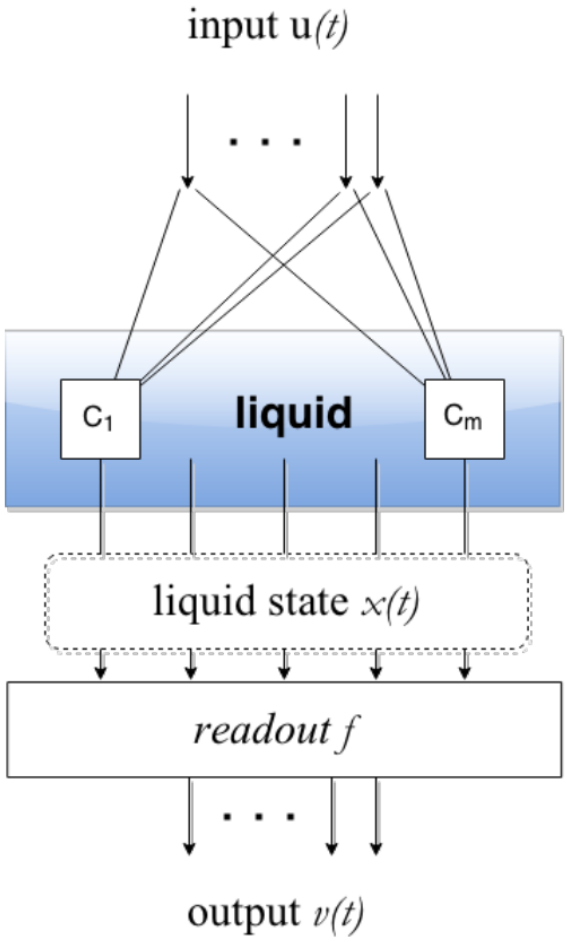


Figure 4.2: General structure of an LSM.

### 4.1.3 *Liquid state machine*

Liquid State Machine (LSM) approach is based on the idea concept of "Liquid Computer" [92]. This idea was imagined by Maass that consists in a liquid medium that act as a filter perturbed by time series inputs in function of time, and a readout that captures all state changes in the liquid without memorize them. A mathematical model of "liquid computer" is called LSM and consists of a reservoir, in this case called liquid, which processes an input time-series $u(t)$ into a liquid state $x(t)$ who integrates influences from inputs at all times prior t. In the ESN approach, this task is solved by the following steps.

**Step 1. Separation.**

**Step 2. Approximation.** The readout has the capability to approximate any given continuous function $f$ that maps current liquid states $x(t)$ on current outputs $y(t)$. This property should be fulfilled by the readout function.

### 4.1.4 *Application in neuroscience*

From a neuroscience perspective, reservoir computing aims to mimic how the brain processes information. In this context, reservoir in [93] introduced neurons were embedded in a complex network whose intrinsic activity was altered by external stimuli. By sustaining the network activity of nerve cells, information processing for given stimuli could be processed. Information processing takes place in the context of the response to previous stimuli. The network activity was then projected onto other cortical areas that interpret or classify the output. This biology-inspired idea motivated one of the archetypes of reservoir computing, the liquid state machine.

## 4.2 EXPERIMENT

### 4.2.1 *Introduction*

Understanding human thought and behavior can take many approaches, but to really understand how the brain works, you need to look inside it. Recently, an electroencephalogram, or EEG, is attracted the researchers due to its quicker, affordable, and accessible insights about brain function, with a tight temporal resolution. EEG is a recording signal of brain activity that mainly use for diagnosing and treating brain disorders. To discover more abilities of the EEG, current research has focused on understanding how the brain works, the identification of biomarkers, and the construction of BCI. A promising approach to better understand the brain is through computing models [7]. These models are adjusted to preproduce signals collected from the brain. Our research aims to build a model that not only reproduce EEG signals of both healthy and epileptic conditions but also forecast EEG signals.

We built the model by using the complex network of weakly connected dynamical system called CAS [7]. Particularly, we simulate neural networks by Hindmarsh-Rose neurons and Kuramoto oscillators described a CAS [94]. Then, a simple linear regression model takes the simulated neural network as an input and produces the generated EEG signals which has high correlation with the original EEG signals. Finally, the model also was used to predict the onforward EEG signals. Our proposed model not only successfully reproduced EEG data from both healthy and epileptic EEG signals, but it also predicted EEG features well. However, the linear regression model provides an approximation of the experimental EEG signals by utilizing a lot of constrains, such as a unique set of constant weight

coefficients, a network with invariant topology, and constant coupling strength connecting the nodes. EEG signals are nonstationary in nature [95]. Therefore, for long-term predictions, our model should incorporate some time-varying configurations tuned to adapt to the varying nature of the experimental signals being modelled.

In order to overcome the issues of linear regression model, another way is to use a novel approach for time-series forward prediction that was developed based on a CAS regime with an extension of an adaptive RC method. Importantly, the reservoir's fixed nature opens up using any dynamic system such as CAS. Theoretical advantages of the proposed method are the model learn and adapt to the time-varying nature of EEG signal. Our method implement the RC model to predict the EEG signals using the simulated CAS as an input. The reservoir's dynamics transforms the CAS neural network stream into a high-dimensional state space, capturing its nonlinearities and time-dependent information for computation tasks.

### 4.2.2 *ESN computation method*

To simplify the reservoir construction, we propose a structured topology template as Fig. 4.4. We compare the results to the linear regression results which have shown in section 3. We consider a non-linear reservoir consisting of neurons with the commonly used tangent hyperbolic (tanh) activation function.

$$X_{n+1} = F(x_n, u_n) = (1 - \alpha)\, x_n + \alpha \tanh\left(WE_n + W_{in}u_n\right) \tag{4.2}$$

We consider ESN with $N$ internal nodes, $k$ input signals, and a single output node. $W^{in}$ and $W^{res}$ are generated as random matrix in the interval $[-0.5, 0.5]$, and were fully connected. In the experiments where relevant, the reservoir weight matrix is rescaled such that its spectral radius 0.9. The default input scaling used is 0.8. $W_{out}$ is adapted with linear regression, using Ordinary Least Squares routines. This is found to lead to the best stable and precise results. For all experiment runs, the first 100 states of each run are discarded to provide a washout of the initial reservoir state. The input $u(n)$ is simulated with the same criteria with HR neurons simulation which explaned in chapter 3.

This experiment was organised along five degrees of freedom:

- Reservoir topology $W$.
- Reservoir activation function $F$.
- Input weight structure $W_{in}$.

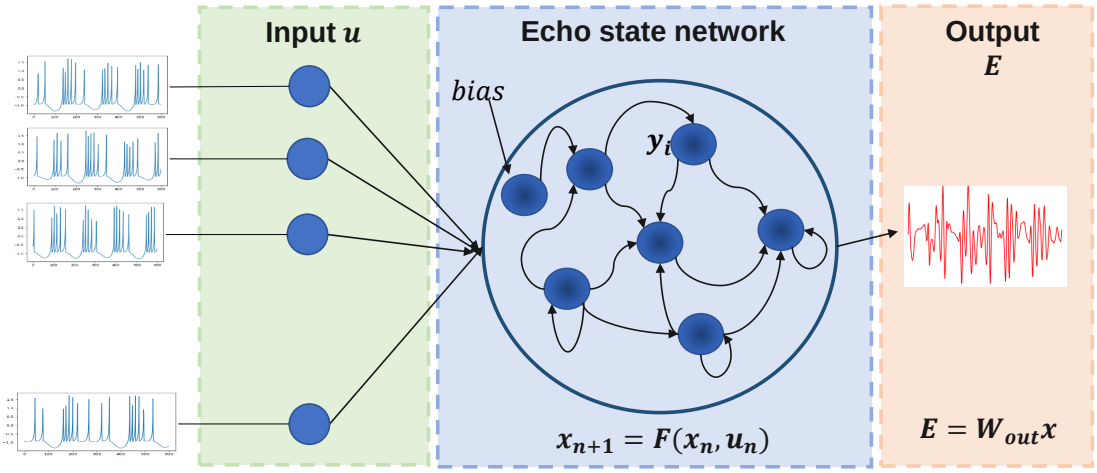


Figure 4.3: An architecture of proposed model.

- Readout learning $W_{out}$.
- Reservoir size.

### 4.2.3 *Dataset*

In this chapter, we also used an open-source database from Bonn University: A (closed eyes, healthy records), B (opened eyes, healthy records), C and D (seizure-free interval, epileptic records), and E (during seizure activity, epileptic records) [78]. Each set consisted of 100 single-channel EEGs under a sampling rate of 173.61 Hz. The datasets were band-pass filtered (0.5–30 Hz, EEGLAB embedded Fourier infrared (FIR) filter). 3000 sampling points collected over approximately 17.28 s were used. The first 2000 points were training data and the last 1000 points were predicted data.

## 4.3 RESULT

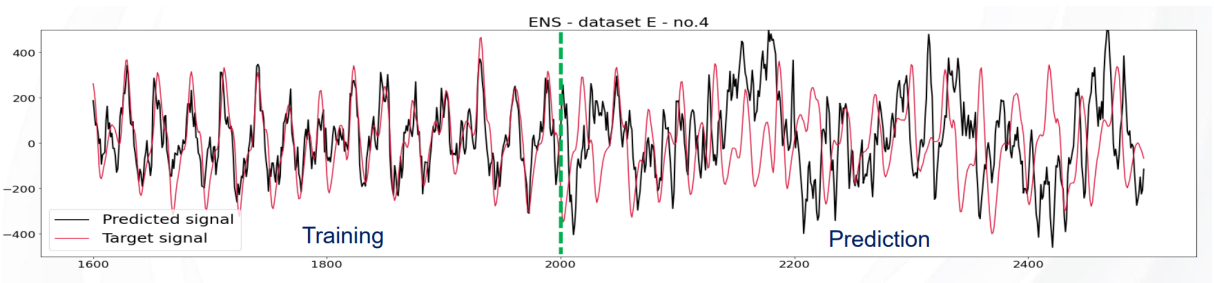


Figure 4.4: An example of prediction.

| Dataset | Linear regression [7] | | ESN | |
|---|---|---|---|---|
| | MSE | Hurst | MSE | Hurst |
| A | $19.05 \pm 16.75$ | $7.20 \pm 5.15$ | $\mathbf{13.96 \pm 1.55}$ | $\mathbf{5.91 \pm 4.35}$ |
| B | $17.03 \pm 10.89$ | $\mathbf{9.49 \pm 7.02}$ | $\mathbf{13.97 \pm 1.51}$ | $15.50 \pm 7.95$ |
| C | $17.02 \pm 14.49$ | $8.71 \pm 16.53$ | $\mathbf{13.70 \pm 1.80}$ | $\mathbf{4.57 \pm 3.36}$ |
| D | $16.00 \pm 9.10$ | $6.76 \pm 5.28$ | $\mathbf{14.07 \pm 2.51}$ | $\mathbf{5.70 \pm 4.29}$ |
| E | $\mathbf{13.79 \pm 3.33}$ | $\mathbf{17.37 \pm 10.06}$ | $16.97 \pm 4.02$ | $24.09 \pm 12.25$ |

Table 4.1: The prediction error in comparison on ESN model with linear regression model. Bold values represent the better results in each data set.

The Fig. 4.4 shown the example for prediction result. EEG signal evolves in time up until time t = 2000. After this point, the autonomous ESN predicts a future trajectory (black line), which is compared to the actual signal (red line). The average error scores computed using the MAE quantity in Eq. (3.12) for the different prediction models are presented in Table 4.1. Owing to the differences in range between the five datasets, the MAE was divided by the range of EEG signal to obtain the ratio. For quantitative performance results described in the previous study, we refer to Table 3.1. The ESN model gives a better prediction for signal prediction – compare with the linear regression model for healthy EEG. The ESN gave outperformance for Hurst prediction in data sets A, C, and D. The linear regression is better for epileptic EEG prediction.

## 4.4 DISCUSSION

This chapter has shown that the RC, which is fed by a weakly coupled regime called CAS, can be used to reproduce EEG signals. This approach could predict better healthy EEG conditions and reproduce the characteristics of the EEG signals in terms of the Hurst exponent. The weighted sum of CAS neurons yields a better prediction for epileptic EEG signals.

Moreover, the difficulty in predicting EEG signals is due to the nonstationary nature of the EEG signals. The proposed method is fundamentally based on a nonlinear network with nodes set to operate in a CAS regime and RC, which can lead to a successful prediction of time intervals of the order of 5.76 s.

However, some limitations need to be addressed to improve this model in the future. The proposed model is based on a simple ESN that provides a good approximation of the experimental EEG signal but includes various coefficients, a constant network topology, and missing feedback memory. Therefore, for long-

term predictions, our model should incorporate some memory feedback tuned to adapt to the varying nature of the experimental signal being modeled.

# 5

# CAS MODELING USED FOR MOTOR IMAGERY EEG CLASSIFICATION

## 5.1 INTRODUCTION

EEG is a useful biological signal to distinguish different brain diseases and mental states. It is an easy and cheap technique for recording human brain signals, and is crucial for the BCI. In BCI research, MI is an important topic, which concerns the process in which a person imagine to be performing some tasks, i.e., intention to perform hand or leg movements. Detecting different MI tasks from EEG signals has attracted much attention by researchers, and several feature extraction methods and classifiers were suggested to recognize imagery action ([96]). In recent years, there have been several studies aimed to use MI for wheelchair control ([97, 98]), neuronal game ([99]), robotic hand control ([100, 101]), and autonomous driving ([102, 103]). Moreover, EEG pattern recognition is significantly more appealing than facial and speech-based recognition methods, given that internal nerve fluctuations cannot be deliberately masked or controlled ([104]). In previous studies, subject-independent EEG classification was shown to be difficult to achieve compared with classification from EEG of subject-dependent ones. Therefore, there is great interest to study the improving of the performance of EEG recognition across subjects. Lu et al. proposed to use a deep learning scheme based on a restricted Boltzmann machine to learn EEG features for MI classification ([105]). The best recognition accuracy across subjects was 70%, significantly lower than 84% achieved using subject-dependent MI classification. In the work from [106], a supervised learning-based method called hybrid-scale Convolutional Neural Network (HS-CNN) reached 87.6% of subject-dependent classification using dataset 2b of BCI Competition-IV ([107]), but its performance drops as 65.3% in a subject-independent setting.

To overcome this problem, besides classification techniques, feature extraction is crucial. EEG contains intense noise level, high non-stationarity, and non-linearity. All these are great challenges to find effective representations for EEG data fea-

tures ([108]). Several studies have proposed classic feature extraction methods for MI-EEG, such as FFT ([101, 109]), Wavelet Transform (WT) ([110, 111]), empirical mode decomposition (EMD) ([112, 113]), typical spatial pattern ([114–116]), AR ([15, 117, 118]), and so on. More recently, researchers suggested combining the time domain and frequency domain methods to describe the characteristics of MI-EEG ([119]) more effectively. However, linear transform methods failed to address the non-linear characteristic of EEG signals ([120]). Human brain can be considered as a complex network of connected nonlinear dynamical systems. Recently, it was shown that the brain activity measured by EEG signals could be modeled by nonlinear oscillators ([5, 121]). This opens up the idea to propose feature extraction methods that explores the dynamical nature of EEG signals, and which can improve classification accuracy in BCI. Several aspects of the CAS method have been considered in EEG modelling ([5, 7]). CAS is a phenomenon characterized by the existence of a local cluster of neurons possessing roughly constant local mean fields, a consequence of the fact that neurons are very weakly connected ([94]). This phenomenon can be studied using computational models of dynamical systems such as Hindmarsh-Rose neurons connected by small coupling strengths. Similar to what is done in the AR modelling approach, experimental EEG signal can be reproduced as a linear combination of a set of selected neurons in a network of weakly connected HR. The coefficients of the linear regression model matching the EEG signal are then used as the feature vectors in the BCI system. Extracted features are then input to a suitable classifier to perform the final recognition of the state of MI.

Recently, Deep Learning (DL) received much attention for its superior performance. Convolutional Neural Network (CNN) is one of the DL methods, which is showed a remarkable success concerning image classification and computer vision ([122]). CNN is also widely used for EEG classification ([123]). Several studies showed that it is suitable for complex EEG recognition tasks ([124–126]). This classifier can also be applied to various BCI paradigms such as MI and emotion classifications, and obtained competitive high accuracy to state-of-the-art methods ([124, 127, 128]).

To this end, this study proposes a novel EEG feature extraction method using our CAS-based nonlinear network modeling. We use a MI-EEG dataset 2b from BCI competition-IV ([129]) and set both intra-subject and across-subjects frameworks classification. The main contribution of the study is as follows: (1) We propose a novel EEG feature extraction method in which EEG signals are modeled by a complex network of chaotic HR neurons that are weakly connected and behaving in the CAS state. The weight coefficients of the model are used as an EEG feature. (2) A CNN is used for classification performance. (3) The performance of the pro-

posed method is compared with state-of-the-art methods in both intra-subject and across-subjects MI-EEG classification. To the best of our knowledge, this study is the first to show an application of a large dimensional nonlinear dynamical system constructed as a model of the brain to extract features expressed in MI-EEG signals.

## 5.2 BACKGROUND

### 5.2.1 *Feature extraction*

EEG signals are generally complex and contain large amounts of information. Therefore, the ability to extract appropriate features from the EEG signal is an essential factor for the success of the classification algorithm. The feature extraction aims to transform the data into a low-dimensional space while preserving the critical information transmitted by the EEG signal [15]. According to the literature, many feature extraction methods have been proposed based on specific tasks such as time domain, frequency domain, time-frequency domain, and spatial information of signals [10, 130–132].

Furthermore, from the point of view of pattern recognition, some studies have excluded the steps of "subject normalization" and "subject selection", while many other studies use very few cases (observations) [133, 134]. More details on the feature extraction methods are provided in the sections below.

#### 5.2.1.1 *Time-domain analysis*

Time-domain analysis works for the stationary signals, but biosignals are non-stationary. One method to quantify a non-stationary time series is to consider it as a large number of stationary segments. There are key features in three categories:

- Mean and standard deviation for a time series with symmetric distribution.
- Median, mode, range, first quartile, and third quartile to measure the locations of a time series.
- Maximum, minimum, variation, skewness, kurtosis to pull out the shape characteristics of a time series.

Besides, existing works have used the change sign slope, Willison amplitude, Lyapunov exponent and Hjorth parameter to extract features from EEG signal [135–137].

#### 5.2.1.2 *Frequency-domain analysis*

There are three basic techniques for frequency-domain analysis: FFT, eigenvector, and model coefficient.

The FFT decomposes a time function (signal) into a frequency component rapidly by rearranging the input elements in bit-reverse order and constructing the decay over time. The FFT is suitable only when we are concerned with which frequency components exist, not the frequency components of the occurrence time. However, the timing during which a particular frequency component occurs is essential for biological symbology analysis. To solve this problem, a STFT uses the idea that some parts of the signal that are not static at any given time interval are the stop signal. A Power spectral density (PSD) values were extracted for each 1 Hz compartment from EEG 1–40 Hz to check the sleep state.

Eigenvector is used to calculate the frequency and power of the signals from artifact dominant measurements. These methods are based on their own analysis of the correlation matrix of the disturbed signal and produce high resolution frequency spectrum even at low SNR. There are three methods of eigenvector with higher resolutions. The Pisarenko algorithm is especially useful for estimating the spectrum containing sharp peaks at expected frequencies. The MUSIC method eliminates the effect of false zeros by using the average spectrum of all eigenvectors corresponding to the noise subspace. The Minimum-Norm method places false zeros inside the unit circle and computes the desired noise subspace vector from the eigenvectors.

AR method estimated PSD of EEG signal using parametric method. These methods solve the spectrum leakage problem and yield better frequency resolution. The Yule-Walker method can lead to inaccurate parameter estimation in the case of quasi-periodic signals. Instead, Burg's method first estimates the reflectivity, then estimates the parameters determined by the Levinson-Durbin algorithm. Recently, there are some studies used the model coefficient for the EEG pattern recognition such as dynamic system model-based EEG.

The power spectrum-based frequency method is often used to extract MI-related characteristics. Specifically, PSD was used for a linear and nonlinear classifier to classify left and right hand MI tasks [138, 139]. A power spectral features is also used for the latent random field method to improve the accuracy of the MI classification. However, for reasons of non-linear and non-Gaussianity EEG signals, conventional power spectroscopy techniques are limited to analyzing MI-related EEG signals. Since the power spectrum rejects information about the phase relationship between frequency components, it is not possible to extract non-linear and non-Gaussian information useful for MI classification.

Bispectrum is proposed to solve the power spectrum problem [140]. Bispectrum is able to quantify the interaction of two frequency components in a non-linear and non-Gaussian signal, so it can further explore non-linear and non-Gaussian characteristics from the associated EEG signals related to MI. Zhou, Gan and Sepulveda estimate the sum of the power spectrum and the total logarithmic amplitude of the bisector for the two MI classes [141]. Shahid and Prasad normalized the total logarithmic amplitude of the bisector and used Fisher's LDA classifier to distinguish right-hand and left-handed MI duties [142]. However, the representative extraction feature used in the above works adds all the bisector values to a feature. Therefore, it can reduce the validity of the classifier and the performance of the MI classification because of the sensitivity to non-linearity.

Using both time- and frequency-domain features can improve seizure classification performance. Three frequency-domain features (dominant frequency, average power in the primary energy zone, and normalized spectral entropy) and two time-domain features (spike rhythmicity and relative spike amplitude) are used. Iscan et al. combined time and frequency features to distinguish between seizure and healthy EEG segments. They got time-domain features using the cross-correlation method and frequency-domain features calculating the PSD [143].

#### 5.2.1.3 *Time-frequency features*

Time-frequency domain analysis studies a signal in both the time and frequency-domains simultaneously. Time-frequency distribution (TFD) and WT analysis are the principal techniques of time-frequency domain analysis.

The basic idea of TFD is to devise a joint distribution of time and frequency that describes the energy density or intensity of a signal simultaneously in time and frequency. In this distribution, we can calculate the fraction of energy in a specific frequency and time range, and the distribution of frequency at a particular time. It is done by constructing a joint time-frequency function with the desired attributes and then obtaining the signal that produces the distribution. Boashash et al. performed TFD feature extraction on multi-channel recordings for seizure detection in newborn EEG signals [144]. Many studies used short-time Fourier transform (STFT) for applying MI classification [145, 146].

WT is an alternative to STFT. STFT gives information about the spectral components at any given interval of time, but not at a specific time instant. It causes a problem of resolution. WT gives a variable resolution using the characteristics that high frequencies are better resolved in time-domain, and low frequencies are in frequency-domain. WT can capture very minute details, sudden changes, and similarities in the EEG signals [147]. It is more effective than other methods because

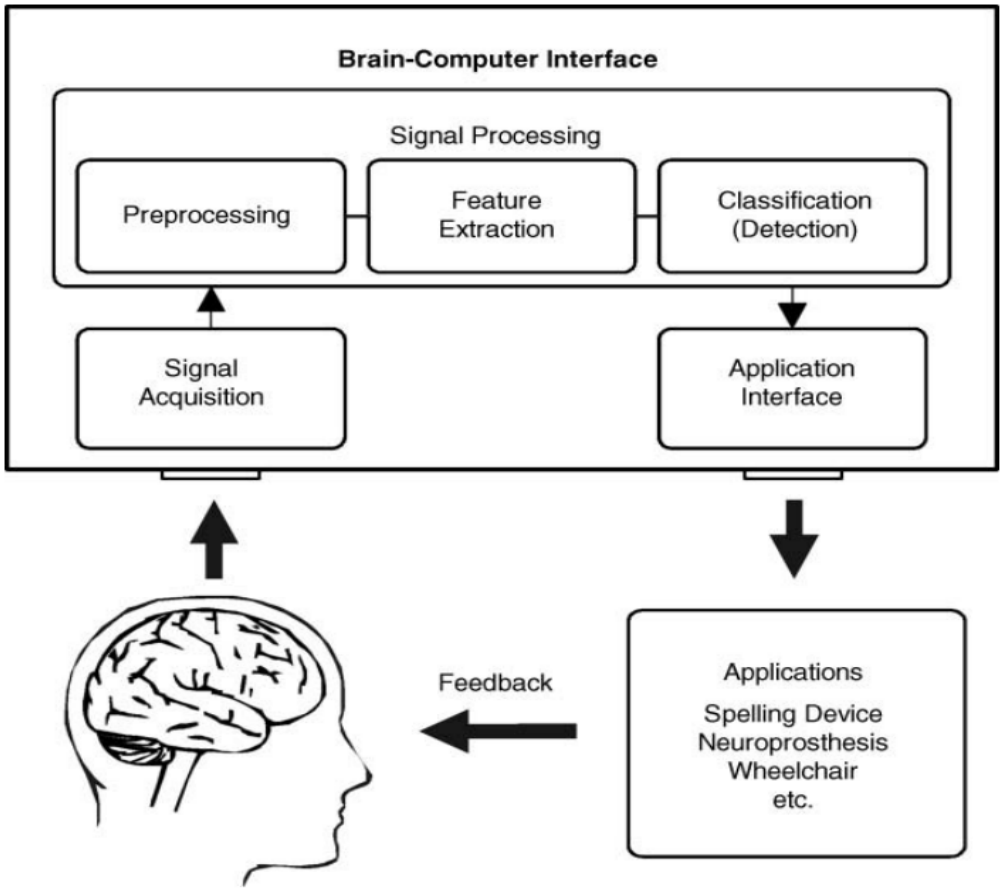


Figure 5.1: Components of a BCI system [148].

biosignals are non-stationary. WT transforms a small wave (a mother wavelet) as a pattern and expresses an arbitrary waveform on the scale of magnification and reduction. WT classified into continuous wavelet transform and discrete wavelet transform.

### 5.2.2 *EEG classification*

Over the years, deep CNN has become highly successful in many application areas, such as computer vision and speech recognition, often outperforming previous modern methods [122, 149–151]. For example, a deep CNN reduced error rate in the ImageNet image recognition challenge, where 1.2 million images must be classified into 1000 different layers, from over 26% to below 4% within 4 year. CNN also reduced error rates when it came to speech recognition, for example, from English news broadcasts [152, 153]. However, hybrid models that combine CNN with other machine learning components, especially repeating networks and non-convolution deep neural networks are also competitive .


Figure 5.2: Example of original EEG signals [154].

The EEG signal has characteristics that make it different from the inputs that CNN has had most success with, namely images. In contrast to the two-dimensional static image, the EEG signal is a dynamic time series from electrode measurements obtained on the surface of the three-dimensional scalp. In addition, EEG signals have a relatively low signal-to-noise ratio, meaning that sources without mission-related information often affect EEG signals more strongly than mission-related sources (see Fig. 5.2).

To address whether the CNN can achieve competitive decoding accuracy, a statistical comparison of their decoding accuracy was made with the results obtained when decoding against the filter bank common space sample, a method widely used in EEG decoding and has won several EEG decoding competitions such as BCI Competition 2b [119, 155–157].

## 5.3 PROPOSED SCHEME

Specific brain activity recorded via EEG has its own frequency band. The MI activities frequency band which is widely used is the one at 8-35 Hz ([105, 158]). Our approach is to use the multi-sub-bands decomposition. Regarding Figure 5.3, the diagram of the proposed method is as in these following steps:

- Multichannel EEG signal is decomposed into four sub-bands: 4-9 Hz, 8-15 Hz, 14-31 Hz, and 30-42 Hz, then the data is split into training and test data sets.
- CAS-based features are extracted from each sub-band EEG signals.

- The features obtained from multi-sub-bands are combined and standardized. The feature refers to the coefficients to match the EEG signals with states of the neurons in the HR network by a linear regression.
- The CNN classifier is trained with extracted features in the training dataset, and classification test is performed using the test dataset.

### 5.3.1 *Feature extraction*

CAS is defined as a universal way of how patterns can appear in complex networks with nodes connected by small coupling strengths. The HR neuron model is a well-known model for designing the neuron activity. Some studies used HR neuron model to describe a CAS pattern models the EEG signal ([5, 7]). In this study, we considered a HR network formed by $L = 1000$ neurons. The HR neurons model is as below:

$$\begin{cases} \dot{\Xi}_{x_i} = \Xi_{y_i} - a\Xi_{x_i}^3 + b\Xi_{x_i}^2 - \Xi_{z_i} - R\Xi_{xi} + Q_i \\ \dot{\Xi}_{y_i} = c - d\Xi_{x_i}^2 - \Xi_{y_i} \\ \dot{\Xi}_{z_i} = -r\Xi_{z_i} + sr\left(\Xi_{x_i} + x_0\right) \end{cases} \tag{5.1}$$

where $R_i = p_i$, $Q_i = p_i C_i$, $p_i = \sigma k_i$, $C_i \approx (1/k_i)\sum_{j=1}^{N} \mathbf{K}_{ij} x_j$. $k_i$ is the electrical coupling degree of neuron $i^{th}$. The parameters of model were chosen as following:$a = 1, b = 3, c = 1, d = 5, r = 0.005, x_0 = 1.618, I_{ext} = 3.23$, and the coupling strength $\sigma = 0.001$. $K_{ij}$ was a small-world matrix generated by Watts-Strogatz network approach with a rewiring probability equal to 0.01. The network had a mean degree of 10. The HR neurons were simulated using the Brain Dynamics Toolbox, and time-series were obtained with the same length of that of the EEG signal time-points. After that, a dimension of all membrane potential $X = \{x_i\} \in \mathbb{R}^{L\times N}$ was reduced by PCA. The final $X = \{x_i\} \in \mathbb{R}^{l\times N}$ was used to model the EEG signal. For more details see Refs. [5, 7].

We applied a parametric method using a linear regression model for EEG. Let $E = \left\{E_{ij}\right\}_{i=1:T,j=1:C}$ , where $E_{ij} \in \mathbb{R}^{1\times N}$, is the sub-band EEG training trials. Here, T is the number of trials, C defines a number of channels, and N is the number of data points. The linear regression model for EEG defines as below:

$$A_{ij}X = E_{ij} \tag{5.2}$$

where $A_{ij} = [\alpha_0, \alpha_1, \cdots, \alpha_l]$ is the vector of coefficients, which we regard as the feature extracted from the MI-EEG signals. $X \in \mathbb{R}^{l\times N}$ corresponds to the states of

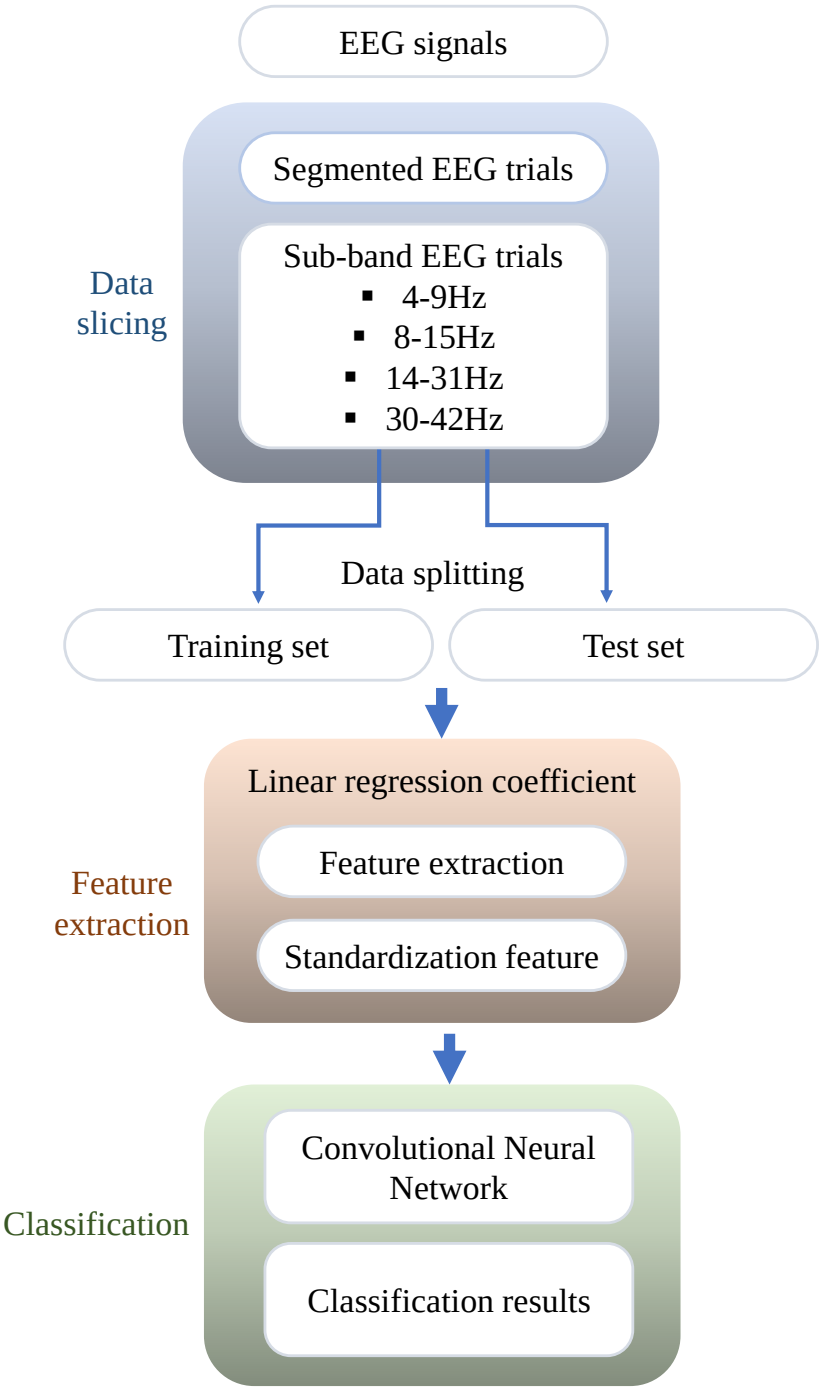


Figure 5.3: Block diagram of the proposed method.

HR neuron network operated in CAS regime. The estimation of $A_{ij}$ is calculated by using least square error method as below:

$$A_{ij} = X^{+} E_{ij} \tag{5.3}$$

where $X^+$ is the Moore-Penrose pseudoinverse of $X$.

### 5.3.2 *Feature standardization*

Normalization or standardization is a critical step needed to change features to the same scale. Different from normalization, standardization requires the data has a normal distribution. The values of $\alpha_0$ have changed much for different experiments, and this variation would have resulted in a distribution of the coefficients skewed. Therefore, $\alpha_0$ was then removed from $A_{ij}$. After confirming that the features satisfy the requirement, they were standardized as follows:

$$\acute{A} = \frac{A - \mu}{\alpha} \tag{5.4}$$

where $A$ is the original feature value, $\acute{A}$ is the normalized feature value. $\mu$ is the mean and $\alpha$ is the standard deviation of the feature.

### 5.3.3 *Convolutional Neural Network classifier*

CNN can take multidimensional data as input and generally works well for image classification. Various studies used a deep learning approach such as CNN to classify EEG signals. Based on their experimental results, we argue that CNN-based methods significantly improves on classical classification methods ([125]). In the present study, we used a simple CNN architecture shown in Figure 5.4. It had two contiguous blocks of a convolution layer followed by a max-pooling layer, a flatten layer, and finally a dense layer. The CNN model was trained with the SGD optimizer algorithm. Also, we used regularization techniques such as dropout to prevent over fitting problem. The settings used for training the CNN model are as follows:

- ReLU was used as an activation function in the convolution layer..
- The final fully connected layer derived the probabilities for two output classes using the sigmoid function.
- Stochastic gradient descent with an initial learning rate of 0.01.
- Dropout with a probability of 0.2, 0.3, and 0.4 in each convolution layer and flatten layer, respectively.

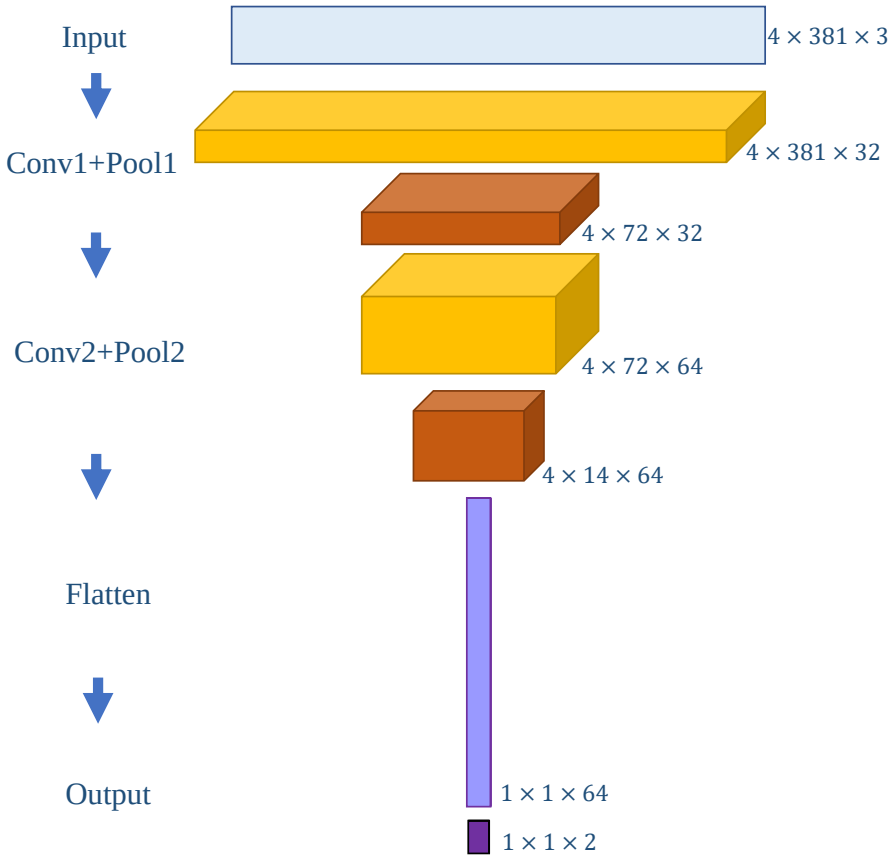


Figure 5.4: The illustration of the CNN block diagram. The model consists of two convolutional layers, two max pooling layers as well as flatten layer.

## 5.4 EXPERIMENTS

### 5.4.1 *Dataset*

To evaluate the performance of the proposed method, we executed MI-EEG classification experiments. For this aim, we used the BCI competition IV dataset 2b[159], because it is commonly used in this field. The dataset contains two types of experiments from nine healthy participants. Each experiment was recorded on separate days for one subject. The timing scheme of each trail is shown in Figure 5.5. The MI classification task aims to predict the label of the second experiment from the supervised information of the first experiment.

EEG signals were recorded in three channels: C3, Cz, and C4, with a frequency 250 Hz. Participants executed five recording sessions in total. In the first experiment, two sessions were done without feedback with 120 trials per session, and the rest three sessions in the second experiment incorporated online feedback with

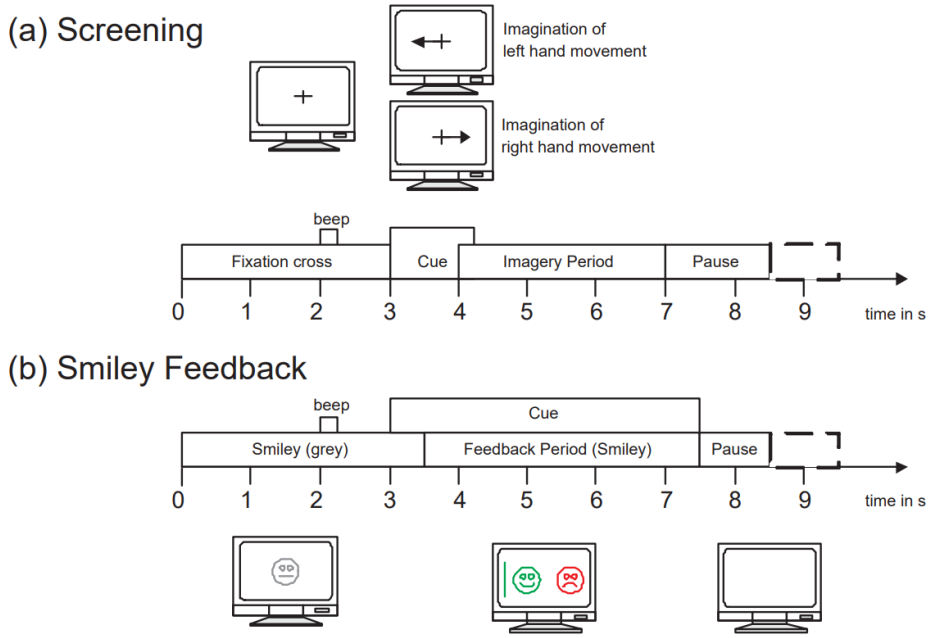


Figure 5.5: Timing scheme of the paradigm.

160 trials per session. An EEG time segment was extracted from the first 4 to 7 s, resulting in 750 data points per trial. In the pre-processing stage, raw EEG data were segmented into trials and band-pass filtered into four sub-bands: delta (4-9Hz), alpha (8-15Hz), beta (14-31Hz), and gamma (30-42Hz).

### 5.4.2 *Experimental setup and comparative experiments*

HR neuron network $X \in \mathbb{R}^{1000\times750}$ was simulated using Brain Dynamics Toolbox ([73]). An example of the dynamic behavior of a single HR neuron is shown in Figure 5.6. $X = \{x_i\} \in \mathbb{R}^{1000\times750}$ is used to model the EEG signal. Then, the dimension of X was reduced into $X \in \mathbb{R}^{l\times750}$ by selecting the top $l$ eigenvectors with the highest eigenvalues. The value of $l$ was chosen so that principal component contains 99% of the information. The linear regression model was performed to extract the feature for each channel and sub-band frequency data. The weight coefficients were calculated by Eq. (3). Thus, we had a set of

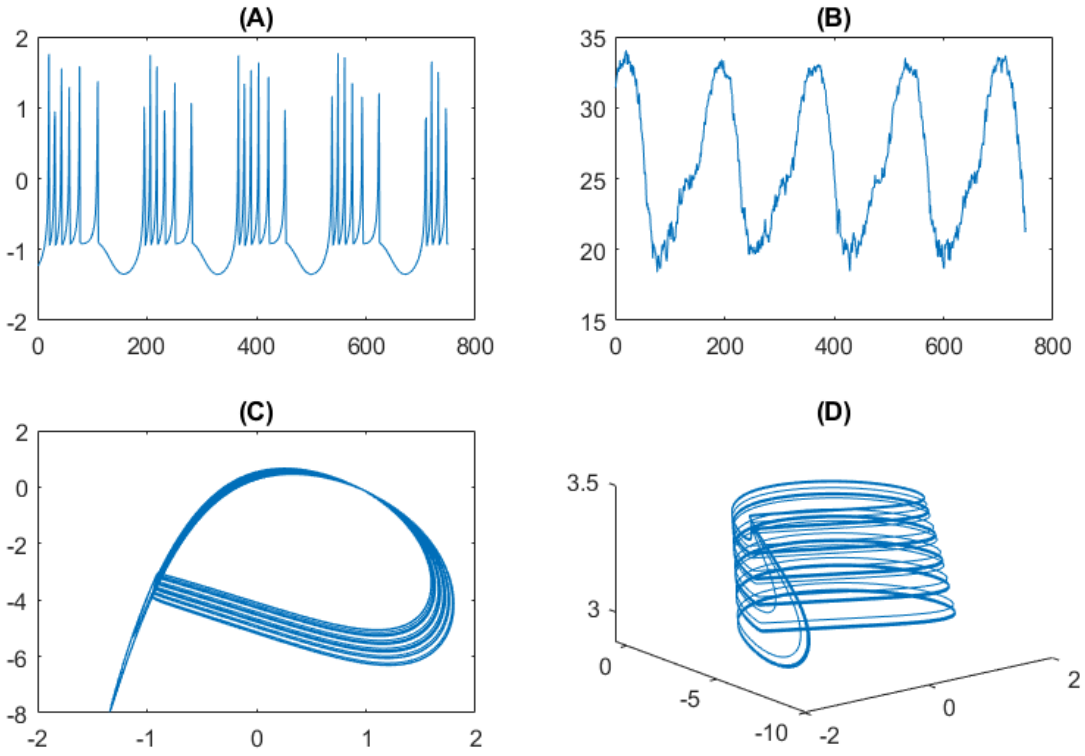


Figure 5.6: The activities of HR neuron. **(A)** action of membrane potential, **(B)** first principal component of membrane potential applying PCA, **(C)** and **(D)** a phase portrait.

$[frequency \times coefficient \times channel]$ arrays for every trials. Furthermore, the correlation between generated signals $\left(\hat{E}_{ij}\right)$ and original EEG was calculated as below:

$$Corr\left(E_{ij}, \hat{E}_{ij}\right) = \frac{\mathbb{E}\left[\left(E_{ij} - \mathbb{E}\left(E_{ij}\right)\right)\left(\hat{E}_{ij} - \mathbb{E}\left(\hat{E}_{ij}\right)\right)\right]}{Var\left(E_{ij}\right) Var\left(\hat{E}_{ij}\right)} \tag{5.5}$$

To evaluate the performance of proposed method for MI classification, we conducted two experiments. In the first experiment, the session-to-session transfer classification, in which one session was for the training and one session was for the test, was conducted for each subject. Training and test sessions were recorded on different days for all subjects. Therefore, the session-to-session transfer classification is more challenging ([160]). Whereas in the second experiment, we investigated across-subjects classification by using Leave-one-subject-out (LOSO) cross-validation, namely the data measured from eights subjects were used as the training set, while the data from the remaining one corresponded to the test set.

To demonstrate the efficiency of the proposed feature extraction method, accuracy and *Kappa* statistic defined as follows were used as the performance measure.

$$Accuracy = \frac{TP + TN}{TP + TN + FP + FN} \times 100(\%) \tag{5.6}$$

where TP indicates for true positive, meaning the correct classification as left-hand; TN indicates for true negative, meaning correct classification as right-hand; FP indicates for false positive, meaning incorrect classification as left-hand; and FN represents false negative, meaning incorrect classification as right-hand.

$$Kappa = \frac{P_0 - P_e^C}{1 - P_e^C} \tag{5.7}$$

where $P_0$ represents the probability of overall agreement between label assignment, classifier, and true process; and $P_e^C$ is defined by the chance agreement for all labels, i.e., the sum of the proportion of instances assigned to class multiplies in proportion to accurate labels of that specific class in the data set. Finally, to verify whether the performance difference between the proposed method and other methods is statistically significant, the two-side paired *t-test* has been conducted.

## 5.5 RESULTS

### 5.5.1 *Examine the results of extracted features*

Figure 5.7 illustrates the distributions of correlation coefficients between original and generated EEG signals. This result shows that the HR neuron model could fit the EEG signal with strong correlations (larger than 0.7). The highest correlation comes from the results in beta band (mean correlation coefficients was 0.85), while the smallest is found in delta band with mean values was 0.74. The mean values were 0.78 and 0.76 for alpha band and gamma band, respectively.

### 5.5.2 *Results on intra-subject classification*

To evaluate the CAS-based feature for MI classification, the intra-subject classification performance obtained by the proposed method was compared with FFT method and non-feature extraction works. The comparison is presented in Table 5.1. Considering the accuracy of 9 subjects, the proposed method yields the highest accuracy in 7 subjects.

In comparison, its accuracy in the other two subjects is very competitive (less than 4.13% and 0.25% compared with the highest ones). The results indicate that

| Subjects | No feature extraction [119] | | FFT [156] | Proposed method |
|---|---|---|---|---|
| | Shallow CNN | Deep CNN | CNN | |
| 1 | 71.56 | 67.25 | 69.78 | **75.31** |
| 2 | 53.57 | 56.10 | 54.75 | **60.25** |
| 3 | 53.12 | 54.87 | 52.88 | **56.26** |
| 4 | 95.93 | 94.52 | 95.31 | **96.56** |
| 5 | 85.00 | 84.59 | 85.91 | **86.15** |
| 6 | 76.87 | 74.46 | 78.03 | **85.21** |
| 7 | **76.56** | 74.46 | 69.75 | 72.86 |
| 8 | 85.93 | **87.75** | 87.56 | 87.50 |
| 9 | 82.18 | 79.25 | 80.91 | **84.06** |
| Average | 75.64 | 75.10 | 74.99 | **78.23** |
| P-value | 0.02742 | 0.03254 | 0.00219 | |

Table 5.1: The accuracy in comparison on inter-subject with the CNN-based methods. Bold values represent the best result in each row.

| Works | No feature extraction | | Proposed method |
|---|---|---|---|
| | Shallow CNN | Deep CNN | CNN |
| Kappa value | 0.63 | 0.59 | 0.64 |

Table 5.2: The Kappa values in comparison on inter-subject with the CNN-based methods.

the proposed CAS-based feature extraction method is superior to other methods with 3.1% on the average level. The CAS-based method significantly improves the classification accuracy in comparison with common method. The significant difference between the proposed and state-of-the-art methods is conducted by statistical test whose results were shown in the bottom row of Table 5.1. A two-sided paired *t-test* at the significance level of $\alpha < 0.5$ reveals that the performance improvement achieved by our proposed method is statistically significant. Table 5.2 summarizes the average *kappa* values of the proposed method and non-feature extraction works. The kappa statistic has a value between 0 and 1, and the higher value indicates the better model consistency. Table 5.2 suggests that the proposed method performs better than non-feature extraction methods.

### 5.5.3 *Results on across-subjects classification*

In the test of across-subjects, Table 5.3 shows the accuracy of the proposed methods for 9-folds cross validation. The dataset contained EEG data of 9 subjects with 600 trials per subject. Among 5400 trials, the CAS-based feature was classified using the CNN model. Specifically, study from [105] reported that DBN classification

| K-fold | 1 | 2 | 3 | 4 | 5 | 6 | 7 | 8 | 9 |
|---|---|---|---|---|---|---|---|---|---|
| Accuracy(%) | 73.11 | 63.91 | 58.67 | 92.14 | 69.43 | 80.75 | 69.92 | 78.84 | 79.50 |

Table 5.3: The accuracy on across-subjects with 9-fold validation.

| Works | DBN | HS-CNN | Proposed |
|---|---|---|---|
| Accuracy(%) | 70 | 65.3 | 74.0 |

Table 5.4: The accuracy in comparison on cross-subject with state-of-the-art methods.

performance reached 84%, but the performance dropped to 70% when the model was trained in across-subjects setting. The HS-CNN reached 87.6% of intra-subject classification, but performance drops as 65.3% in across-subjects setting ([107]). Our approach achieved 74.03% (±10.02%) mean accuracy (Table 5.4).

In comparison with other works, this study has two advantages. First, our study indicates that the CAS-based method is more robust and can extract distinguishable features from EEG signals than FFT. The linear regression model uses a simple linear algebra formula and reduce the consumption of calculation, which is more beneficial for online BCI application. Second, our proposed method can improve the inconvenience of the parameter dependency such as time window, model order referred in ([15]).

The average processing time for the proposed methods was 15 ms per epoch on a PC with Intel® Core™ i7 4.20 GHz processor and 48 GB RAM. The code was developed on the Python Jupyter notebook.

## 5.6 CONCLUSION

In this study, the EEG signals are reproduced using a linear combination of the states of dynamical neurons connected in a network by weak couplings and operating in the CAS regime. We provide the evidence that MI-EEG data can be generated well using CAS model in four frequency bands, as demonstrated by the results from Figure 5.7. Furthermore, the coefficients of the linear regression to model the EEG signals were used as feature vectors for classification. The performance of the proposed feature extraction method is compared with CNN-based methods for both intra-subject and across-subjects MI-EEG classification. Through the results of experiments, we first found that the CAS-based method successfully maintains important features of EEG signals, thereby improving the performance. Compared with non-feature extraction and FFT method, our proposed methods achieved superior classification performance for the intra-subject setting. Furthermore, our

proposed method outperformed the classification accuracy with the state-of-the-art methods such as HS-CNN and DBN for across-subjects classification.

In conclusion, this work demonstrates the superior performance and promising potential of the proposed EEG feature extraction (by the CAS model approach) and further classification method (by the CNN approach) using fewer assumptions. This article could pave the way for the practical implementation of an across-subject BCI. In recent years, researchers have tried their best to design online BCI systems for commercial use. The accuracy and non-stationarity characteristics of this signal are still a challenge for real-time BCI implementation. An online BCI system requires that the algorithm has a high performance. The method proposed in this study could achieve superior classification performance for both intra-subject and across-subjects settings. Using the linear combination of the time series obtained from simulations of HR neural networks, our proposed method is independent from the model order, not the case for autoregressive methods. Moreover, the time-domain-based feature extraction approach allows a short-segmented data. Therefore, the proposed method would potentially contribute to the online BCI system design.

However, there are still several challenging issues that need to be addressed for future investigations. Firstly, the proposed method was compared with FFT features with one dataset. Further works on different features should be implemented to give reliable results. In addition, we used a simple CNN structure in this study. Several new architectures are worthwhile to explore to boost the performance further.

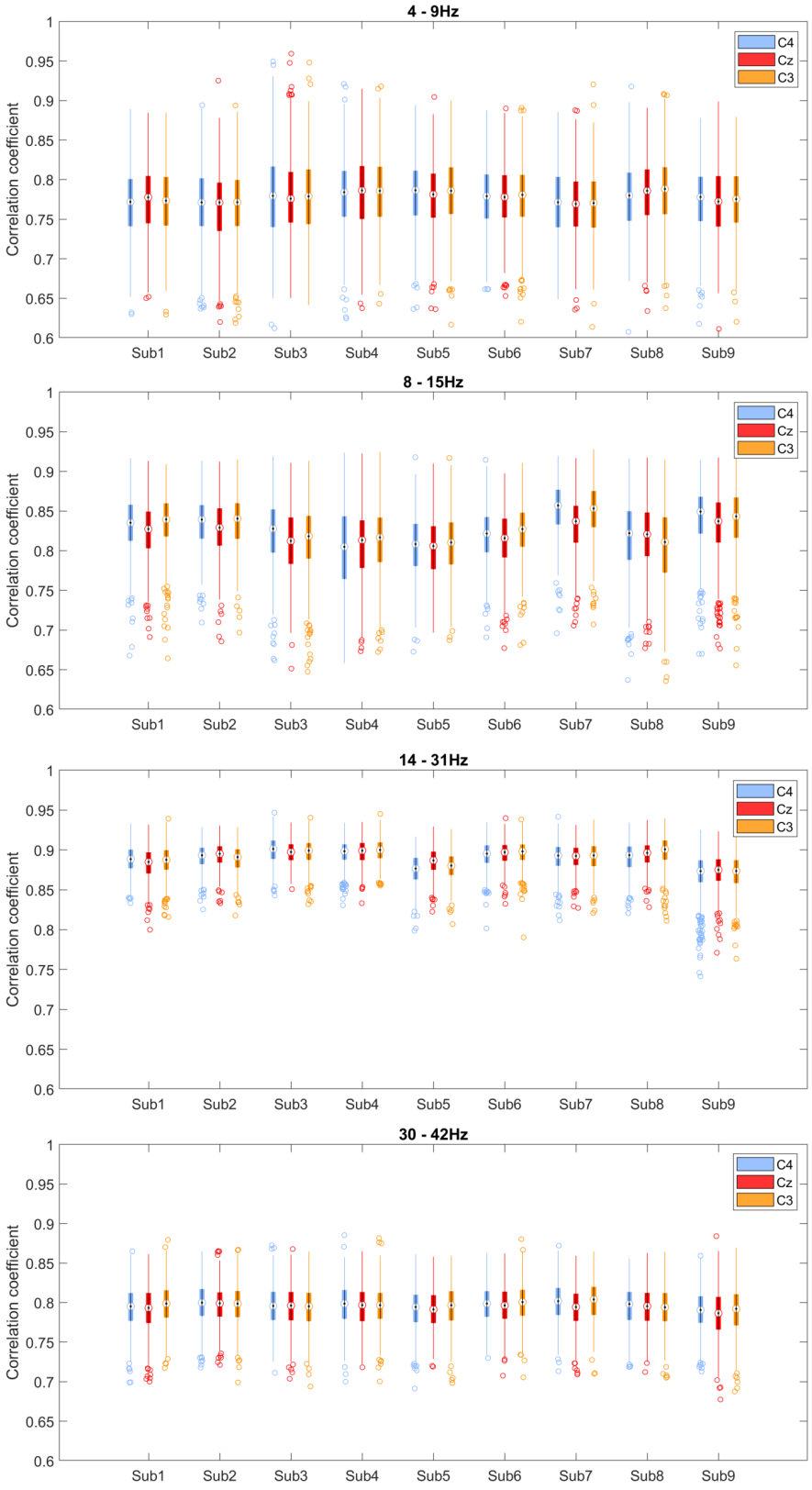


Figure 5.7: Boxplot of estimated correlation values between actual EEG trials and generated EEG by HR neurons in four frequency bands.

# 6

# IMPACT AND FUTURE DIRECTION

## 6.1 IMPACT

This thesis will have a broader impact on the fields of the neuroscience of movement, neuronal processes in EEG analysis, and BCI. This will significantly contribute to improving the understanding of brain operation. The dynamical networks formed by Kuramoto phase oscillators and HR neuron models can be used to reproduce EEG signals. This gives a deeper insight into the neuronal mechanisms and provides a new novel method for EEG signal modeling. This research has a long prediction period sufficient for classifying epilepsy seizure detection and several analyses during a short period as motor imagery classification. EEG measurement has long been a favorite as a neuroimaging technique for developing BCI applications because of its compactness, portability, and ease of use. However, EEG signals are often noisy and affect the performance of the BCI system. It is also susceptible to noise and artifacts. The EEG signal is roughly the result of the accumulation of nerve spike information beneath the scalp's surface. In the practical application of BCI, it is difficult to collect large data sets, which may lead to overfitting of classifiers and weak generalization. Also, acquiring low-noise data is very expensive. The proposed EEG modeling may help reinforce the EEG signal and thus improve the performance of the BCI.

This thesis shows that the EEG signals could be functioning in a reservoir network and CAS regime. It will be possible to carry out methods and analyses of its mechanism. In addition, if the mechanism can be elucidated, it will be possible to eliminate changes in brain activity related to the type of disease, imagery action, or emotion. This thesis is expected to improve the accuracy of observation of characteristics of brain activities, lead to further elucidation of the brain's mechanism, and significantly contribute to the progress of neuroscience. Especially forecasting EEG signals have a number of potential benefits for BCI systems.

EEG signal classification, in general, requires investigation of feature extraction. Feature extraction of EEG signals is a challenging problem and has received much attention over the past decade. AR model and FFT are widely used to extract

features from EEG signals. This thesis also contributed a new method for EEG feature extraction that can improve the disadvantage of the AR model and get higher accuracy than FFT. Moreover, EEG recognition has greater potential in security with respect to research than facial and speech-based methods, given that internal nerve fluctuations cannot be deliberately masked or controlled. In previous studies, subject-independent recognition was difficult to achieve when compared with subject-dependent EEG classification. Our proposed method developed for MI classification subject-independent was found to be effective.

## 6.2 FUTURE DIRECTION

The novel approach of reproducing EEG could be used as a new research tool in neuroscience and it will be interesting to find its applications. In the field of modeling EEG, we have many challenges. EEG signals are nonstationary in nature. For long-term predictions, our model should incorporate some time-varying configurations tuned to adapt to the varying nature of the experimental signal being modeled. It will be interesting to study whether the combination of CAS regime and RC can be used to learn parameters for an EEG model.

Secondly, for studying EEG generation further, it would also be interesting to look at a method that can be obtained a surrogate EEG data. The work done by [161] has spiking neural network (SNN) to enhance the classification performance by generating task-related multi-channel EEG template signals. The node in an SNN adheres to the dynamics of a spiking neuron. The new approach with CAS-regime can give a further method for generating surrogate EEG data.

Finally, the proposed feature extraction method was compared with FFT features with one dataset. Further works on different features should be implemented to give reliable results. In addition, we used a simple CNN structure in this study. Several new architectures are worthwhile exploring to boost the performance further.

# BIBLIOGRAPHY


[1] A. Biasiucci, B. Franceschiello and M. M. Murray, 'Electroencephalography', *Current Biology*, vol. 29, 3 2019, ISSN: 09609822. DOI: 10.1016/j.cub.2018.11.052.

[2] R. Shalbaf, H. Behnam and H. J. Moghadam, 'Monitoring depth of anesthesia using combination of eeg measure and hemodynamic variables', *Cognitive Neurodynamics*, vol. 9, 1 2015, ISSN: 18714099. DOI: 10.1007/s11571-014-9295-z.

[3] J. Britton, L. Frey, J. Hopp, P. Korb, M. Koubeissi, W. Lievens, E. Pestana-Knight and E. S. Louis, 'Electroencephalography (eeg): An introductory text and atlas of normal and abnormal findings in adults, children, and infants', *Chicago: American Epilepsy Society*, 2016.

[4] M. A. Bell and K. Cuevas, 'Using eeg to study cognitive development: Issues and practices', *Journal of Cognition and Development*, vol. 13, 3 2012, ISSN: 15248372. DOI: 10.1080/15248372.2012.691143.

[5] H. P. Ren, C. Bai, M. S. Baptista and C. Grebogi, 'Weak connections form an infinite number of patterns in the brain', *Scientific Reports*, vol. 7, 2017, ISSN: 20452322. DOI: 10.1038/srep46472.

[6] C. E. Stevens and D. L. Zabelina, 'Creativity comes in waves: An eeg-focused exploration of the creative brain', *Current Opinion in Behavioral Sciences*, vol. 27, 2019, ISSN: 23521546. DOI: 10.1016/j.cobeha.2019.02.003.

[7] P. T. M. Nguyen, Y. Hayashi, M. D. S. Baptista and T. Kondo, 'Collective almost synchronization-based model to extract and predict features of eeg signals', *Scientific Reports*, vol. 10, 1 Dec. 2020, ISSN: 20452322. DOI: 10.1038/s41598-020-73346-z.

[8] G. Tanaka, T. Yamane, J. B. Héroux, R. Nakane, N. Kanazawa, S. Takeda, H. Numata, D. Nakano and A. Hirose, 'Recent advances in physical reservoir computing: A review', *Neural Networks*, vol. 115, pp. 100–123, 2019, ISSN: 18792782. DOI: 10.1016/j.neunet.2019.03.005. [Online]. Available: https://doi.org/10.1016/j.neunet.2019.03.005.

[9] D. J. Gauthier, E. Bollt, A. Griffith and W. A. Barbosa, 'Next generation reservoir computing', *Nature Communications*, vol. 12, 1 2021, ISSN: 20411723. DOI: 10.1038/s41467-021-25801-2.

[10] T. Kim and B. R. King, 'Time series prediction using deep echo state networks', *Neural Computing and Applications*, vol. 32, 23 2020, ISSN: 14333058. DOI: 10.1007/s00521-020-04948-x.

[11] F. A. Araujo *et al.*, 'Role of non-linear data processing on speech recognition task in the framework of reservoir computing', *Scientific Reports*, vol. 10, 1 2020, ISSN: 20452322. DOI: 10.1038/s41598-019-56991-x.

[12] F. Cincotti, D. Mattia, F. Aloise, S. Bufalari, G. Schalk, G. Oriolo, A. Cherubini, M. G. Marciani and F. Babiloni, 'Non-invasive brain-computer interface system: Towards its application as assistive technology', *Brain Research Bulletin*, vol. 75, 6 2008, ISSN: 03619230. DOI: 10.1016/j.brainresbull.2008.01.007.

[13] M. Zhuang, Q. Wu, F. Wan and Y. Hu, 'State-of-the-art non-invasive brain–computer interface for neural rehabilitation: A review', *Journal of Neurorestoratology*, vol. 08, 01 2020, ISSN: 2324-2426. DOI: 10.26599/jnr.2020.9040001.

[14] M. T. Heideman, D. H. Johnson and C. S. Burrus, 'Gauss and the history of the fast fourier transform', *IEEE ASSP Magazine*, vol. 1, 4 1984, ISSN: 07407467. DOI: 10.1109/MASSP.1984.1162257.

[15] A. S. Al-Fahoum and A. A. Al-Fraihat, 'Methods of eeg signal features extraction using linear analysis in frequency and time-frequency domains', *ISRN Neuroscience*, vol. 2014, 2014, ISSN: 2314-4661. DOI: 10.1155/2014/730218.

[16] M. Frigo and S. G. Johnson, 'Fftw: An adaptive software architecture for the fft', vol. 3, 1998. DOI: 10.1109/ICASSP.1998.681704.

[17] Z. Huang and M. Wang, 'A review of electroencephalogram signal processing methods for brain-controlled robots', *Cognitive Robotics*, vol. 1, 2021, ISSN: 26672413. DOI: 10.1016/j.cogr.2021.07.001.

[18] A. Zabidi, W. Mansor, Y. L. Khuan and C. W. C. W. Fadzal, 'Classification of imagined writing from eeg signals using autoregressive features', 2012. DOI: 10.1109/ISCAIE.2012.6482097.

[19] C. Yang, R. L. B. Jeannes, J. J. Bellanger and H. Shu, 'A new strategy for model order identification and its application to transfer entropy for eeg signals analysis', *IEEE Transactions on Biomedical Engineering*, vol. 60, 5 2013, ISSN: 00189294. DOI: 10.1109/TBME.2012.2234125.

[20] Z. Tayeb, J. Fedjaev, N. Ghaboosi, C. Richter, L. Everding, X. Qu, Y. Wu, G. Cheng and J. Conradt, 'Validating deep neural networks for online decoding of motor imagery movements from eeg signals', *Sensors (Switzerland)*, vol. 19, 1 2019, ISSN: 14248220. DOI: 10.3390/s19010210.

[21] M. Le Van Quyen, L. E. Muller, B. Telenczuk, E. Halgren, S. Cash, N. G. Hatsopoulos, N. Dehghani and A. Destexhe, 'High-frequency oscillations in human and monkey neocortex during the wake–sleep cycle', *Proceedings of the National Academy of Sciences*, vol. 113, no. 33, pp. 9363–9368, Aug. 2016, ISSN: 0027-8424. DOI: 10.1073/pnas.1523583113.

[22] L. F. Haas, 'Hans berger (1873-1941), richard caton (1842-1926), and electroencephalography.', *Journal of neurology, neurosurgery, and psychiatry*, vol. 74, 1 2003, ISSN: 00223050. DOI: 10.1136/jnnp.74.1.9.

[23] P. Ghorbanian, S. Ramakrishnan, H. Ashrafiuon and F. Liao, 'Stochastic non-linear oscillator models of EEG : the Alzheimer ' s disease case', *Frontiers in Computational Neuroscience*, vol. 9, no. April, pp. 1–14, 2015. DOI: 10.3389/fncom.2015.00048.

[24] F. Shayegh, R. A. Fattahi, S. Sadri and K. Ansari-Asl, 'A brief survey of computational models of normal and epileptic EEG signals: A guideline to model-based seizure prediction', *Journal of Medical Signals and Sensors*, vol. 1, no. 1, pp. 62–72, Jan. 2011. DOI: 10.4103/2228-7477.83521.

[25] J. Schumann-Bischoff, S. Luther and U. Parlitz, 'Estimability and dependency analysis of model parameters based on delay coordinates', *Physical Review E*, vol. 94, no. 3, Sep. 2016. DOI: 10.1103/PhysRevE.94.032221.

[26] F. Mansouri, K. Dunlop, P. Giacobbe, J. Downar and J. Zariffa, 'A fast EEG forecasting algorithm for phase-locked transcranial electrical stimulation of the human brain', *Frontiers in Neuroscience*, vol. 11, no. 410, Jul. 2017. DOI: 10.3389/fnins.2017.00401.

[27] G. Ibagon, C. A. Kothe and T. Mullen, 'Deep Neural Networks for Forecasting Single-Trial Event-Related Neural Activity', *2018 IEEE International Conference on Systems, Man, and Cybernetics (SMC)*, pp. 1070–1075, 2018. DOI: 10.1109/SMC.2018.00189.

[28] P. P. Paul and H. Leung, 'Combining temporal and frequencybased prediction for EEG signals', in *Proceedings of the Third International Conference on Bio-inspired Systems and Signal Processing*, 2010, pp. 29–36, ISBN: 0002696800. DOI: 10.5220/0002696800290036.

[29] A. S. Benjamin, H. L. Fernandes, T. Tomlinson, P. Ramkumar, C. Versteeg, R. H. Chowdhury, L. E. Miller and K. P. Kording, 'Modern machine learning as a benchmark for fitting neural responses', *Frontiers in Computational Neuroscience*, vol. 12, no. July, pp. 1–13, 2018, ISSN: 16625188. DOI: 10.3389/fncom.2018.00056.

[30] J. Gonzalez-Castillo, C. W. Hoy, D. A. Handwerker, M. E. Robinson, L. C. Buchanan, Z. S. Saad and P. A. Bandettini, 'Tracking ongoing cognition in individuals using brief, whole-brain functional connectivity patterns', *Proceedings of the National Academy of Sciences*, vol. 112, no. 28, pp. 8762–8767, Jul. 2015, ISSN: 0027-8424. DOI: 10.1073/PNAS.1501242112. [Online]. Available: https://www.pnas.org/content/112/28/8762.

[31] P. Barttfeld, L. Uhrig, J. D. Sitt, M. Sigman, B. Jarraya and S. Dehaene, 'Signature of consciousness in the dynamics of resting-state brain activity', *PNAS*, vol. 98, no. 2, pp. 676–682, 2015. DOI: 10.1073/pnas.98.2.676. [Online]. Available: https://www.pnas.org/content/112/3/887.

[32] I. Cribben, R. Haraldsdottir, L. Y. Atlas, T. D. Wager and M. A. Lindquist, 'Dynamic connectivity regression: Determining state-related changes in brain connectivity', *NeuroImage*, vol. 61, 4 2012, ISSN: 10538119. DOI: 10.1016/j.neuroimage.2012.03.070.

[33] E. Damaraju *et al.*, 'Dynamic functional connectivity analysis reveals transient states of dysconnectivity in schizophrenia', *NeuroImage: Clinical*, vol. 5, 2014, ISSN: 22131582. DOI: 10.1016/j.nicl.2014.07.003.

[34] E. A. Allen, E. Damaraju, T. Eichele, L. Wu and V. D. Calhoun, 'EEG Signatures of Dynamic Functional Network Connectivity States', *Brain Topography*, vol. 31, no. 1, pp. 101–116, Jan. 2018, ISSN: 15736792. DOI: 10.1007/s10548-017-0546-2.

[35] H. A. Marusak, V. D. Calhoun, S. Brown, L. M. Crespo, K. Sala-Hamrick, I. H. Gotlib and M. E. Thomason, 'Dynamic functional connectivity of neurocognitive networks in children', *Human Brain Mapping*, vol. 38, no. 1, pp. 97–108, Jan. 2017, ISSN: 10970193. DOI: 10.1002/hbm.23346.

[36] A. H. C. Fong, K. Yoo, M. D. Rosenberg, S. Zhang, C. S. R. Li, D. Scheinost, R. T. Constable and M. M. Chun, 'Dynamic functional connectivity during task performance and rest predicts individual differences in attention across studies', *NeuroImage*, vol. 188, pp. 14–25, Mar. 2019, ISSN: 10959572. DOI: 10.1016/j.neuroimage.2018.11.057.

[37] Y. Ma, C. Hamilton and N. Zhang, 'Dynamic Connectivity Patterns in Conscious and Unconscious Brain', *Brain Connectivity*, vol. 7, no. 1, pp. 1–12, 2016, ISSN: 2158-0014. DOI: 10.1089/brain.2016.0464.

[38] A. S. Ghuman, J. R. McDaniel and A. Martin, 'A wavelet-based method for measuring the oscillatory dynamics of resting-state functional connectivity in meg', *NeuroImage*, vol. 56, 1 2011, ISSN: 10538119. DOI: 10.1016/j.neuroimage.2011.01.046.

[39] J. P. Lachaux, E. Rodriguez, M. L. V. Quyen, A. Lutz, J. Martinerie and F. J. Varela, 'Studying single-trials of phase synchronous activity in the brain', *International Journal of Bifurcation and Chaos in Applied Sciences and Engineering*, vol. 10, 10 2000, ISSN: 02181274. DOI: 10.1142/S0218127400001560.

[40] M. Newman and M. E. J. Newman, 'Mathematics of networks', in *Networks*, Oxford University Press, Sep. 2010, pp. 109–167. DOI: 10.1093/acprof:oso/9780199206650.003.0006.

[41] A. N. Langville and C. D. Meyer, 'Google's pagerank and beyond: The science of search engine rankings', *Google's PageRank and Beyond: The Science of Search Engine Rankings*, 2011, ISSN: 0343-6993. DOI: 10.1007/bf02985759.

[42] P. Bonacich, 'Factoring and weighting approaches to status scores and clique identification', *The Journal of Mathematical Sociology*, vol. 2, no. 1, pp. 113–120, Aug. 2010, ISSN: 0022-250X. DOI: 10.1080/0022250x.1972.9989806.

[43] J. R. Sato *et al.*, 'Connectome hubs at resting state in children and adolescents: Reproducibility and psychopathological correlation', *Developmental Cognitive Neuroscience*, vol. 20, pp. 2–11, Aug. 2016, ISSN: 18789307. DOI: 10.1016/j.dcn.2016.05.002.

[44] A. Corduneanu and C. M. Bishop, 'Variational Bayesian Model Selection for Mixture Distributions', *In Artificial Intelligence and Statistics*, pp. 27–34, 2001. [Online]. Available: http://research.microsoft.com/âĹijcmbishop.

[45] M. P. van den Heuvel and O. Sporns, 'Network hubs in the human brain', *Trends in Cognitive Sciences*, vol. 17, no. 12, pp. 683–696, 2013, ISSN: 13646613. DOI: 10.1016/j.tics.2013.09.012. [Online]. Available: http://dx.doi.org/10.1016/j.tics.2013.09.012.

[46] E. N. Davison, K. J. Schlesinger, D. S. Bassett, M. E. Lynall, M. B. Miller, S. T. Grafton and J. M. Carlson, 'Brain Network Adaptability across Task States', *PLoS Computational Biology*, vol. 11, no. 1, 2015, ISSN: 15537358. DOI: 10.1371/journal.pcbi.1004029.

[47] J. R. Cohen, 'The behavioral and cognitive relevance of time-varying, dynamic changes in functional connectivity', *NeuroImage*, vol. 180, 2018, ISSN: 10959572. DOI: 10.1016/j.neuroimage.2017.09.036.

[48] T. M. P. Nguyen, X. Li, Y. Hayashi, S. Yano and T. Kondo, 'Estimation of brain dynamics under visuomotor task using functional connectivity analysis based on graph theory', in *2019 IEEE 19th International Conference on Bioinformatics and Bioengineering (BIBE)*, 2019, pp. 577–582. DOI: 10.1109/BIBE.2019.00110.

[49] P. Bashivan, I. Rish, M. Yeasin and N. Codella, 'Learning Representations from EEG with Deep Recurrent-Convolutional Neural Networks', Nov. 2015. [Online]. Available: http://arxiv.org/abs/1511.06448.

[50] N. Lu, T. Li, X. Ren and H. Miao, 'A Deep Learning Scheme for Motor Imagery Classification based on Restricted Boltzmann Machines', *IEEE Transactions on Neural Systems and Rehabilitation Engineering*, vol. 25, no. 6, pp. 566–576, 2017, ISSN: 15344320. DOI: 10.1109/TNSRE.2016.2601240.

[51] S. Sakhavi, C. Guan and S. Yan, 'Learning Temporal Information for Brain-Computer Interface Using Convolutional Neural Networks', *IEEE Transactions on Neural Networks and Learning Systems*, vol. 29, no. 11, 2018, ISSN: 21622388. DOI: 10.1109/TNNLS.2018.2789927.

[52] H. Yang, S. Sakhavi, K. K. Ang and C. Guan, 'On the use of convolutional neural networks and augmented CSP features for multi-class motor imagery of EEG signals classification', *Proceedings of the Annual International Conference of the IEEE Engineering in Medicine and Biology Society, EMBS*, vol. 2015-Novem, pp. 2620–2623, 2015, ISSN: 1557170X. DOI: 10.1109/EMBC.2015.7318929.

[53] R. T. Schirrmeister, J. T. Springenberg, L. D. J. Fiederer, M. Glasstetter, K. Eggensperger, M. Tangermann, F. Hutter, W. Burgard and T. Ball, 'Deep learning with convolutional neural networks for EEG decoding and visualization', *Human Brain Mapping*, vol. 38, no. 11, pp. 5391–5420, 2017, ISSN: 10970193. DOI: 10.1002/hbm.23730.

[54] H. K. Lee and Y. S. Choi, 'A convolution neural networks scheme for classification of motor imagery EEG based on wavelet time-frequecy image', *International Conference on Information Networking*, vol. 2018-Janua, pp. 906–909, 2018, ISSN: 19767684. DOI: 10.1109/ICOIN.2018.8343254.

[55] O. Orenstein and H. Keren, 'Development of cortical networks under continuous stimulation', *Frontiers in Molecular Neuroscience*, vol. 10, no. 18, Jan. 2017. DOI: 10.3389/fnmol.2017.00018.

[56] H. Ju, M. R. Dranias, G. Banumurthy and A. M. Vandongen, 'Spatiotemporal memory is an intrinsic property of networks of dissociated cortical neurons', *Journal of Neuroscience*, vol. 35, no. 9, pp. 4040–4051, 2015. DOI: 10.1523/JNEUROSCI.3793-14.2015.

[57] A. H. Marblestone *et al.*, 'Physical principles for scalable neural recording', *Frontiers in Computational Neuroscience*, vol. 7, p. 137, Oct. 2013. DOI: 10.3389/fncom.2013.00137.

[58] C. Siettos and J. Starke, 'Multiscale modeling of brain dynamics: from single neurons and networks to mathematical tools', *Wiley Interdisciplinary Reviews: Systems Biology and Medicine*, vol. 8, no. 5, pp. 438–458, Sep. 2016. DOI: 10.1002/wsbm.1348.

[59] G. J. Goodhill, 'Theoretical Models of Neural Development', *iScience*, vol. 8, pp. 183–199, 2018. DOI: 10.1016/j.isci.2018.09.017. [Online]. Available: https://doi.org/10.1016/j.isci.2018.09.017.

[60] S. G. Tewari, M. K. Gottipati and V. Parpura, 'Mathematical modeling in neuroscience: Neuronal activity and its modulation by astrocytes', *Frontiers in Integrative Neuroscience*, vol. 10, no. 3, 2016. DOI: 10.3389/fnint.2016.00003.

[61] G. T. Einevoll, 'Mathematical modelling of neural activity', in *Dynamics of Complex Interconnected Systems: Networks and Bioprocesses*, Springer Netherlands, Dec. 2006, pp. 127–145. DOI: 10.1007/1-4020-5030-5{_}8.

[62] M. T. Lo, P. H. Tsai, P. F. Lin, C. Lin and Y. L. Hsin, 'The nonlinear and nonstationary properties in EEG signals: Probing the complex fluctuations by Hilbert-huang transform', *Advances in Adaptive Data Analysis*, vol. 1, no. 3, pp. 461–482, Jul. 2009, ISSN: 17935369. DOI: 10.1142/S1793536909000199.

[63] P. Ghorbanian, S. Ramakrishnan, A. J. Simon and H. Ashrafiuon, 'Stochastic Dynamic Modeling of the Human Brain EEG Signal', in *Proceedings of the ASME 2013 Dynamic Systems and Control Conference*, Oct. 2013. DOI: 10.1115/dscc2013-3881.

[64] P. I. Keeton, F. S. Schlindwein and D. H. Evans, 'A study of the spectral broadening of simulated Doppler signals using FFT and AR modelling', *Ultrasound in Medicine and Biology*, vol. 23, no. 7, pp. 1033–1045, 1997, ISSN: 03015629. DOI: 10.1016/S0301-5629(97)00020-3.

[65] M. Wairagkar, Y. Hayashi and S. J. Nasuto, 'Modeling the Ongoing Dynamics of Short and Long-Range Temporal Correlations in Broadband EEG During Movement', *Frontiers in Systems Neuroscience*, vol. 13, p. 66, 2019. DOI: 10.3389/fnsys.2019.00066.

[66] Y. Roy, H. Banville, I. Albuquerque, A. Gramfort, T. H. Falk and J. Faubert, 'Deep learning-based electroencephalography analysis: A systematic review', *Journal of Neural Engineering*, vol. 16, no. 5, Aug. 2019. DOI: 10.1088/1741-2552/ab260c.

[67] G Pfurtscheller and F. H. Lopes Da Silva, 'Event-related EEG/MEG synchronization and desynchronization: basic principles', *Clinical Neurophysiology*, vol. 110, no. 11, pp. 1842–1857, 1999. DOI: 10.1016/s1388-2457(99)00141-8. [Online]. Available: www.elsevier.com/locate/clinph.

[68] Y. Aoh, H. J. Hsiao, M. K. Lu, A. Macerollo, H. C. Huang, M. Hamada, C. H. Tsai and J. C. Chen, 'Event-related desynchronization/synchronization in spinocerebellar ataxia type 3', *Frontiers in Neurology*, vol. 10, p. 822, 2019. DOI: 10.3389/fneur.2019.00822. [Online]. Available: https://www.frontiersin.org/article/10.3389/fneur.2019.00822.

[69] W. Klonowski, 'Everything you wanted to ask about EEG but were afraid to get the right answer', *Nonlinear Biomedical Physics*, vol. 3, no. 1, p. 2, May 2009, ISSN: 17534631. DOI: 10.1186/1753-4631-3-2.

[70] J. L. Hindmarsh and R. M. Rose, 'A model of neuronal bursting using three coupled first order differential equations.', *Proceedings of the Royal Society of London. Series B, Containing papers of a Biological character. Royal Society (Great Britain)*, vol. 221, 1222 1984, ISSN: 00804649. DOI: 10.1098/rspb.1984.0024.

[71] S. H. Strogatz, 'From kuramoto to crawford: Exploring the onset of synchronization in populations of coupled oscillators', *Physica D: Nonlinear Phenomena*, vol. 143, 1-4 2000, ISSN: 01672789. DOI: 10.1016/S0167-2789(00)00094-4.

[72] M. S. Baptista, H. P. Ren, J. C. Swarts, R. Carareto, H. Nijmeijer and C. Grebogi, 'Collective Almost Synchronisation in Complex Networks', *PLoS ONE*, vol. 7, no. 11, e48118, 2012. DOI: 10.1371/journal.pone.0048118.

[73] S. Heitmann, M. J. Aburn and M. Breakspear, 'The brain dynamics toolbox for matlab', *Neurocomputing*, vol. 315, 2018, ISSN: 18728286. DOI: 10.1016/j.neucom.2018.06.026.

[74] X. Chen and J. Ji, 'The minimum-norm least-squares solution of a linear system and symmetric rank-one updates', *Electronic Journal of Linear Algebra*, vol. 22, 480–489, 2011. DOI: 10.13001/1081-3810.1451.

[75] Q. Yan and Y. Liu, 'A predictive dynamic neural network model based on principal component analysis (PCA) and its application', in *Applied Mechanics and Materials*, vol. 127, 2012, pp. 19–24, ISBN: 9783037852835. DOI: 10.4028/www.scientific.net/AMM.127.19.

[76] H. Abdi and L. J. Williams, 'Principal component analysis', *Wiley Interdisciplinary Reviews: Computational Statistics*, vol. 2, no. 4, pp. 433–459, Jul. 2010. DOI: 10.1002/wics.101.

[77] B. Rahmani, C. K. Wong, P. Norouzzadeh, J. Bodurka and B. McKinney, 'Dynamical Hurst analysis identifies EEG channel differences between PTSD and healthy controls', *PLoS ONE*, vol. 14, no. 3, e0214527, 2018. DOI: 10.1371/journal.pone.0199144.

[78] R. G. Andrzejak, K. Lehnertz, F. Mormann, C. Rieke, P. David and C. E. Elger, 'Indications of nonlinear deterministic and finite-dimensional structures in time series of brain electrical activity: Dependence on recording region and brain state', *Physical Review E - Statistical Physics, Plasmas, Fluids, and Related Interdisciplinary Topics*, vol. 64, no. 6, p. 6 061 907, 2001. DOI: 10.1103/PhysRevE.64.061907.

[79] S. Madan, K. Srivastava, A. Sharmila and P. Mahalakshmi, 'A case study on Discrete Wavelet Transform based Hurst exponent for epilepsy detection', *Journal of Medical Engineering and Technology*, vol. 42, no. 1, pp. 9–17, Jan. 2018, ISSN: 1464522X. DOI: 10.1080/03091902.2017.1394390.

[80] D. P. Subha, P. K. Joseph, R. Acharya U and C. M. Lim, 'EEG signal analysis: a survey.', *Journal of medical systems*, vol. 34, no. 2, pp. 195–212, 2010, ISSN: 01485598. DOI: 10.1007/s10916-008-9231-z.

[81] Q. Yuan, W. Zhou, S. Li and D. Cai, 'Epileptic EEG classification based on extreme learning machine and nonlinear features', *Epilepsy Research*, vol. 96, no. 1-2, pp. 29–38, Sep. 2011, ISSN: 09201211. DOI: 10.1016/j.eplepsyres.2011.04.013.

[82] S. Lahmiri, 'Generalized Hurst exponent estimates differentiate EEG signals of healthy and epileptic patients', *Physica A: Statistical Mechanics and its Applications*, vol. 490, pp. 378–385, Jan. 2018, ISSN: 03784371. DOI: 10.1016/j.physa.2017.08.084.

[83] H. E. Hurst, 'Long-term Storage Capacity of Reservoirs', *Transactions of the American Society of Civil Engineers*, vol. 116, pp. 770–799, 1951.

[84] O. Dressler, G. Schneider, G. Stockmanns and E. F. Kochs, 'Awareness and the EEG power spectrum: Analysis of frequencies', *British Journal of Anaesthesia*, vol. 93, no. 6, pp. 806–809, 2004, ISSN: 00070912. DOI: 10.1093/bja/aeh270.

[85] M. G. Tsipouras, 'Spectral information of EEG signals with respect to epilepsy classification', *Eurasip Journal on Advances in Signal Processing*, vol. 2019, Dec. 2019. DOI: 10.1186/s13634-019-0606-8.

[86] M. K. van Vugt, P. B. Sederberg and M. J. Kahana, 'Comparison of spectral analysis methods for characterizing brain oscillations', *Journal of Neuroscience Methods*, vol. 162, no. 1-2, pp. 49–63, May 2007, ISSN: 01650270. DOI: 10.1016/j.jneumeth.2006.12.004.

[87] K. Nakayashiki, M. Saeki, Y. Takata, Y. Hayashi and T. Kondo, 'Modulation of event-related desynchronization during kinematic and kinetic hand movements', *Journal of NeuroEngineering and Rehabilitation*, vol. 11, p. 90, 2014. DOI: 10.1186/1743-0003-11-90. [Online]. Available: http://www.jneuroengrehab.com/content/11/1/90.

[88] B. Yan and P. Li, 'The emergence of abnormal hypersynchronization in the anatomical structural network of human brain', *NeuroImage*, vol. 65, pp. 34–51, Jan. 2013, ISSN: 10538119. DOI: 10.1016/j.neuroimage.2012.09.031.

[89] H. Schmidt, G. Petkov, M. P. Richardson and J. R. Terry, 'Dynamics on Networks: The Role of Local Dynamics and Global Networks on the Emergence of Hypersynchronous Neural Activity', *PLoS Computational Biology*, vol. 10, no. 11, e1003947, 2014. DOI: 10.1371/journal.pcbi.1003947.

[90] J. Dong, M. Rafayelyan, F. Krzakala and S. Gigan, 'Optical reservoir computing using multiple light scattering for chaotic systems prediction', *IEEE Journal of Selected Topics in Quantum Electronics*, vol. 26, 1 2020, ISSN: 15584542. DOI: 10.1109/JSTQE.2019.2936281.

[91] H. Jaeger, 'The "echo state" approach to analysing and training recurrent neural networks', *GMD Report*, vol. 148, 2001.

[92] W. Maass, T. Natschläger and H. Markram, 'Real-time computing without stable states: A new framework for neural computation based on perturbations', *Neural Computation*, vol. 14, 11 2002, ISSN: 08997667. DOI: 10.1162/089976602760407955.

[93] W. Maass, P. Joshi and E. D. Sontag, 'Computational aspects of feedback in neural circuits', *PLoS Computational Biology*, vol. 3, 1 2007, ISSN: 1553734X. DOI: 10.1371/journal.pcbi.0020165.

[94] M. S. Baptista, H. P. Ren, J. C. Swarts, R. Carareto, H. Nijmeijer and C. Grebogi, 'Collective almost synchronisation in complex networks', *PLoS ONE*, vol. 7, 11 2012, ISSN: 19326203. DOI: 10.1371/journal.pone.0048118.

[95] A. Y. Kaplan, A. A. Fingelkurts, A. A. Fingelkurts, S. V. Borisov and B. S. Darkhovsky, 'Nonstationary nature of the brain activity as revealed by EEG/MEG: Methodological, practical and conceptual challenges', *Signal Processing*, vol. 85, no. 11, 2005, ISSN: 01651684. DOI: 10.1016/j.sigpro.2005.07.010.

[96] S. Aggarwal and N. Chugh, 'Signal processing techniques for motor imagery brain computer interface: A review', *Array*, vol. 1-2, 2019, ISSN: 25900056. DOI: 10.1016/j.array.2019.100003.

[97] K. Choi and A. Cichocki, 'Control of a wheelchair by motor imagery in real time', vol. 5326 LNCS, 2008. DOI: 10.1007/978-3-540-88906-9_42.

[98] F. Galán, M. Nuttin, E. Lew, P. W. Ferrez, G. Vanacker, J. Philips and J. del R. Millán, 'A brain-actuated wheelchair: Asynchronous and non-invasive brain-computer interfaces for continuous control of robots', *Clinical Neurophysiology*, vol. 119, 9 2008, ISSN: 13882457. DOI: 10.1016/j.clinph.2008.06.001.

[99] A. Vourvopoulos, S. Bermudez i Badia and F. Liarokapis, 'Eeg correlates of video game experience and user profile in motor-imagery-based brain–computer interaction', *Visual Computer*, vol. 33, 4 2017, ISSN: 01782789. DOI: 10.1007/s00371-016-1304-2.

[100] J. Cantillo-Negrete, R. I. Carino-Escobar, P. Carrillo-Mora, D. Elias-Vinas and J. Gutierrez-Martinez, 'Motor imagery-based brain-computer interface coupled to a robotic hand orthosis aimed for neurorehabilitation of stroke patients', *Journal of Healthcare Engineering*, vol. 2018, 2018, ISSN: 20402309. DOI: 10.1155/2018/1624637.

[101] C. Yang, H. Wu, Z. Li, W. He, N. Wang and C. Y. Su, 'Mind control of a robotic arm with visual fusion technology', *IEEE Transactions on Industrial Informatics*, vol. 14, 9 2018, ISSN: 15513203. DOI: 10.1109/TII.2017.2785415.

[102] N. S. Karuppusamy and B. Y. Kang, 'Driver fatigue prediction using eeg for autonomous vehicle', *Advanced Science Letters*, vol. 23, 10 2017, ISSN: 19367317. DOI: 10.1166/asl.2017.9747.

[103] L. Yang, R. Ma, H. M. Zhang, W. Guan and S. Jiang, 'Driving behavior recognition using eeg data from a simulated car-following experiment', *Accident Analysis and Prevention*, vol. 116, 2018, ISSN: 00014575. DOI: 10.1016/j.aap.2017.11.010.

[104] F. Yang, X. Zhao, W. Jiang, P. Gao and G. Liu, 'Multi-method fusion of cross-subject emotion recognition based on high-dimensional eeg features', *Frontiers in Computational Neuroscience*, vol. 13, 2019, ISSN: 16625188. DOI: 10.3389/fncom.2019.00053.

[105] N. Lu, T. Li, X. Ren and H. Miao, 'A deep learning scheme for motor imagery classification based on restricted boltzmann machines', *IEEE Transactions on Neural Systems and Rehabilitation Engineering*, vol. 25, 6 2017, ISSN: 15344320. DOI: 10.1109/TNSRE.2016.2601240.

[106] S. An, S. Kim, P. Chikontwe and S. H. Park, 'Few-shot relation learning with attention for eeg-based motor imagery classification', 2020. DOI: 10.1109/IROS45743.2020.9340933.

[107] G. Dai, J. Zhou, J. Huang and N. Wang, 'Hs-cnn: A cnn with hybrid convolution scale for eeg motor imagery classification', vol. 17, 2020. DOI: 10.1088/1741-2552/ab405f.

[108] Y. Li, W. Zheng, L. Wang, Y. Zong and Z. Cui, 'From regional to global brain: A novel hierarchical spatial-temporal neural network model for eeg emotion recognition', *IEEE Transactions on Affective Computing*, 2019, ISSN: 19493045. DOI: 10.1109/TAFFC.2019.2922912.

[109] J. Sun, R. Cao, M. Zhou, W. Hussain, B. Wang, J. Xue and J. Xiang, 'A hybrid deep neural network for classification of schizophrenia using eeg data', *Scientific Reports*, vol. 11, 1 2021, ISSN: 20452322. DOI: 10.1038/s41598-021-83350-6.

[110] N. Kumar, K. Alam and A. H. Siddiqi, 'Wavelet transform for classification of eeg signal using svm and ann', *Biomedical and Pharmacology Journal*, vol. 10, 4 2017, ISSN: 24562610. DOI: 10.13005/bpj/1328.

[111] R. Akut, 'Wavelet based deep learning approach for epilepsy detection', *Health Information Science and Systems*, vol. 7, 1 2019, ISSN: 2047-2501. DOI: 10.1007/s13755-019-0069-1.

[112] O. K. Cura, S. K. Atli, H. S. Türe and A. Akan, 'Epileptic seizure classifications using empirical mode decomposition and its derivative', *BioMedical Engineering Online*, vol. 19, 1 2020, ISSN: 1475925X. DOI: 10.1186/s12938-020-0754-y.

[113] D. X. Zhang, X. P. Wu and X. J. Guo, 'The eeg signal preprocessing based on empirical mode decomposition', 2008. DOI: 10.1109/ICBBE.2008.862.

[114] K. K. Ang, Z. Y. Chin, C. Wang, C. Guan and H. Zhang, 'Filter bank common spatial pattern algorithm on bci competition iv datasets 2a and 2b', *Frontiers in Neuroscience*, MAR 2012, ISSN: 16624548. DOI: 10.3389/fnins.2012.00039.

[115] H. Yu, H. Lu, S. Wang, K. Xia, Y. Jiang and P. Qian, 'A general common spatial patterns for eeg analysis with applications to vigilance detection', *IEEE Access*, vol. 7, 2019, ISSN: 21693536. DOI: 10.1109/ACCESS.2019.2934519.

[116] P. K. Saha, M. A. Rahman, M. K. Alam, A. Ferdowsi and M. N. Mollah, 'Common spatial pattern in frequency domain for feature extraction and classification of multichannel eeg signals', *SN Computer Science*, vol. 2, 3 2021, ISSN: 2662-995X. DOI: 10.1007/s42979-021-00586-9.

[117] V. Lawhern, W. D. Hairston, K. McDowell, M. Westerfield and K. Robbins, 'Detection and classification of subject-generated artifacts in eeg signals using autoregressive models', *Journal of Neuroscience Methods*, vol. 208, 2 2012, ISSN: 01650270. DOI: 10.1016/j.jneumeth.2012.05.017.

[118] R. Chai, G. R. Naik, T. N. Nguyen, S. H. Ling, Y. Tran, A. Craig and H. T. Nguyen, 'Driver fatigue classification with independent component by entropy rate bound minimization analysis in an eeg-based system', *IEEE Journal of Biomedical and Health Informatics*, vol. 21, 3 2017, ISSN: 21682194. DOI: 10.1109/JBHI.2016.2532354.

[119] Y. R. Tabar and U. Halici, 'A novel deep learning approach for classification of eeg motor imagery signals', *Journal of Neural Engineering*, vol. 14, 1 2017, ISSN: 17412552. DOI: 10.1088/1741-2560/14/1/016003.

[120] C. J. Stam, 'Nonlinear dynamical analysis of eeg and meg: Review of an emerging field', *Clinical Neurophysiology*, vol. 116, 10 2005, ISSN: 13882457. DOI: 10.1016/j.clinph.2005.06.011.

[121] P. Ghorbanian, S. Ramakrishnan and H. Ashrafiuon, 'Stochastic non-linear oscillator models of eeg: The alzheimer's disease case', *Frontiers in Computational Neuroscience*, vol. 9, APR 2015, ISSN: 16625188. DOI: 10.3389/fncom.2015.00048.

[122] J. Song, S. Gao, Y. Zhu and C. Ma, 'A survey of remote sensing image classification based on cnns', *Big Earth Data*, vol. 3, 3 2019, ISSN: 25745417. DOI: 10.1080/20964471.2019.1657720.

[123] P. Bashivan, I. Rish, M. Yeasin and N. Codella, 'Learning representations from eeg with deep recurrent-convolutional neural networks', 2016.

[124] N. K. N. Aznan, S. Bonner, J. Connolly, N. A. Moubayed and T. Breckon, 'On the classification of ssvep-based dry-eeg signals via convolutional neural networks', 2019. DOI: 10.1109/SMC.2018.00631.

[125] B. E. Olivas-Padilla and M. I. Chacon-Murguia, 'Classification of multiple motor imagery using deep convolutional neural networks and spatial filters', *Applied Soft Computing Journal*, vol. 75, 2019, ISSN: 15684946. DOI: 10.1016/j.asoc.2018.11.031.

[126] X. Lun, Z. Yu, T. Chen, F. Wang and Y. Hou, 'A simplified cnn classification method for mi-eeg via the electrode pairs signals', *Frontiers in Human Neuroscience*, vol. 14, 2020, ISSN: 16625161. DOI: 10.3389/fnhum.2020.00338.

[127] V. J. Lawhern, A. J. Solon, N. R. Waytowich, S. M. Gordon, C. P. Hung and B. J. Lance, 'Eegnet: A compact convolutional neural network for eeg-based brain-computer interfaces', *Journal of Neural Engineering*, vol. 15, 5 2018, ISSN: 17412552. DOI: 10.1088/1741-2552/aace8c.

[128] G. Xu, X. Shen, S. Chen, Y. Zong, C. Zhang, H. Yue, M. Liu, F. Chen and W. Che, 'A deep transfer convolutional neural network framework for eeg signal classification', *IEEE Access*, vol. 7, 2019, ISSN: 21693536. DOI: 10.1109/ACCESS.2019.2930958.

[129] R. Leeb, F. Lee, C. Keinrath, R. Scherer, H. Bischof and G. Pfurtscheller, 'Brain-computer communication: Motivation, aim, and impact of exploring a virtual apartment', *IEEE Transactions on Neural Systems and Rehabilitation Engineering*, vol. 15, 4 2007, ISSN: 15344320. DOI: 10.1109/TNSRE.2007.906956.

[130] M. Saeidi, W. Karwowski, F. V. Farahani, K. Fiok, R. Taiar, P. A. Hancock and A. Al-Juaid, 'Neural decoding of eeg signals with machine learning: A systematic review', *Brain Sciences*, vol. 11, 11 2021, ISSN: 20763425. DOI: 10.3390/brainsci11111525.

[131] M. F. Mridha, S. C. Das, M. M. Kabir, A. A. Lima, M. R. Islam and Y. Watanobe, 'Brain-computer interface: Advancement and challenges', *Sensors*, vol. 21, 17 2021, ISSN: 14248220. DOI: 10.3390/s21175746.

[132] I. Stancin, M. Cifrek and A. Jovic, 'A review of eeg signal features and their application in driver drowsiness detection systems', *Sensors*, vol. 21, 11 2021, ISSN: 14248220. DOI: 10.3390/s21113786.

[133] V. Harpale and V. Bairagi, 'An adaptive method for feature selection and extraction for classification of epileptic eeg signal in significant states', *Journal of King Saud University - Computer and Information Sciences*, 2018, ISSN: 22131248. DOI: 10.1016/j.jksuci.2018.04.014.

[134] M. R. Islam, T. Tanaka and M. K. I. Molla, 'Multiband tangent space mapping and feature selection for classification of eeg during motor imagery', *Journal of Neural Engineering*, vol. 15, 4 2018, ISSN: 17412552. DOI: 10.1088/1741-2552/aac313.

[135] E. D. Übeyli, 'Lyapunov exponents/probabilistic neural networks for analysis of eeg signals', *Expert Systems with Applications*, vol. 37, 2 2010, ISSN: 09574174. DOI: 10.1016/j.eswa.2009.05.078.

[136] C. Vidaurre, N. Krämer, B. Blankertz and A. Schlögl, 'Time domain parameters as a feature for eeg-based brain-computer interfaces', *Neural Networks*, vol. 22, 9 2009, ISSN: 08936080. DOI: 10.1016/j.neunet.2009.07.020.

[137] A. Khorshidtalab, M. J. Salami and M. Hamedi, 'Robust classification of motor imagery eeg signals using statistical time-domain features', *Physiological Measurement*, vol. 34, 11 2013, ISSN: 13616579. DOI: 10.1088/0967-3334/34/11/1563.

[138] R. Ortner, B. Z. Allison, G. Korisek, H. Gaggl and G. Pfurtscheller, 'An SSVEP BCI to control a hand orthosis for persons with tetraplegia', *IEEE Transactions on Neural Systems and Rehabilitation Engineering*, vol. 19, no. 1, 2011, ISSN: 15344320. DOI: 10.1109/TNSRE.2010.2076364.

[139] B. Blankertz, C. Sannelli, S. Halder, E. M. Hammer, A. Kübler, K. R. Müller, G. Curio and T. Dickhaus, 'Neurophysiological predictor of SMR-based BCI performance', *NeuroImage*, vol. 51, no. 4, 2010, ISSN: 10538119. DOI: 10.1016/j.neuroimage.2010.03.022.

[140] L. Sun, Z. Feng, N. Lu, B. Wang and W. Zhang, 'An advanced bispectrum features for EEG-based motor imagery classification', *Expert Systems with Applications*, vol. 131, pp. 9–19, 2019, ISSN: 09574174. DOI: 10.1016/j.eswa.2019.04.021.

[141] S. M. Zhou, J. Q. Gan and F. Sepulveda, 'Classifying mental tasks based on features of higher-order statistics from EEG signals in brain-computer interface', *Information Sciences*, vol. 178, no. 6, 2008, ISSN: 00200255. DOI: 10.1016/j.ins.2007.11.012.

[142] S. Shahid and G. Prasad, 'Bispectrum-based feature extraction technique for devising a practical brain-computer interface', *Journal of Neural Engineering*, vol. 8, no. 2, 2011, ISSN: 17412560. DOI: 10.1088/1741-2560/8/2/025014.

[143] Z. Iscan, Z. Dokur and T. Demiralp, 'Classification of electroencephalogram signals with combined time and frequency features', *Expert Systems with Applications*, vol. 38, no. 8, 2011, ISSN: 09574174. DOI: 10.1016/j.eswa.2011.02.110.

[144] L. Rankine, N. Stevenson, M. Mesbah and B. Boashash, 'A nonstationary model of newborn EEG', *IEEE Transactions on Biomedical Engineering*, vol. 54, no. 1, pp. 19–28, Jan. 2007, ISSN: 00189294. DOI: 10.1109/TBME.2006.886667.

[145] Z. Tayeb, J. Fedjaev, N. Ghaboosi, C. Richter, L. Everding, X. Qu, Y. Wu, G. Cheng and J. Conradt, 'Validating deep neural networks for online decoding of motor imagery movements from eeg signals', *Sensors (Switzerland)*, vol. 19, no. 1, Jan. 2019, ISSN: 14248220. DOI: 10.3390/s19010210.

[146] K. W. Ha and J. W. Jeong, 'Motor imagery EEG classification using capsule networks', *Sensors (Switzerland)*, vol. 19, no. 13, 2019, ISSN: 14248220. DOI: 10.3390/s19132854.

[147] O. Faust, U. R. Acharya, H. Adeli and A. Adeli, 'Wavelet-based eeg processing for computer-aided seizure detection and epilepsy diagnosis', *Seizure*, vol. 26, 2015, ISSN: 15322688. DOI: 10.1016/j.seizure.2015.01.012.

[148] G. Pfurtscheller, C. Neuper and N. Birbaumer, 'Human Brain—Computer Interface', in Dec. 2004. DOI: 10.1201/9780203503584.ch14. [Online]. Available: http://www.crcnetbase.com/doi/abs/10.1201/9780203503584.ch14.

[149] J. Cheng, P. song Wang, G. Li, Q. hao Hu and H. qing Lu, 'Recent advances in efficient computation of deep convolutional neural networks', *Frontiers of Information Technology and Electronic Engineering*, vol. 19, 1 2018, ISSN: 20959230. DOI: 10.1631/FITEE.1700789.

[150] J. Gu *et al.*, 'Recent advances in convolutional neural networks', *Pattern Recognition*, vol. 77, 2018, ISSN: 00313203. DOI: 10.1016/j.patcog.2017.10.013.

[151] Q. Zhang, M. Zhang, T. Chen, Z. Sun, Y. Ma and B. Yu, 'Recent advances in convolutional neural network acceleration', *Neurocomputing*, vol. 323, 2019, ISSN: 18728286. DOI: 10.1016/j.neucom.2018.09.038.

[152] P. Swietojanski, A. Ghoshal and S. Renals, 'Convolutional neural networks for distant speech recognition', *IEEE Signal Processing Letters*, vol. 21, 9 2014, ISSN: 10709908. DOI: 10.1109/LSP.2014.2325781.

[153] O. Abdel-Hamid, A. R. Mohamed, H. Jiang, L. Deng, G. Penn and D. Yu, 'Convolutional neural networks for speech recognition', *IEEE Transactions on Audio, Speech and Language Processing*, vol. 22, 10 2014, ISSN: 15587916. DOI: 10.1109/TASLP.2014.2339736.

[154] N. I. Wolf, A. García-Cazorla and G. F. Hoffmann, *Epilepsy and inborn errors of metabolism in children*, 2009. DOI: 10.1007/s10545-009-1171-3.

[155] K. W. Ha and J. W. Jeong, 'Motor imagery eeg classification using capsule networks', *Sensors (Switzerland)*, vol. 19, 13 2019, ISSN: 14248220. DOI: 10.3390/s19132854.

[156] D. Lee, S.-H. Park, H.-J. Lee and S.-G. Lee, 'Eeg-based motor imagery classification using convolutional neural network', *Journal of Korean Institute of Information Technology*, vol. 15, 6 2017, ISSN: 1598-8619. DOI: 10.14801/jkiit.2017.15.6.103.

[157] Z. Chen, Y. Wang and Z. Song, 'Classification of motor imagery electroencephalography signals based on image processing method', *Sensors*, vol. 21, 14 2021, ISSN: 14248220. DOI: 10.3390/s21144646.

[158] M. K. I. Molla, A. A. Shiam, M. R. Islam, T. Tanaka, T. Tanaka and T. Tanaka, 'Discriminative feature selection-based motor imagery classification using eeg signal', *IEEE Access*, vol. 8, 2020, ISSN: 21693536. DOI: 10.1109/ACCESS.2020.2996685.

[159] M. Tangermann *et al.*, 'Review of the bci competition iv', *Frontiers in Neuroscience*, JULY 2012, ISSN: 16624548. DOI: 10.3389/fnins.2012.00055.

[160] X. Li, C. Guan, H. Zhang, K. K. Ang and S. H. Ong, 'Adaptation of motor imagery eeg classification model based on tensor decomposition', *Journal of Neural Engineering*, vol. 11, 5 2014, ISSN: 17412552. DOI: 10.1088/1741-2560/11/5/056020.

[161] S. K. R. Singanamalla and C.-T. Lin, 'Spike-representation of eeg signals for performance enhancement of brain-computer interfaces', *Frontiers in Neuroscience*, vol. 16, 2022, ISSN: 1662-453X. DOI: 10.3389/fnins.2022.792318. [Online]. Available: https://www.frontiersin.org/article/10.3389/fnins.2022.792318.

# A

# APPENDIX

Figures 1, 2, 3, and 4 show the total errors between EEG signals and generated EEG signals for each network model and different coupling strengths. Small $\sigma$ values that produce CAS can lead to the smaller errors i.e., better prediction of the EEG signals after the training session.

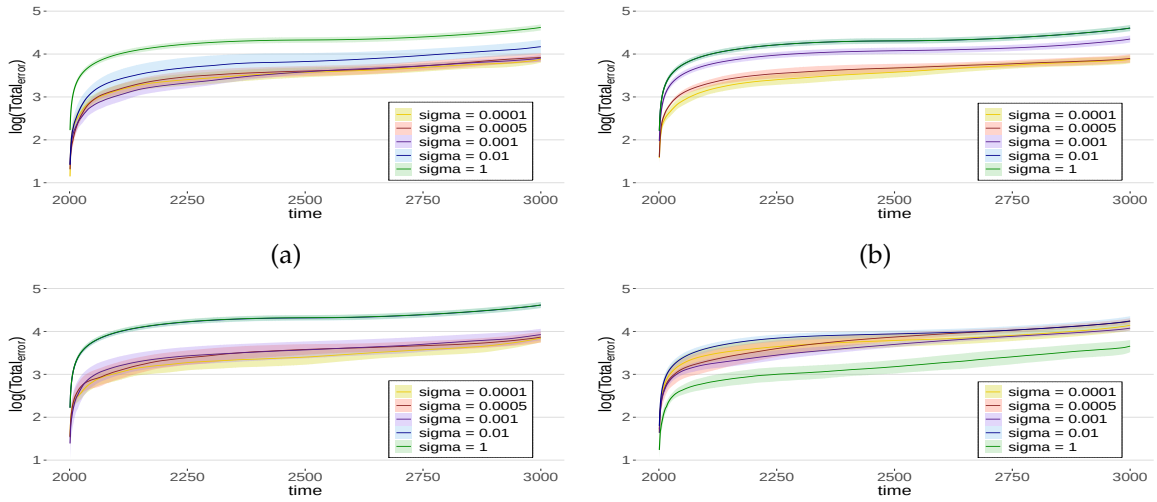


Figure A.1: Total error of prediction from channel 4 of five subjects in dataset B.

*Supplementary Figure B*

Figures 5, 6, 7, and 8 show the spectrum calculated directly from the EEG signals and the predicted EEG signals of channel Fp1 for each network model and different coupling strengths. The rows of this figure represent the power spectra ("actual" and "prediction") for several values of $\sigma$ increased from up to down.

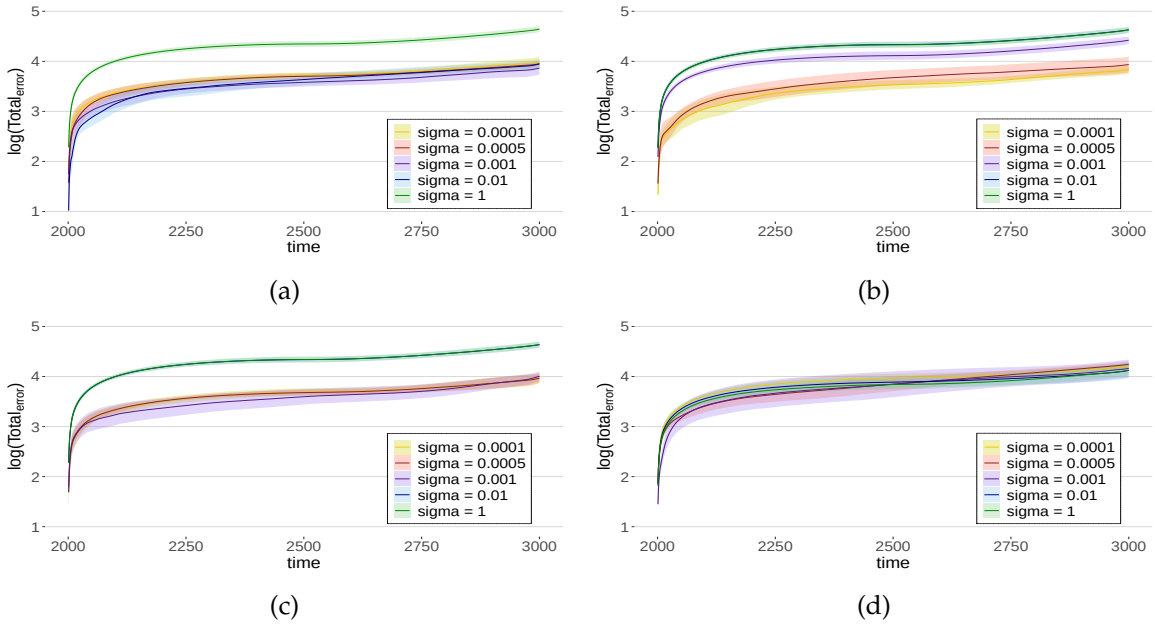


Figure A.2: Total error of prediction from channel 4 of five subjects in dataset C.

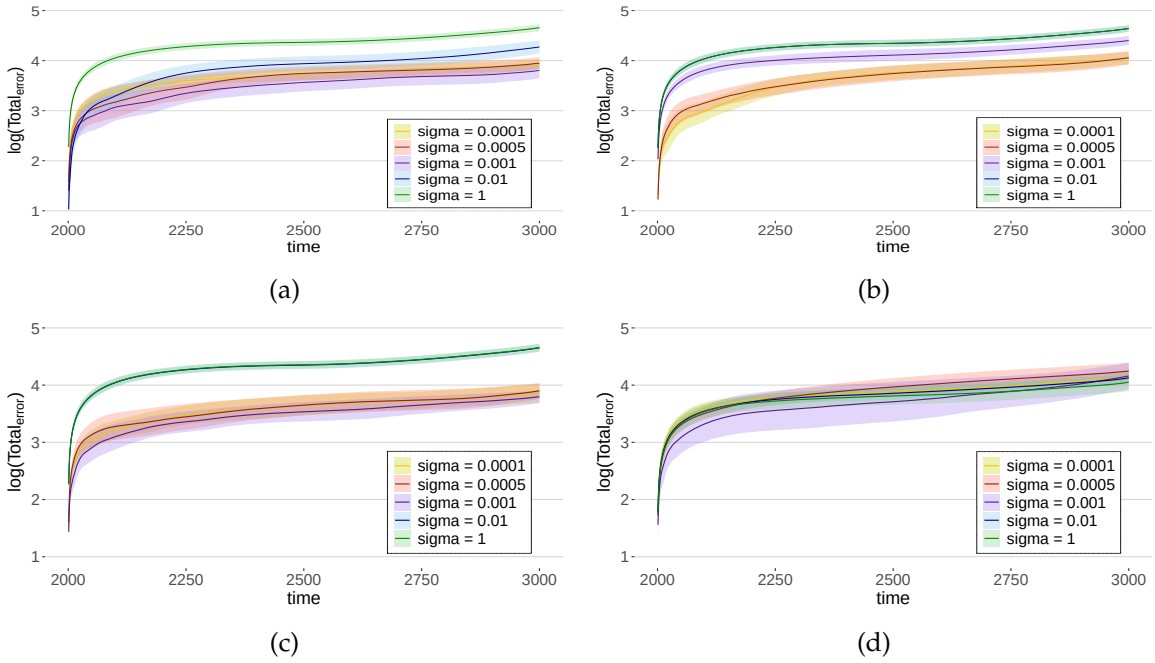


Figure A.3: Total error of prediction from channel 4 of five subjects in dataset D.

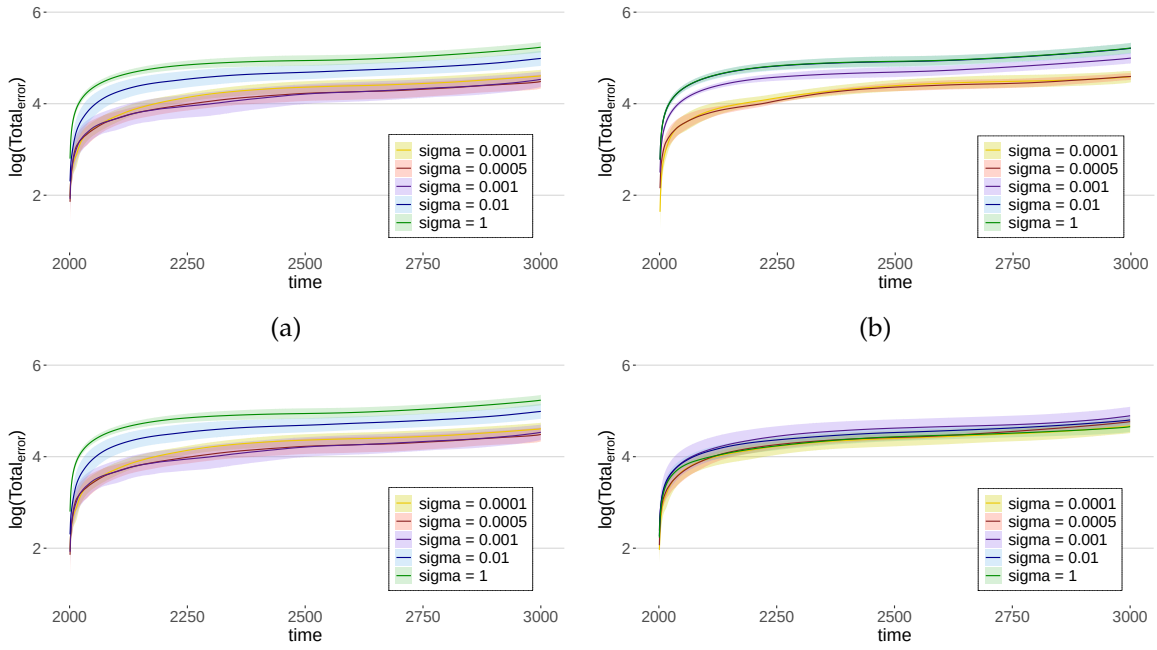


Figure A.4: Total error of prediction from channel 4 of five subjects in dataset E.

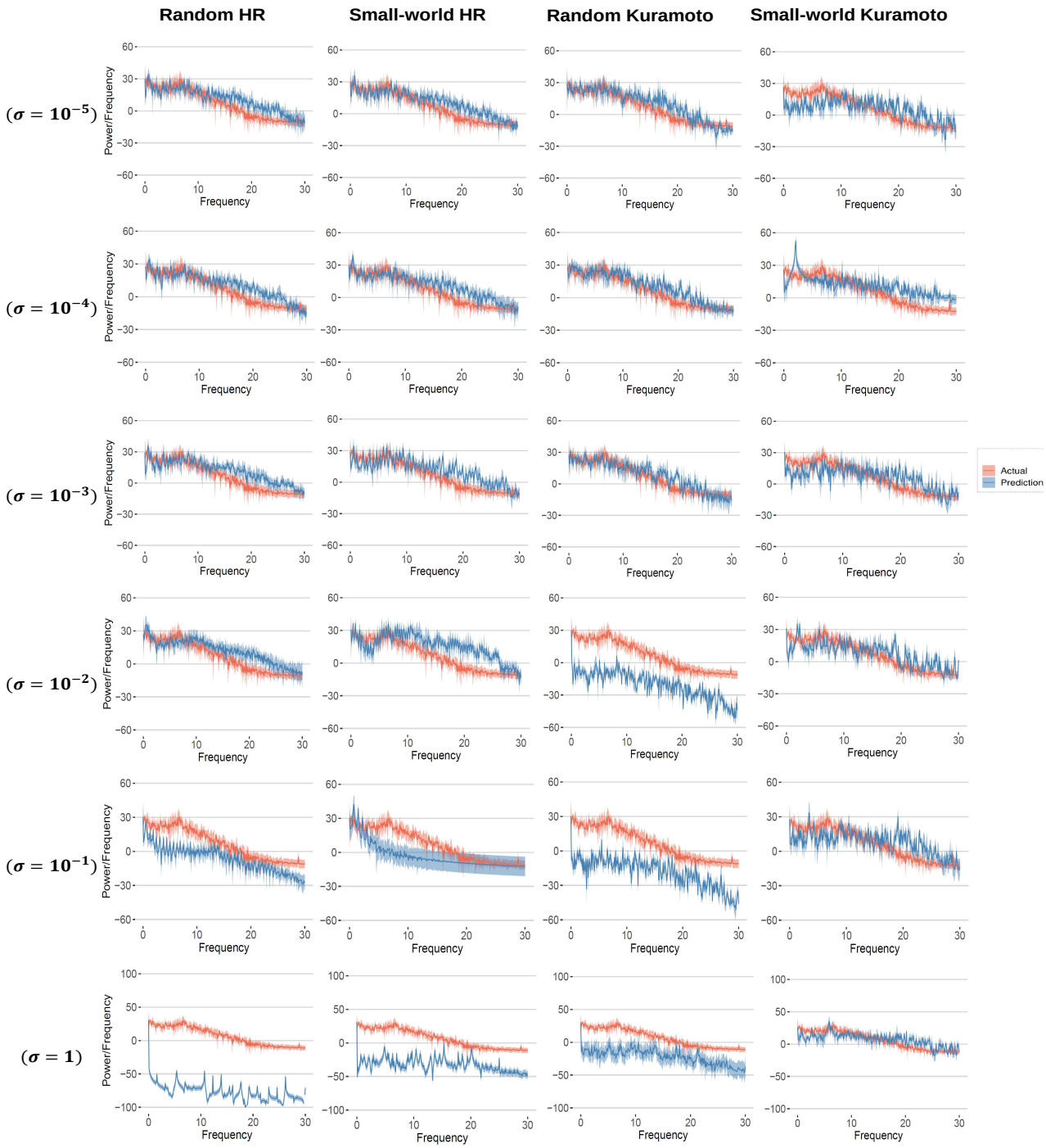


Figure A.5: Experimental and predicted power spectrum for dataset B.

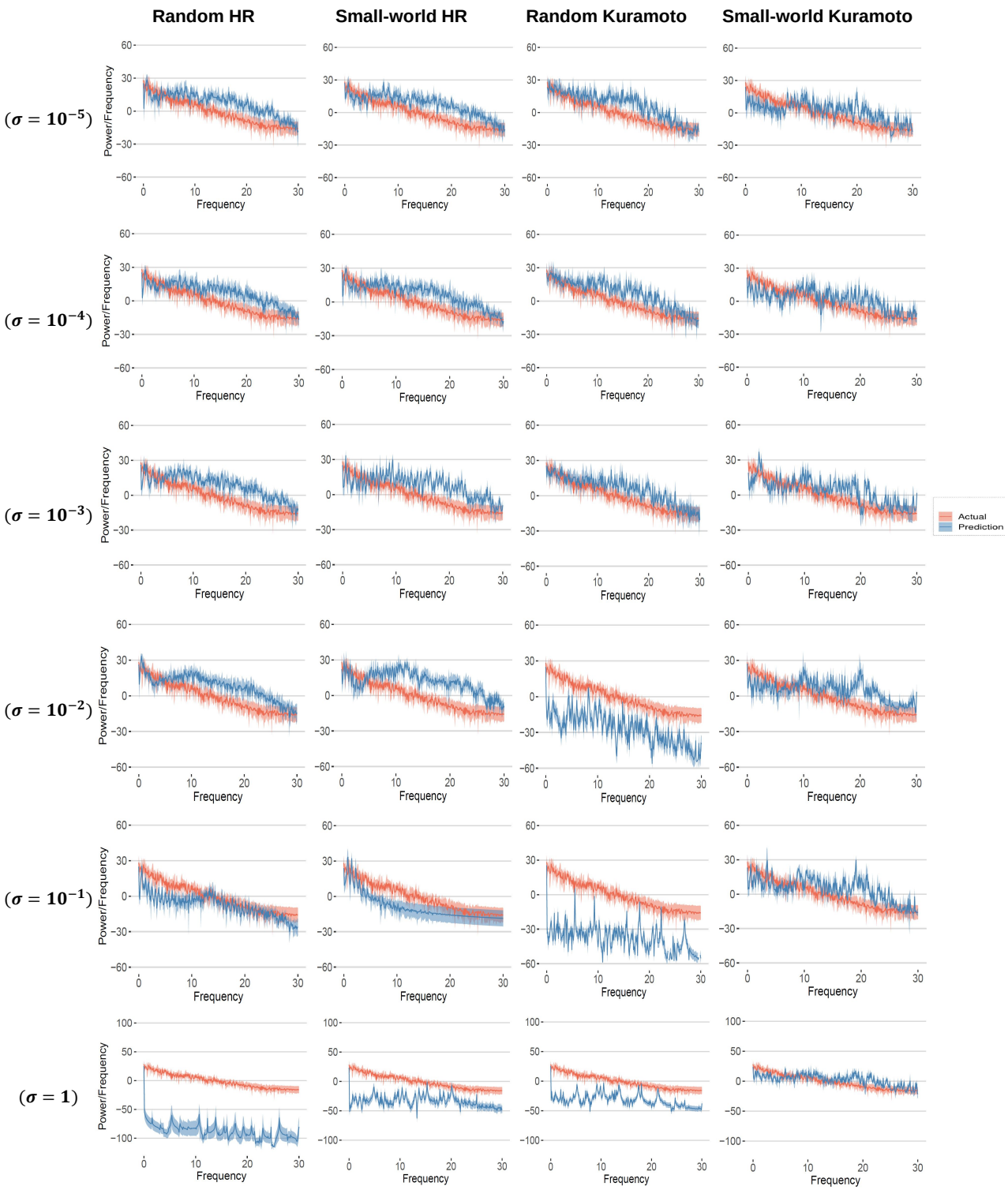


Figure A.6: Experimental and predicted power spectrum for dataset C.

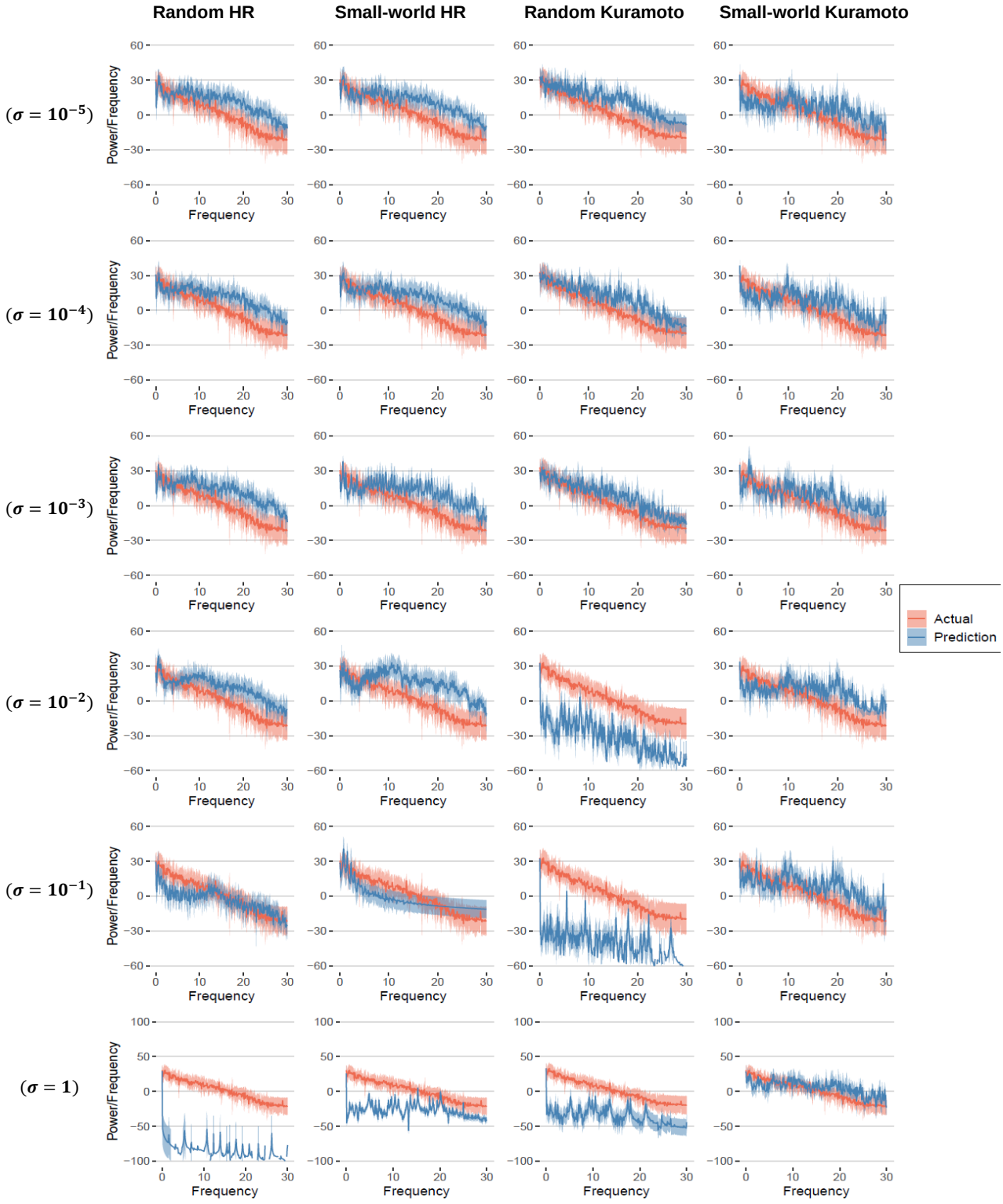


Figure A.7: and predicted power spectrum for dataset D.

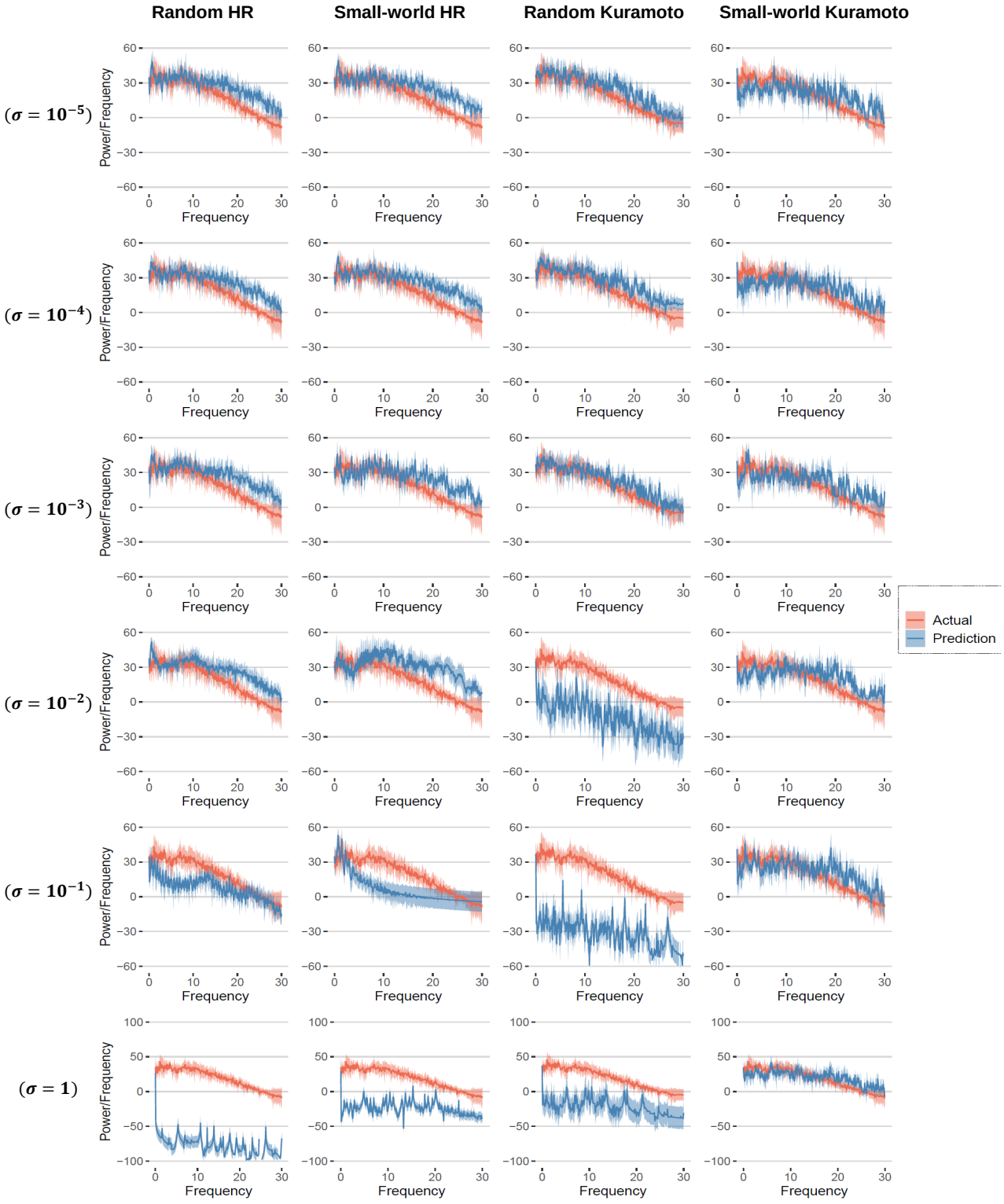


Figure A.8: Experimental and predicted power spectrum for dataset E.

# B

# PUBLICATIONS

Journal paper

- Thi Mai Phuong Nguyen, Yoshikatsu Hayashi, Murilo Da Silva Baptista, and Toshiyuki Kondo, "**Collective Almost Synchronization-based model to extract and predict features of EEG signals**" , Scientific Reports, 10, 16342, 2020 (peer-reviewed).
- Hoa Le, Uyen Pham, Phuong Nguyen, and The Bao Pham, "**Improvement on Monte Carlo estimation of HPD intervals**", Communications in Statistics - Simulation and Computation, 49:8, pp2164-2180, 2020 (peer-reviewed).

International Conference

- Thi Mai Phuong Nguyen, Xinzhe Li, Yoshikatsu Hayashi, Shiro Yano and Toshiyuki Kondo, "**Estimation of brain dynamics under visuomotor task using functional connectivity analysis based on graph theory**", Proceedings of the 19th annual IEEE International Conference on Bioinformatics and Bioengineering, Athens, Greece, Oct 2019 (oral, peer-reviewed).
- Thi Mai Phuong Nguyen, Yoshikatsu Hayashi, Murilo Da Silva Baptista, and Toshiyuki Kondo, "**Synthesis of EEG time-series using collective almost synchronization model**", 1st International Symposium on Hyper Adaptability, Virtual, May 2021 (poster, not peer-reviewed).
- Maro G. Machizawa, Giuseppe Lisi, Thi Mai Phuong Nguyen, Ryohei Mizuochi, Noriaki Kanayama, Kai Makita, Takafumi Sasaoka, and Shigeto Yamawaki, "**Dissociable neural markers for integrative emotional states relates to separable types of personality traits**", Technologies for Neuroengineering, Virtual, May 2021 (poster, not peer-reviewed).
- Thi Mai Phuong Nguyen, Minh Khanh Phan, Yoshikatsu Hayashi, Murilo Da Silva Baptista, and Toshiyuki Kondo, "**Collective Almost Synchronization Modeling Used for Motor Imagery EEG Classification**", 43rd Annual International Conference of the IEEE Engineering in Medicine and Biology Society, Virtual, Oct 2021 (poster, peer-reviewed).

Domestic Conference

- Thi Mai Phuong Nguyen, Maro G. Machizawa, Ryohei Mizuochi, and Shigeto Yamawaki."**Validation of personality dependent optimized emotion (KANSEI) decoding using EEGs**", The 44th Annual Meeting of the Japan Neuroscience Society, Kobe, Japan, July 2021 (poster, not peer-reviewed).